Carnegie Mellon University

CARNEGIE INSTITUTE OF TECHNOLOGY

THESIS

SUBMITTED IN PARTIAL FULFILLMENT OF THE REQUIREMENTS

FOR THE DEGREE OF Doctor of Philosophy

TITLE Measurement and Recovery of Rare Earth Elements from Hypersaline Fluids

PRESENTED BY Clinton W. Noack

ACCEPTED BY THE DEPARTMENTS OF

Civil and Environmental Engineering

Athanasios Karamalidis CO-ADVISOR, MAJOR PROFESSOR	December 28, 2015 DATE
David A. Dzombak CO-ADVISOR, MAJOR PROFESSOR	December 28, 2015 DATE
David A. Dzombak DEPARTMENT HEAD	December 28, 2015 DATE

APPROVED BY THE COLLEGE COUNCIL

Vijayakumar Bhagavatula DEAN	January 4, 2016 DATE

Measurement and Recovery of Rare Earth Elements from Hypersaline Fluids

Submitted in partial fulfillment of the requirements for

the degree of

Doctor of Philosophy

in

Civil & Environmental Engineering

Clinton W. Noack

B.S., Environmental Systems Engineering, Pennsylvania State University

M.S., Civil & Environmental Engineering, Carnegie Mellon University

Carnegie Mellon University

Pittsburgh, PA

December, 2015

Abstract

The rare earth elements (REE) constitute much of Group 3 of the periodic table, a group of 16 transition metals, including the lanthanide series (La to Lu, excluding Pm), yttrium (Y) and scandium (Sc). Modern technologies — including catalysts, high-strength alloys, high-efficiency phosphors, lasers, and magnets — are dependent upon the unique properties of the REE for their efficacy of operation. However, global REE material-flows are prone to complex environmental, technical, and geopolitical forces on both the supply- and demand side. Development of economically-viable technologies for the extraction of the REE and other critical materials from unconventional sources (such as geothermal fluids, oil and gas produced waters, or coal combustion residuals) has great potential value to: generate a consistent domestic supply of materials critical to green energy and defense technologies; valorize high-volume wastes or low-value industrial byproducts; and avoid environmental impacts from primary REE mining. This research addressed the potential for REE extraction and recovery from aqueous sources.

The primary goal of this thesis research was to assess the potential for aqueous sources to serve as alternative resources for the rare earth elements. This was accomplished through a combination of a literature analysis, method development, and experimentation. Three specific objectives were pursued in order to meet this goal, with each comprising a separate chapter of this thesis. First, to determine the abundance of dissolved REE in waters of various

compositions and investigate trends to better understand solubility controlling processes. Second, to develop an extraction and preconcentration method, robust to a range of water chemistries, for the analysis of dissolved REE in hypersaline fluids. Finally, to compare technologies for the economic extraction of REE from hypersaline fluids.

For the first objective, reported dissolved REE concentration data over a wide range of natural water types (groundwater, ocean-, river-, and lake water) and groundwater chemistries (e.g. fresh, brine, and acidic) were compiled and analyzed with the goal of quantifying the extent of natural REE variability, especially for groundwater systems. Reported measurements of rare earth elements in natural waters range over nearly ten orders of magnitude, though the majority of measurements are within two to four orders of magnitude, and are highly correlated with one another. Few global correlations exist among dissolved abundance and bulk solution properties in groundwaters indicating the complex nature of source-sink terms and the need for care when comparing results between studies. This collection, homogenization, and analysis of a disparate literature facilitates inter-study comparison and provides insight into the wide range of variables that influence REE geochemistry.

Accurate quantitation in complex, aqueous matrices is necessary for evaluation and implementation of systems aimed at recovering critical materials. For the second objective, we modified and optimized previously published liquid-liquid extraction (LLE) techniques, using bis(2-ethylhexyl) phosphate as the extractant in a heptane diluent, and studied its efficacy for REE recovery as a function of three primary variables: background salinity (as NaCl), concentration of a competing species (here Fe), and concentration of dissolved organic carbon (DOC). Results showed that the modified LLE was robust to a range of salinity, Fe, and DOC concentrations studied as well as constant, elevated Ba concentrations. With proper characterization of the natural samples of interest, this method could be deployed for accurate analysis of REE in small volumes of hyper-saline and chemically complex brines.

Finally, aminated silica gels were functionalized with different REE-reactive ligands and tested under a range of chemical conditions. A suite of characterization techniques and batch adsorption experiments were used to test the REE-uptake chemistry of the functionalized materials. Results showed that DTPA-dianhydride yielded the most REE reactive adsorbent of the three tested, with measured partitioning coefficients commensurate with some of the highest reported in the literature. Additional development is required to implement an REE recovery scheme using these materials, however it is clear that DTPA-based adsorbents offer a highly-reactive adsorbent warranting further study.

This dissertation improved the understanding of the occurrence of REE in waters and the potential for their economic recovery. Each chapter detailing novel research constitutes a unique contribution to the scientific literature on this topic. These contributions can be summarized as: (1) the compilation and standardization of reported REE concentrations (and associated water chemistry measurements) to encourage inter-study comparisons while discouraging generalizations; (2) the validation of an efficient and robust analytical technique for the determination of dissolved REE concentrations in chemically complex aqueous solutions; and (3) the demonstration of silica based, REE-reactive adsorbents at previously untested salinities and with environmentally relevant REE concentrations. This knowledge will be useful to compare REE concentrations and values among aqueous sources and to measure and recover these elements with efficient and environmentally benign technologies.

Acknowledgements

This technical effort was partially performed under the RES contract DE-FE0004000 through the National Energy Technology Laboratory (NETL) of the U.S. Department of Energy (DOE). Latter parts of this research, the development of functionalized adsorbents, was funded by the DOE Office of Energy Efficiency and Renewable Energy under contract DE-EE0006749.0000. Additionally, this research was supported in part by an appointment to the U.S. DOE Postgraduate Research Program administered by the Oak Ridge Institute for Science and Education.

I would like to thank my advisors, Dr. Athanasios Karamalidis and Dr. David Dzombak for their support throughout this study. Both Thanasis and Dave have taught me invaluable lessons about science, research, education, and professionalism I would also like to thank my committee members, Dr. Ale Hakala from NETL and Dr. Mitch Small, who have continued their involvement with this thesis despite the aforementioned changes. Lastly, I would like to thank Dr. Newell Washburn for his invaluable input into the development and testing of functionalized adsorbents.

Throughout my time at Carnegie Mellon, numerous faculty and staff have contributed invaluably to my progress. My first project at CMU focused on the sequestration of CO_2 using alkaline industrial wastes. This project was co-advised by my current advisor Dr. Dzombak as well as Dr. Dave Nakles. Dr. Nakles quickly became a valued advisor, mentor, and friend,

whom has stayed involved in my thesis studies, despite no longer being directly involved in the research. As with every student performing research in the Hauck Environmental Lab, my success and progress was directly facilitated by the dedicated work of lab manager, Ron Ripper. I, and many of my lab mates, have told Ron that he has the worst job in the world: constantly bailing needy, inconsiderate graduate students (myself chief among them) out of minor and major binds. That he disagrees with this assessment is a testament to his excellence. Also, I ate *way* too many donuts on account of Ron, and I love donuts.

Many students, past and present, have helped me to complete this journey, including Drs. Arvind Murali Mohan, Djuna Gulliver, Hariprasad Parthasarathy, and Aniela Burant as well as Adam Cadwallader, Jon Callura, Nizette Consolazio, Megan Leitch, Eric McGivney, Joe Moore, Kedar Perkins, John Stegemeier, and Lauren Strahs. Through their involvement in the CCUS/Shale Gas research groups, 207C Journal Club, and everyday banter about the occasional absurdities of doctoral studies, these individuals have enriched my experience at CMU. While his time physically at CMU was brief, Dr. Nick Azzolina and I bonded over a shared value of self-reliance and self-discovery in topics ranging from "finding a way to generate random numbers in Excel on a Mac", to discussing the relative merits of the Wallenius versus the Fisher noncentral hypergeometric distributions. In addition to Dr. Mitch Small, Nick is primarily responsible for my love of statistics and data analysis and (through his own struggles as a programmer) my fierce dedication to and moderate skill in the R programming language.

In making Pittsburgh my adoptive home, I have been welcomed into an incredible family, that has supported me physically and emotionally. The Taylors (and the George, Masters, and Wolff families) — specifically Sam, Jan, Kathy, Hilary, Jen, Bryan, and little Hillary — have all shown me love and support every day throughout my studies. We have shared too many exquisite meals, relaxing vacations, and simple moments of family to keep track

of, each of which has sustained me in some way, small or large. I am so fortunate for and grateful to these wonderful people.

Every day of my life, my parents, Michele and Ralph, have shown me love, given me encouragement, and truly believed in me. I have not always been effusive about my appreciation of their efforts, but they have always and continue to guide me down a path of success and fulfillment. I love them both for their tireless dedication to me, above their own needs, and am so happy that (after nearly 27 years) they will see me get a real job and stop relying on them for help with the rent.

Finally, and most importantly, I want to acknowledge my fiancée, Robin Taylor. In the last month of this dissertation alone, you have brought an imbalance of love, support, and selflessness to our relationship that I can never hope to equalize. But it has been far more than a month. From the beginning of our lives together you have put me ahead of yourself and been dedicated to my success, never more so than throughout this dissertation. I would never have made it without the chance to laugh with you at the start and end of every day, regardless of what happened in between. I am so lucky for the chance to spend the rest of our lives together and the daily opportunity to remind you of how much I love and appreciate you.

Contents

List of Tables

List of Figures

Chapter 1

Introduction, problem identification, and research goals

1.1 Introduction

Modern technologies — including catalysts, high-strength alloys, high-efficiency phosphors, lasers, and magnets — are dependent upon the unique properties of the rare earth elements (REE) for their efficacy of operation. However, global REE material-flows are prone to complex environmental, technical, and geopolitical forces on both the supply- and demand side. Development of economically-viable technologies for the extraction of the REE and other critical materials from unconventional sources (such as geothermal fluids, oil and gas produced waters, or coal combustion residuals) has great potential value to: generate a consistent domestic supply of materials critical to green energy and defense technologies; valorize high-volume wastes or low-value industrial byproducts; and avoid environmental impacts from primary REE mining. This research seeks to address the potential for REE extraction and recovery from aqueous sources.

1.2 Problem identification

1.2.1 Drivers of REE demand

The constantly increasing consumer products incorporating the REE, and the ensuing demand for these products, have established the REE as valuable global commodities. Domestic demand in 2012 was 11,300 tons, while the global demand was more than 113,000 tons (Frost & Sullivan 2013). Much of that demand is a result of a booming green energies market. In particular, the permanent magnets sector (which uses neodymium, praseodymium, and samarium with dysprosium and terbium additives) is expected to experience significant growth between 2013 and 2020. The U.S. Department of Energy has projected the supply risk and clean-energy demand of the REE across all sectors found a variety of criticalities for the elements (Figure 1.1).

Even at the height of domestic REE production at Mountain Pass in CA (2012), the U.S. imported $520MM worth of REE compounds, with nearly 40% coming from China, in order to support a demand of 11,300 tons (Gambogi 2012). A booming green energies industry fueled, and continues to fuel, both domestic and global demand, where the REE provide superior performance and efficiency compared to alternative materials (Graedel et al. 2015; Nassar et al. 2015). The distribution of REE demand by use sector and country/region is shown in Table 1.1, while typical REE compositions within those applications are shown in Table 1.2. Sustained growth in these technologies is dependent on diversifying REE sources given projected supply shortages in the medium- to long-term. Traditional mining of REE from ore deposits is unlikely to fulfill this demand for technical and economic reasons, especially in the US where traditional mining of REE is suspended. China, the world's leading source of REE and primary supplier of global demand for many years (Figure 1.2), has indicated partial control of exports, or punitive tariffs, in the near future. This emphasizes

the need for REE separation and recovery from unconventional matrices, such as geothermal fluids.

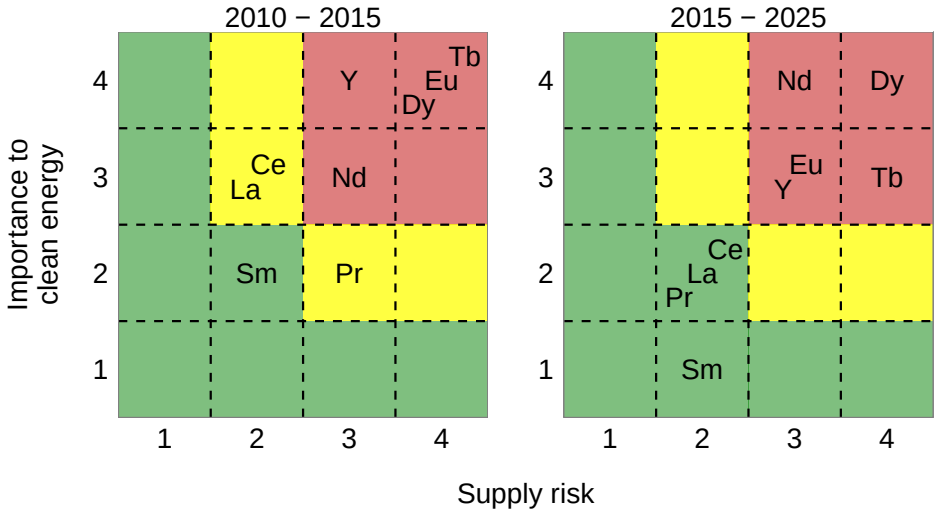

Figure 1.1: U.S. Department of Energy critical material matrix. Adapted from Bauer et al. (2010). Elements in red are considered critical, yellow are considered near-critical, and green are considered non-critical.

Table 1.1: Estimated global rare earth demand in 2010 by use sector (tonnes REO ±15%). Data adapted from Kingsnorth (2010).

Application	China	Japan & NE Asia	USA	Others	**Total**
Catalysts	9,000	3,000	9,000	3,500	24,500
Glass	7,000	1,500	1,000	1,500	11,000
Polishing	9,500	7,000	1,000	1,500	19,000
Metal alloys	14,500	5,500	1,000	1,000	2,200
Magnets	20,500	4,000	500	1,000	26,000
Phosphors	5,500	2,000	1,500	500	8,500
Ceramics	2,500	2,500	1,500	500	7,000
Other	4,000	2,500	500	500	7,000
Total	72,500	27,500	15,000	10,000	**125,000**

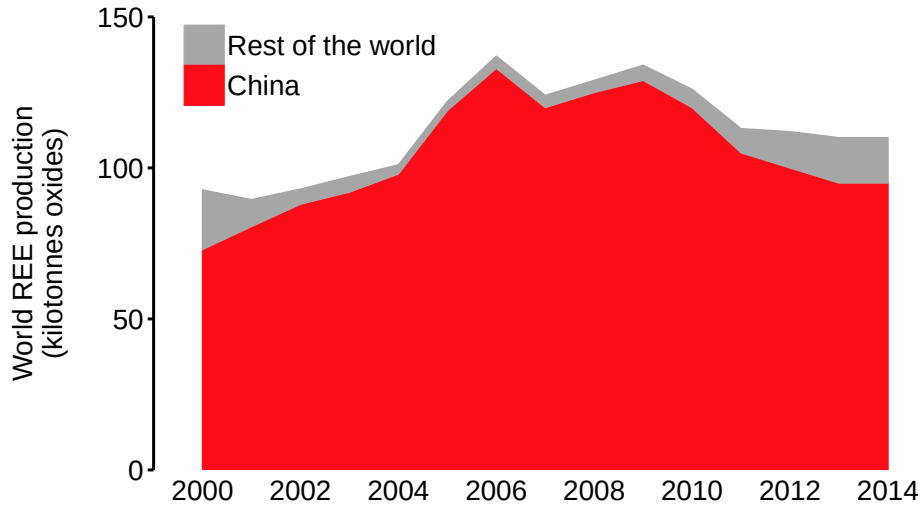

Figure 1.2: Global, primary REE production, 2000-2014. Data from U.S. Geological Survey (2015).

Table 1.2: Intra-element distribution (wt% of total REE usage) for REE-based components of common products containing REE. Data reproduced from Long et al. (2012). Rows sum to 100%, columns do not. Untabulated REE are grouped as "Other". Rows represent typical values, actual compositions may vary.

	La	Ce	Pr	Nd	Sm	Eu	Gd	Tb	Dy	Y	Other
Magnets			23.4	69.4			2	0.2	5		
Battery alloys	50	33.4	3.3	10	3.3						
Metal alloys	26	52	5.5	16.5							
Auto catalysts	5	90	2	3							
Petroleum refining	90	10									
Polishing compounds	31.5	65	3.5								
Glass additives	24	66	1	3						2	4
Phosphors	8.5	11				4.9	1.8	4.6		69.2	
Ceramics	17	12	6	12						53	

1.2.2 Limitations of REE supply

Global REE reserves are estimated at 130 million metric tons (U.S. Geological Survey 2015), much of which is located in low-concentration deposits or ocean-floor manganese nodules, which are both extremely expensive to mine with current methods. This limits the number of readily mineable REE deposits and, ultimately, our ability to increase REE supply (Alonso et al. 2012; Moss et al. 2011). Aqueous media such as brines or produced waters from geothermal energy, conventional oil/gas, and shale gas extraction operations are potentially significant, but unexplored sources of REE.

Presently, REE extraction is accomplished by traditional mining (e.g. open-pit) followed by chemically-, and energy-intensive element separations, which incur a significant environmental burden (Figure 1.3; (Zaimes et al. 2015)). Even when present in ores at appreciable levels, REE are commonly commingled with radioactive thorium and uranium, which need to be safely separated and stored in addition to standard waste management associated with mining (e.g. tailings) (Gupta and Krishnamurthy 1992; Sprecher et al. 2014). Stringent environmental regulations, time-intensive processes, and expensive permits complicate the opening of new, domestic mines because of these inherent risks. On this basis, projections expect that exploiting traditional REE sources to meet increasing demand will be a significant challenge.

In 2012, China was responsible for more than 95% of the global REE supply (U.S. Geological Survey 2015). China also had the largest demand for REE, at 66% of the total global demand (U.S. Geological Survey 2015). The US was the next largest consumer, at 10–15% of the total demand. In 2011, China announced a 35% reduction in exports of REE, in an effort to meet their domestic needs (Gambogi 2012). This created large instability in the REE market as there were no other major sources for REE (Alonso et al. 2012; Chakhmouradian

and Wall 2012; Hatch 2012). China is expected to continue reduction of exports, through either quotas or tariffs, as a means to reduce stress on its REE reserves (Frost & Sullivan 2013; U.S. Geological Survey 2015).

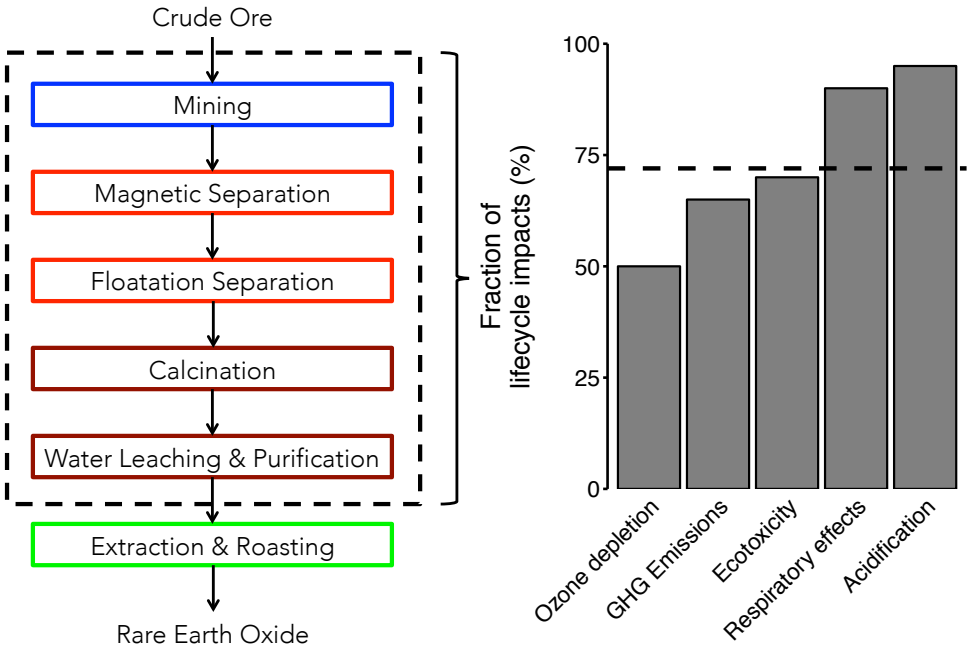

Figure 1.3: Traditional REE production flowsheet (left) and the associated fraction of lifecycle environmental impacts for the boxed boundary (right) using data from Zaimes et al. (2015). Only selected impact categories are shown, however the dashed line (72%) indicates the overall average across ten categories.

Primary mining effectively constitutes 100% of the REE production worldwide (Binnemans et al. 2013; U.S. Geological Survey 2015), but interest in recovery of REE from end-of-life stocks (EOL), from unconventional resources, and from REE-containing industrial wastes has expanded rapidly in recent years (Binnemans et al. 2015). High volumes of REE are deployed in permanent magnets, while high-value REE are used in phosphors (Hatch 2012), making these products two primary targets for recycling from EOL products along with metal hydride batteries (Binnemans et al. 2013; Tunsu et al. 2015). REE are applied in many other products, but the REE content is dissipated in-use or rendered unrecyclable by current

designs (Ciacci et al. 2015). Ferrous shredder waste (where magnets could accumulate) is a promising potential resource for REE and other critical materials. However, Bandara et al. (2015) propose that recycling of ferrous shredder-waste would need to exceed 50% in order to dampen Nd price volatility from recycling alone. The conclusion from these forecasts is the need for novel, alternative feedstocks (Bandara et al. 2015).

1.2.3 Potential alternative REE resources

The United States is a pioneer in utilizing geothermal resources for the production of low-carbon energy. Among energy production approaches, such as solar, wind, conventional oil, and coal, geothermal energy is renewable, abundant and with a small green-house gas footprint. Although variations of geothermal power plants exist, either those being equipped with conventional hydrothermal flash-, conventional hydrothermal binary- or enhanced hydrothermal systems (Clark et al. 2011), all designs produce steam as a working fluid from naturally-heated brines found in deep, crustal reservoirs.

In a simplistic description of a steam-based geothermal power plant, high temperature brine flows to the surface from a geothermal reservoir through a production well. This hot, pressurized fluid is separated from entrained solids and guided to gas-liquid separators, producing steam that is delivered to turbines for electricity production. The cooled brine is mixed with condensed steam and recycled by re-injection into the reservoir without further treatment. These fluids, where the valuable heat has already been extracted, represent an attractive source for mineral extraction that would not interfere with the primary function of the geothermal power plant.

Geothermal brines, as well as groundwater, have been reported to contain REE at typical concentrations ranging from 10^{-9}–10^{-12} g/g of solution, along with other minerals, such as

Fe, Si, Al, Na, and K (Lewis et al. 1998; 1997; Michard 1989; Noack et al. 2014). Depending on the reservoir lithology and the fluid chemistry (e.g. acid-sulfate, acid-sulfate-chloride, etc.), concentrations of total REE can reach µmol/kg solution (10^{-6} mol/kg) levels, as in the case of the geothermal systems from Yellowstone National Park, Wyoming, USA , i.e. $\sum$REE = 1.13 µmol/kg solution (Lewis et al. 1998). Historical data from CDOGGR (2009) show typical geothermal brine production rates of 393,000 – 512,000 gal/day/MWe (for a binary plant) and 93,000 – 171,000 gal/day/MWe (for secondary flash plant). These data optimistically translate to a maximum resource stream of 1.8 – 2.3 mol total REE/day/MWe for a binary plant and 0.4 – 0.8 mol total REE/day/MWe for a secondary flash plant.

Considering the total installed capacity in the US in February 2013 was 3,386 MW with new geothermal projects under development reaching 10,100 MW in 2025 (Geothermal Energy Association 2013), creating new revenue for the industry through REE extraction from brines may be viable. Global geothermal capacity is expected to grow from 11.6 GW in 2012 to 20.7 GW in 2020 and 29.4 GW in 2025. The capacity expansion is largely driven by North America, Asia-Pacific as well as national and regional markets such as Turkey, Iceland and Eastern Africa (Frost & Sullivan 2014). It is apparent that recovery of REE from these streams may be a viable alternative source of critical elements both domestically and globally.

1.3 Research goals

The primary goal of this thesis research was to assess the potential for aqueous sources to serve as alternative resources for the rare earth elements. This was accomplished through a combination of a literature analysis, method development, and experimentation. Three specific objectives were pursued in order to meet this goal, with each comprising a separate

chapter of this thesis.

Objective 1: Determine the abundance of dissolved REE is waters of various compositions and investigate trends to better understand solubility controlling processes.

Objective 2: Develop an extraction and preconcentration method, robust to a range of water chemistries, for the analysis of dissolved REE in hypersaline fluids

Objective 3: Compare technologies for the economic extraction of REE from hypersaline fluids

1.3.1 REE abundance and trends in terrestrial waters

Despite their name, the "rare" earth elements are ubiquitously dispersed in geologic and aqueous systems. Study of the REE systematics in natural and anthropogenically-influenced environments has produced an extensive, but disparate, literature, holding rich insights were it to be compiled, standardized, and analyzed. This objective brought together more than 1000 measurements from 31 studies to constitute the largest aggregation of REE data in the literature.

This objective studied the natural variability of REE in aqueous media, quantitative methods for considering below-detection-limit values, the REE occurrence in brines, and the relationships between REE and bulk solution properties important for REE fate and transport. These data were used to: (1) ascertain an expected range of dissolved REE concentrations in waters of variable chemistries, deriving unbiased estimates of REE distributions and (2) investigate trends in REE abundance in groundwater in relation to other available chemical parameters (e.g. pH, ionic strength, and major solution species). This collection, homogenization, and analysis of a disparate literature facilitates inter-study comparison and provides insight into the wide range of variables that influence REE geochemistry.

1.3.2 Analytical method development for REE measurement in hypersaline fluids

There exists a dearth of methodologies in the analytical literature for quantitation of REE in brines. Many approaches have been applied for separation and concentration of REE from aqueous media including solid- phase extraction (SPE), co-precipitation (co-ppt), and liquid- liquid extraction (LLE). However, nearly all studies in the analytical chemistry literature have focused on fresh water or seawater matrices, neglecting hypersaline waters which could have significant, unknown impacts on the efficiency of separation without proper validation.

Efficiency of REE separation and concentration from synthetic brines using a LLE method for quantitative analysis was studied. The LLE method was adapted, modified, and optimized from previously published studies. The tasks of this work were to: (1) evaluate the feasibility of REE recovery from small volumes of hypersaline solutions by LLE, (2) optimize the LLE methodology for high salinity brines, and (3) study the influence of brine composition on REE recovery.

1.3.3 Novel extractive technologies for REE recovery from geothermal waters

Development of dilute aqueous resource streams is dependent on high-capacity and resource-selective adsorbent materials for the passive capture of the resource from large, continuous volumes of feed solution. Numerous ligands have been developed for strong, selective complexation with the REE, whether for use in medical imaging, or separation of the REE from actinides during nuclear fuel reprocessing. These ligands meet the resource-selective criteria

stated above, while their attachment to a high surface area support will create significant capacity. However, few studies have attempted the surface-grafting of these ligands for this purpose, so little is known about the changes to their reactivity towards the REE.

REE uptake onto silica-based adsorbents with varying surface functionalization was studied. In particular, this work sought to confirm the persistence of REE-selective reactivity and capacity upon surface attachment. This goal was accomplished though a suite of adsorption tests (i.e. adsorption edges, isotherms, and kinetics) under a range of solution conditions (e.g. low and high salt concentrations, with and without various competing cations).

1.4 Thesis organization

This thesis is arranged into distinct chapters to address key knowledge- and technical gaps in the existing literature (Figure 1.4). Chapter 2 provides a background on the aqueous geochemistry of the REE, with a focus on complex, high-salinity systems. The background material concludes in Chapter 3 with a review of the current technologies in use and proposed for REE extraction and recovery from conventional and unconventional sources. The second portion constitutes the novel contributions of this thesis and is comprised of one chapter per objective (as outlined previously). Chapter 4 describes the results of a review and compilation of published REE data, accompanied by an in depth statistical analysis of occurrence distributions and trends. Chapter 5 details the optimization and application of a liquid-liquid extraction to precisely measure REE concentrations in small volumes of complex, hypersaline fluids. Chapter 6 characterizes the performance of surface attached ligands for the extraction and recovery of the REE from synthetic brine solutions. Finally, Chapter 7 summarizes this project in the broader context of alternative REE resources and suggests future work.

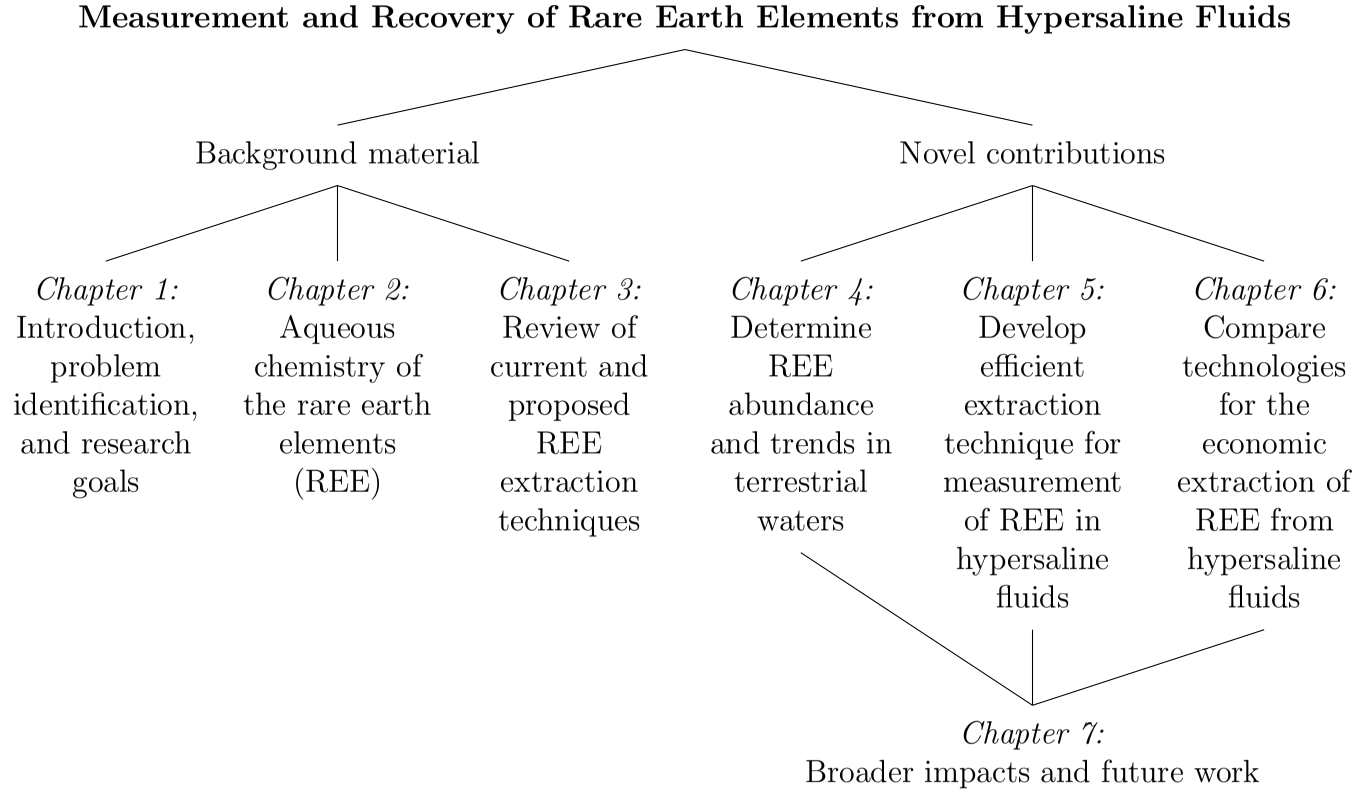

Figure 1.4: Organization of the thesis, including research objectives

1.5 References

Alonso, E., Sherman, A. M., Wallington, T. J., Everson, M. P., Field, F. R., Roth, R., and Kirchain, R. E. Evaluating rare earth element availability: A case with revolutionary demand from clean technologies. *Environmental science & technology*, 46(6):3406–3414, 2012.

Bandara, H. M. D., Mantell, M. A., Darcy, J. W., and Emmert, M. H. Rare earth recycling: Forecast of recoverable Nd from shredder scrap and influence of recycling rates on price volatility. *Journal of Sustainable Metallurgy*, pages 1–10, 2015.

Bauer, D., Diamond, D., Li, J., Sandalow, D., Telleen, P., and Wanner, B. US Department of Energy Critical Materials Strategy. Report, U.S. Department of Energy, 2010.

Binnemans, K., Jones, P. T., Blanpain, B., Van Gerven, T., Yang, Y., Walton, A., and Buchert, M. Recycling of rare earths: a critical review. *Journal of Cleaner Production*, 51:1–22, 2013.

Binnemans, K., Jones, P. T., Blanpain, B., Van Gerven, T., and Pontikes, Y. Towards zero-waste valorisation of rare-earth-containing industrial process residues: a critical review. *Journal of Cleaner Production*, 99(0):17–38, 2015.

CDOGGR. Summary of geothermal operations. Report, California Division of Oil, Gas & Geothermal Resources, 2009.

Chakhmouradian, A. R. and Wall, F. Rare earth elements: Minerals, mines, magnets (and more). *Elements*, 8(5):333–340, 2012.

Ciacci, L., Reck, B. K., Nassar, N. T., and Graedel, T. E. Lost by design. *Environmental Science & Technology*, 49(16):9443–51, 2015.

Clark, C., Harto, C., Sullivan, J., and Wang, M. Water use in the development and operation of geothermal power plants. Report, Argonne National Laboratory, 2011.

Frost & Sullivan. Supply/demand dynamics of rare earth elements. Report, December 2013.

Frost & Sullivan. Annual renewable energy outlook. Report, 2014.

Gambogi, J. *Rare Earths*. Minerals Yearbook. U.S. Geologic Survey, 2012.

Geothermal Energy Association. Annual US geothermal power production and development report. Report, Geothermal Energy Association, 2013.

Graedel, T. E., Harper, E. M., Nassar, N. T., and Reck, B. K. On the materials basis of modern society. *Proceedings of the National Academy of Sciences*, 112(20):6295–6300, 2015.

Gupta, C. and Krishnamurthy, N. Extractive metallurgy of rare earths. *International Materials Reviews*, 37(1):197–248, 1992.

Hatch, G. P. Dynamics in the global market for rare earths. *Elements*, 8(5):341–346, 2012.

Kingsnorth, D. J. Meeting the challenges of rare earths supply in the next decade. *Industrial Minerals Company of Australia Pty Ltd., The Hague Centre for Strategic Studies*, 2010: 30, 2010.

Lewis, A., Komninou, A., Yardley, B., and Palmer, M. Rare earth element speciation in geothermal fluids from Yellowstone National Park, Wyoming, USA. *Geochimica et Cosmochimica Acta*, 62(4):657–663, 1998.

Lewis, A. J., Palmer, M. R., Sturchio, N. C., and Kemp, A. J. The rare earth element geochemistry of acid-sulphate and acid-sulphate-chloride geothermal systems from Yellowstone National Park, Wyoming, USA. *Geochimica et Cosmochimica Acta*, 61(4):695–706, 1997.

Long, K. R., Van Gosen, B. S., Foley, N. K., and Cordier, D. The principal rare earth elements deposits of the United States: a summary of domestic deposits and a global perspective. Technical report, U.S. Geological Survey, 2012.

Michard, A. Rare earth element systematics in hydrothermal fluids. *Geochimica et Cosmochimica Acta*, 53(3):745–750, 1989.

Moss, R., Tzimas, E., Kara, H., Willis, P., and Kooroshy, J. Critical metals in strategic energy technologies. Technical report, European Commission Joint Research Centre Institute for Energy and Transport, 2011.

Nassar, N. T., Du, X., and Graedel, T. E. Criticality of the rare earth elements. *Journal of Industrial Ecology*, In press., 2015. doi: 10.1111/jiec.12237.

Noack, C. W., Dzombak, D. A., and Karamalidis, A. K. Rare earth element distributions and trends in natural waters with a focus on groundwater. *Environmental Science & Technology*, 48(8):4317–4326, 2014.

Sprecher, B., Xiao, Y., Walton, A., Speight, J., Harris, R., Kleijn, R., Visser, G., and Kramer, G. J. Life cycle inventory of the production of rare earths and the subsequent production of NdFeB rare earth permanent magnets. *Environmental Science & Technology*, 48(7): 3951–3958, 2014.

Tunsu, C., Petranikova, M., Gergorić, M., Ekberg, C., and Retegan, T. Reclaiming rare earth elements from end-of-life products: A review of the perspectives for urban mining using hydrometallurgical unit operations. *Hydrometallurgy*, In press., 2015.

U.S. Geological Survey. Mineral commodity summaries 2015. Report, U.S. Geological Survey, 2015.

Zaimes, G. G., Hubler, B. J., Wang, S., and Khanna, V. Environmental life cycle perspective on rare earth oxide production. *ACS Sustainable Chemistry & Engineering*, 3(2):237–244, 2015.

Chapter 2

Aqueous chemistry of the rare earth elements (REE)

2.1 What are the REE?

The REE constitute much of Group 3 of the periodic table, a group of 16 transition metals, including the lanthanide series (La to Lu, excluding Pm), Yttrium (Y) and Scandium (Sc). The "rare" moniker stems from their initial isolation from uncommon mineral phases in the 18th and 19th century (Castor and Hedrick 2006), though the natural abundance of REE in the earth's crust range from 0.52 parts per million (ppm) to 41.5 ppm, in the same range as Pb or Sn and exceeding the natural, crustal abundance of Ag and Hg (Lide 2012).

In the natural sciences, predictable thermodynamic differences between the REE make these elements uniquely capable tools for interpreting natural geologic and chemical processes (Laveuf and Cornu 2009; Murray et al. 1990). Rare earth lithogeochemistries have long been used to infer depositional environments of geologic strata (Hanson 1980; Murray et al. 1990; Nance and Taylor 1976). Similarly, REE serve as benign analogs to the transuranic actinide series for nuclear waste disposal studies (Krauskopf 1986; Millero 1992); as potential markers

of regional authenticity for high value exported food products such as wine, pumpkin-seed oil, and olive oil (Farmaki et al. 2012; Jakubowski et al. 1999; Joebstl et al. 2010); and for studying mixing and metal cycling in the oceans (De Baar et al. 1983; Elderfield et al. 1988).

Many of the same properties that yield the unique and predictable geochemistry of the REE have lead to their use in more consumer products than nearly any other element group (Castor and Hedrick 2006; Graedel et al. 2015). In most applications, the performance of the REE is unmatched (Ciacci et al. 2015; Nassar et al. 2015), making substitution (with more readily available/environmentally benign elements) undesirable.

Based on atomic number, the REE are segregated into light and heavy REE (LREE and HREE, respectively) with the division occurring between Eu and Gd (Castor and Hedrick 2006); some studies further distinguish middle REE (MREE), though the specific elements are inconsistently defined between authors (Choi et al. 2009; Hannigan and Sholkovitz 2001; Tang and Johannesson 2010). These "weight" distinctions allow for simplified description and quantification of the inter-element relationships, typically ratios of normalized concentrations, which are exploited in REE analysis. Similarly, anomalies of certain REE — due to redox lability for Ce and Eu (Brookins 1989) and large anthropogenic emissions for Gd (Bau and Dulski 1996) — are used to interpret geochemical processes. Y and Sc exhibit similar properties to the lanthanides and are thus included in the suite of REE with Y being most similar to HREE and Sc being most similar to LREE in solution (Brookins 1989).

2.2 REE speciation in natural waters

The speciation of dissolved metals governs their reactivity in aqueous systems with respect to solid precipitation/dissolution, oxidation/reduction, microbial processes, and surface pro-

cesses including ion exchange and surface complexation. Thus it is crucial to understand the speciation of the REE in the proposed matrices to maximize extraction and interpret experimental results. The REE exist almost exclusively in a 3+ oxidation state, though Ce is readily oxidized to a 4+ state under oxic conditions and Eu is reduced to a 2+ state under extreme reducing conditions or at high temperatures ($T \sim 200°C$) (Brookins 1983; Sverjensky 1984).

While not indicative in isolation of how the REE will speciate, trends in stability constants for various ligands can be compared to assess reactivity. Thermodynamic data for the REE, compiled from the literature, are shown in Figure 2.1 (values and citations found in Table A.1. From these data, the following order of reactivity is observed for the common, inorganic ligands: $PO_4^{3-} >> CO_3^{2-} > OH^- > F^-/SO_4^{2-} >> NO_3^-/Cl^-$. This order agrees with the general trend of hardness described by Pearson (1963). However, since PO_4^{3-} is significantly less abundant in natural waters than CO_3^{2-}, carbonate complexes are generally understood to be the predominant species of the dissolved REE (Johannesson and Lyons 1994; Johannesson et al. 1995).

Speciation of the REE in multicomponent systems is easily calculated by mass action and mass balance using the geochemical equilibrium model `PHREEQC` with the `llnl.dat` database. This particular database was chosen because it includes numerous reactions of the REE. The relevant reactions and equilibrium constants defined in this database and used in subsequent calculations are given in Table A.2.

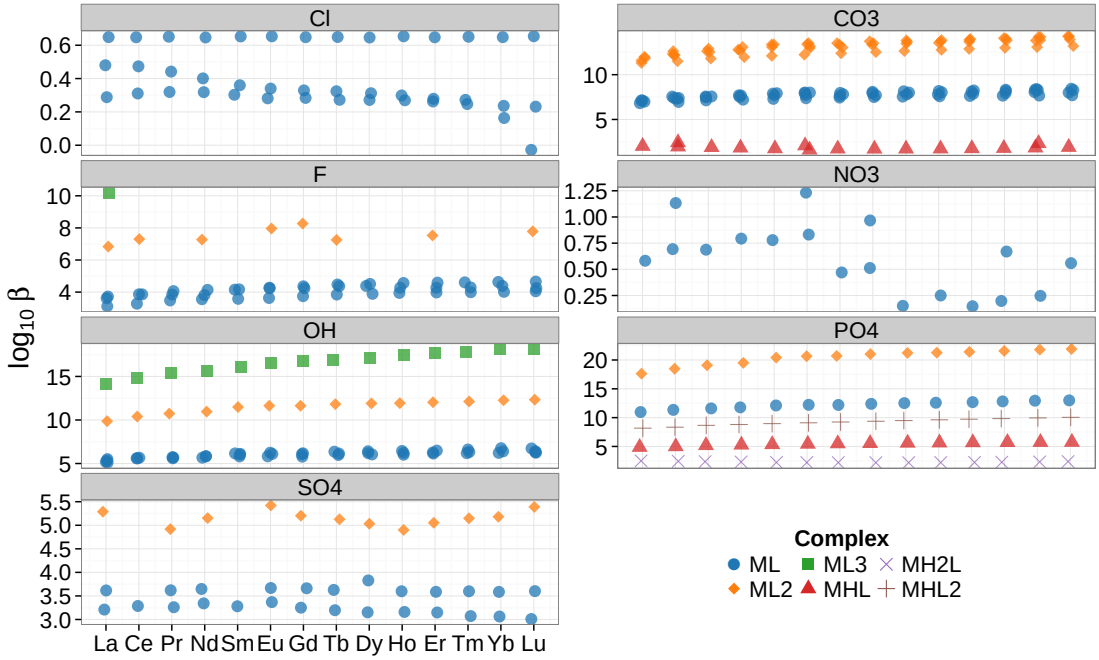

Figure 2.1: REE-ligand complex formation constants ($\log_{10}\beta$) compiled from published literature. Stability constant values are for the general reaction: $M^{3+} + aH^{+} + bL^{z-} \overset{\beta}{\rightleftharpoons} MH_aL_b^{(3+a-bz)}$. Data are not available for all complexes of all elements. Data are tabulated with references in Tables A.1.

2.2.1 Speciation in freshwater

A more practical scenario might be that of the model freshwater presented by Morel and Hering (1993):

$TOTNa = 10^{-3.55}$ M	$TOTCl = 10^{-3.7}$ M
$TOTCa = 10^{-3.43}$ M	$TOTSO_4 = 10^{-4}$ M
$TOTMg = 10^{-3.8}$ M	$TOTCO_3 = 10^{-3}$ M
$TOTK = 10^{-4.22}$ M	

Speciation of three select REE (Nd, Gd, and Ho) in this system at median concentrations of those elements in grounwater (Noack et al. 2014) is shown in Figure 2.2. Under these conditions the free Ln^{3+} species predominates to near pH 6, where the $LnCO_3^+$ species becomes the primary species. As the solution becomes more basic (pH > 8) the $Ln(CO_3)_2^-$ and subsequently (pH > 10) the $Ln(OH)_4^-$ complexes predominate. A small (< 25%) fraction of the REE are found as sulfate complexes at low pH, but these species are rapidly displaced by the carbonate species starting at pH 6. While the practical manifestation is small, increased stability of the HREE-carbonate complexes (Figure 2.1) is apparent as the conversion from $(Ln^{3+} + LnSO_4^+)$ to $LnCO_3^+$ occurs at lower pH values from Nd to Gd to Ho.

2.2.2 Speciation in geothermal waters

This system can be compared to an average geothermal produced water (average values from Breit and Otton 2002):

$TOTNa = 10^{-1.23}$ M	$TOTCl = 10^{-1.14}$ M
$TOTCa = 10^{-2.65}$ M	$TOTSO_4 = 10^{-2.45}$ M
$TOTMg = 10^{-2.53}$ M	$TOTCO_3 = 10^{-2.37}$ M
$TOTK = 10^{-2.71}$ M	

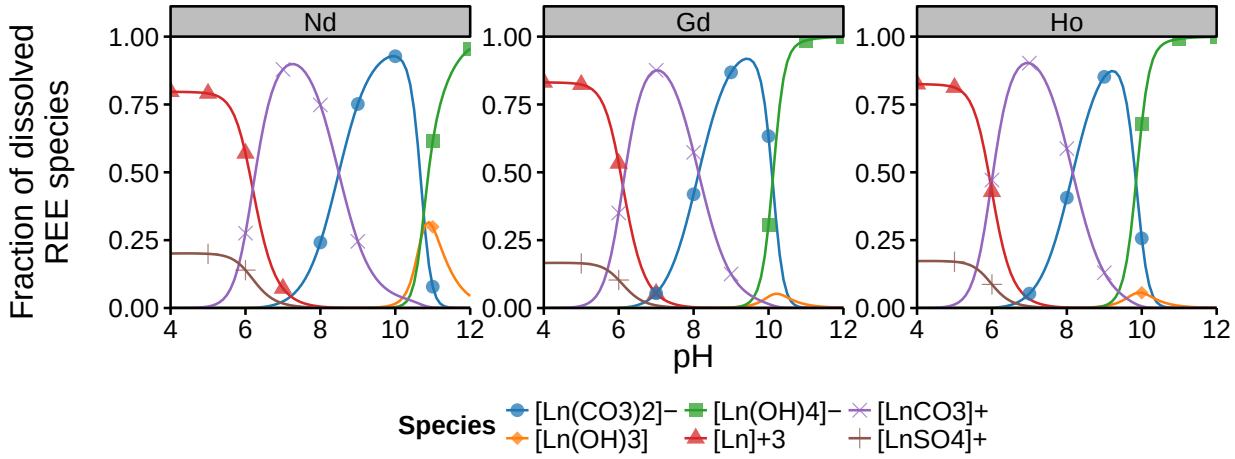

Figure 2.2: Speciation of select REE in a model fresh water (Example 1, pg. 345 from Morel and Hering (1993)) at 25°C. Speciation calculated using `PHREEQC` (Charlton and Parkhurst 2011; Parkhurst and Appelo 2013) in `R` (R Core Team 2014) with the `llnl.dat` thermodynamic database (Table A.2). Total REE concentrations are the medians for the elements in groundwater (Noack et al. 2014): 263 ppt, 76 ppt, and 12 ppt for Nd, Gd, and Ho respectively. Curves are labeled with plot marker symbols at integer pH values for comparison. Species that make up less than 5% at their maximum concentration are not plotted.

The speciation of median REE concentrations in this system is shown as a function of pH in Figure 2.3. The primary difference between the speciation in this model geothermal water, compared to the freshwater system, is the increased prevalence of the $LnSO_4^+$ complexes at low pH (even overtaking the free ion for Nd). However, even after the extraction of useable heat, geothermal waters remain quite hot ($T \sim 70 - 120$°C). This increase in temperature significantly alters the REE speciation for the same bulk solutes (Figure 2.4 shows $T = 90$°C). Here, the sulfate complexes persist to pH ~ 7, while the prevalence of the carbonate complexes is displaced by hydrolysis products.

2.2.3 Summary of REE speciation

In most waters, fresh or saline, the dominant species of the REE will be their sulfate- and carbonate complexes, depending on the pH, though free ions may constitute a significant

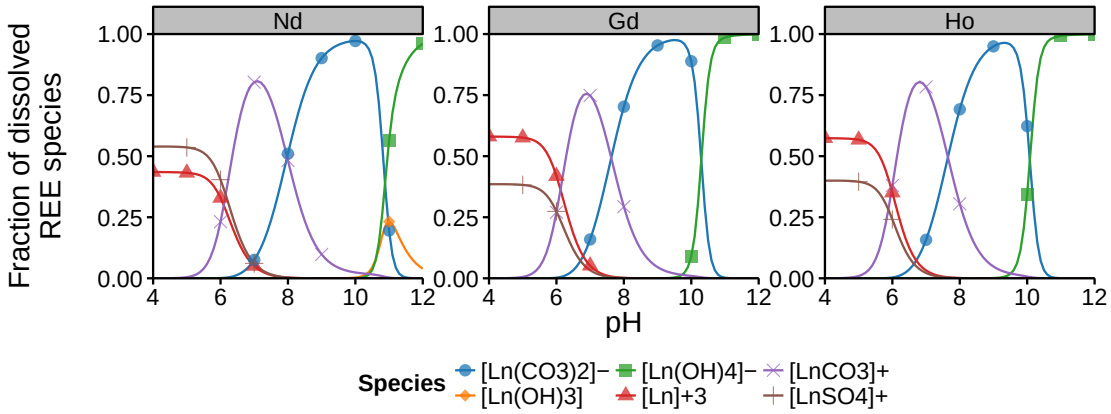

Figure 2.3: Speciation of select REE in a median geothermal water (estimated from Breit and Otton (2002)) at 25°C. Speciation calculated using `PHREEQC` (Charlton and Parkhurst 2011; Parkhurst and Appelo 2013) in `R` (R Core Team 2014) with the `llnl.dat` thermodynamic database (Table A.2). Total REE concentrations are the medians for the elements in groundwater (Noack et al. 2014): 263 ppt, 76 ppt, and 12 ppt for Nd, Gd, and Ho respectively. Curves are labeled with plot marker symbols at integer pH values for comparison. Species that make up less than 5% at their maximum concentration are not plotted.

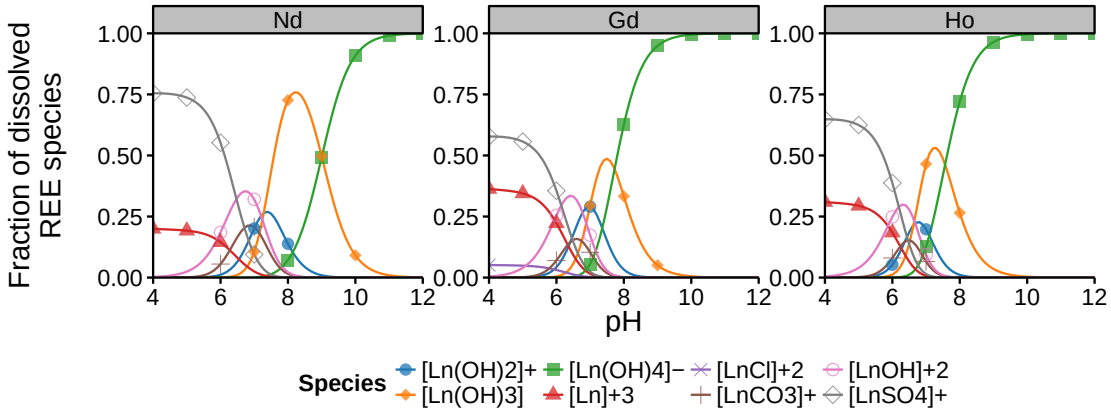

Figure 2.4: Speciation of select REE in a median geothermal water (estimated from Breit and Otton (2002)) at 90°C. Speciation calculated using `PHREEQC` (Charlton and Parkhurst 2011; Parkhurst and Appelo 2013) in `R` (R Core Team 2014) with the `llnl.dat` thermodynamic database (Table A.2). Total REE concentrations are the medians for the elements in groundwater (Noack et al. 2014): 263 ppt, 76 ppt, and 12 ppt for Nd, Gd, and Ho respectively. Curves are labeled with plot marker symbols at integer pH values for comparison. Species that make up less than 5% at their maximum concentration are not plotted.

portion of the speciation in more acidic pH regimes. The order of REE reactivity with inorganic ligands is governed by the Pearson (1963) concept of hard/soft acids and bases. On this basis, even in highly saline waters, chloride complexes are rarely a significant portion of the speciation. Hydrolysis species (i.e. OH^- as the ligand) are only relevant under very alkaline conditions or at elevated temperatures.

These trends represent predictions based on controlled thermodynamic studies under equilibrium assumptions. There is implicitly no consideration of time-dependent effects when applying these observations. Moreover, the species described here are not directly measurable using the analytical techniques in this thesis (inductively-coupled plasma mass spectrometry).

2.3 References

Bau, M. and Dulski, P. Anthropogenic origin of positive gadolinium anomalies in river waters. *Earth and Planetary Science Letters*, 143(1):245–255, 1996.

Breit, G. and Otton, J. Produced waters database, 2002. URL http://energy.cr.usgs.gov/prov/prodwat/contact.htm.

Brookins, D. G. Aqueous geochemistry of rare earth elements. *Reviews in Mineralogy and Geochemistry*, 21(1):201–225, 1989.

Brookins, D. G. Eh-pH diagrams for the rare earth elements at 25 °c and one bar pressure. *Geochem. J*, 17(5):223–229, 1983.

Castor, S. B. and Hedrick, J. B. *Rare Earth Elements*, pages 769–792. SME, 7 edition, 2006.

Charlton, S. R. and Parkhurst, D. L. Modules based on the geochemical model PHREEQC for use in scripting and programming languages. *Computers & Geosciences*, 37(10):1653–1663, 2011.

Choi, H.-S., Yun, S.-T., Koh, Y.-K., Mayer, B., Park, S.-S., and Hutcheon, I. Geochemical behavior of rare earth elements during the evolution of CO_2-rich groundwater: A study from the Kangwon district, South Korea. *Chemical Geology*, 262(3–4):318–327, 2009.

Ciacci, L., Reck, B. K., Nassar, N. T., and Graedel, T. E. Lost by design. *Environmental Science & Technology*, 49(16):9443–51, 2015.

De Baar, H. J. W., Bacon, M. P., and Brewer, P. G. Rare-earth distributions with a positive Ce anomaly in the western North-Atlantic ocean. *Nature*, 301(5898):324–327, 1983.

Elderfield, H., Whitfield, M., Burton, J. D., Bacon, M. P., and Liss, P. S. The oceanic chemistry of the rare-earth elements [and discussion]. *Philosophical Transactions of the Royal Society of London. Series A, Mathematical and Physical Sciences*, 325(1583):105–126, 1988.

Farmaki, E. G., Thomaidis, N. S., Minioti, K. S., Ioannou, E., Georgiou, C. A., and Efstathiou, C. E. Geographical characterization of Greek olive oils using rare earth elements content and supervised chemometric techniques. *Analytical Letters*, 45(8):920–932, 2012.

Graedel, T. E., Harper, E. M., Nassar, N. T., Nuss, P., and Reck, B. K. Criticality of metals and metalloids. *Proceedings of the National Academy of Sciences*, 112(14):4257–4262, 2015.

Hannigan, R. E. and Sholkovitz, E. R. The development of middle rare earth element enrichments in freshwaters: weathering of phosphate minerals. *Chemical Geology*, 175 (3–4):495–508, 2001.

Hanson, G. N. Rare-earth elements in petrogenetic studies of igneous systems. *Annual Review of Earth and Planetary Sciences*, 8:371–406, 1980.

Jakubowski, N., Brandt, R., Stuewer, D., Eschnauer, H. R., and Görtges, S. Analysis of wines by ICP-MS: Is the pattern of the rare earth elements a reliable fingerprint for the provenance? *Fresenius' Journal of Analytical Chemistry*, 364(5):424–428, 1999.

Joebstl, D., Bandoniene, D., Meisel, T., and Chatzistathis, S. Identification of the geographical origin of pumpkin seed oil by the use of rare earth elements and discriminant analysis. *Food Chemistry*, 123(4):1303–1309, 2010. ISSN 0308-8146.

Johannesson, K. H. and Lyons, W. B. The rare-earth element geochemistry of mono lake water and the importance of carbonate complexing. *Limnology and Oceanography*, 39(5): 1141–1154, 1994.

Johannesson, K. H., Lyons, W. B., Stetzenbach, K. J., and Byrne, R. H. The solubility control of rare earth elements in natural terrestrial waters and the significance of PO_4^{3-} and CO_3^{2-} in limiting dissolved rare earth concentrations: A review of recent information. *Aquatic Geochemistry*, 1(2):157–173, 1995.

Krauskopf, K. B. Thorium and rare-earth metals as analogs for actinide elements. *Chemical Geology*, 55(3–4):323–335, 1986.

Laveuf, C. and Cornu, S. A review on the potentiality of rare earth elements to trace pedogenetic processes. *Geoderma*, 154(1):1–12, 2009. ISSN 0016-7061.

Lide, D. R. *CRC handbook of chemistry and physics*. CRC press, 2012. ISBN 1439880492.

Millero, F. J. Stability constants for the formation of rare earth-inorganic complexes as a function of ionic strength. *Geochimica et Cosmochimica Acta*, 56(8):3123–3132, 1992.

Morel, F. M. and Hering, J. G. *Principles and Applications of Aquatic Chemistry*. John Wiley & Sons, Inc., 1993.

Murray, R. W., Buchholtz ten Brink, M. R., Jones, D. L., Gerlach, D. C., and Russ, G. Rare earth elements as indicators of different marine depositional environments in chert and shale. *Geology*, 18(3):268–271, 1990.

Nance, W. B. and Taylor, S. R. Rare earth element patterns and crustal evolution—I. Australian post-Archean sedimentary rocks. *Geochimica et Cosmochimica Acta*, 40(12): 1539–1551, 1976.

Nassar, N. T., Du, X., and Graedel, T. E. Criticality of the rare earth elements. *Journal of Industrial Ecology*, In press., 2015. doi: 10.1111/jiec.12237.

Noack, C. W., Dzombak, D. A., and Karamalidis, A. K. Rare earth element distributions and trends in natural waters with a focus on groundwater. *Environmental Science & Technology*, 48(8):4317–4326, 2014.

Parkhurst, D. L. and Appelo, C. Description of input and examples for PHREEQC version 3: a computer program for speciation, batch-reaction, one-dimensional transport, and inverse geochemical calculations. Technical report, US Geological Survey, 2013.

Pearson, R. G. Hard and soft acids and bases. *Journal of the American Chemical Society*, 85(22):3533–3539, 1963.

R Core Team. *R: A Language and Environment for Statistical Computing*. R Foundation for Statistical Computing, Vienna, Austria, 2014. URL http://www.R-project.org/.

Sverjensky, D. A. Europium redox equilibria in aqueous solution. *Earth and Planetary Science Letters*, 67(1):70–78, 1984.

Tang, J. and Johannesson, K. H. Rare earth elements adsorption onto Carrizo sand: Influence of strong solution complexation. *Chemical Geology*, 279(3–4):120–133, 2010.

Chapter 3

Review of current and proposed REE extraction techniques

3.1 Thermodynamic and economic considerations in mineral resource development

The value of resources, mineral or otherwise, is commonly depicted as a pyramid. The highest value resources are a combination of high ore grade and ease of recovery, but are quite rare. Meanwhile, lower grade-, or more difficult to develop, resources are significantly more abundant. The fraction of a resource's total mass, globally, encapsulated in low-quality reserves dwarfs the fraction found in high-quality reserves. However, without sufficient technical development, these low-quality reserves are essentially unexploitable.

A hypothetical resource pyramid for the REE is depicted in Figure 3.1. Clearly, the established REE mines, such as those at Bayan Obo in China and Mountain Pass in California, sit atop the resource pyramid. The ore grades at each of these operations is exceptional (by REE standards) and the use of well-understood hydrometallurgical unit operations means that the extraction and recovery of REE from these ores is simple, if also economically and

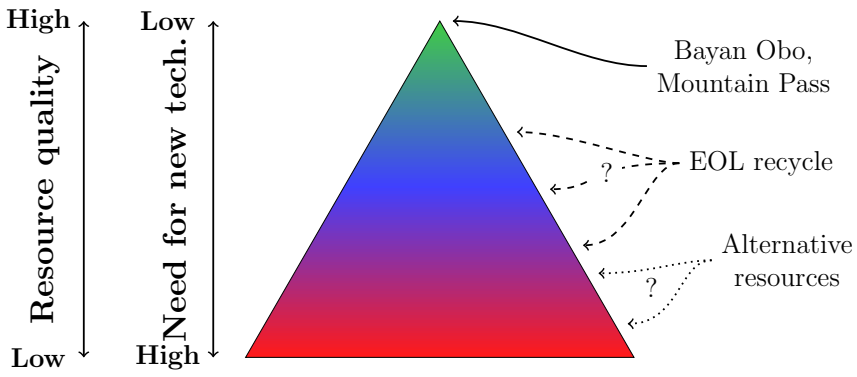

Figure 3.1: Conceptualization of the REE resource pyramid. Established mines such as Bayan Obo and Mountain Pass produce the balance of world demand. Thus there is significant uncertainty regarding the "status" or quality of recyclable products and alternative resources, such as geothermal fluids, because there has never been a pressing need to develop these alternatives.

environmentally burdensome. Likely below these primary resources are end of life (EOL) consumer or industrial products which may have a significant recyclable REE content. Finally, dilute alternative streams (such as geothermal fluids or seawater) form the base of the pyramid, having vast volumes with an enormous cumulative mass, but occurring in trace concentrations.

For any resource, at any level of the pyramid, profitability is defined the same way: sales revenues must exceed the cost to produce. Formally, this can be expressed for a product with market value k_v occurring in ore mass m_p at concentration c_v, which is refined for the unit-mixture price of k_c:

$$\begin{aligned} k_v m_p c_v &> k_c m_p \\ k_c \frac{1}{c_v} &< k_v \end{aligned} \tag{3.1}$$

This relationship between the break-even cost to produce a material and its dilution in a source is referred to as the Sherwood relationship (Dahmus and Gutowski 2007). An equivalent statement of the Sherwood relationship is that the cost of a separation and concentration

process is driven solely by the volume or mass of the unwanted, or gangue, material. Lightfoot and Cockrem (1987) in fact *define* a dilute resource stream as one where the processing costs are dominated by the handling of the undesirable material (here the large volumes of water and dissolved salts).

There are numerous examples of failed, on-going, or successful attempts to exploit a mineral resource at a significantly lower level of the resource pyramid than more conventional resources. Perhaps the most famous example of a failed attempt is the proposal by German chemist Fritz Haber to extract gold from seawater to help pay German war debts following World War I (Falkner and Edmond 1990). Haber proposed an electrochemical method that showed promising results (Haber 1927). However, it is widely held that he overestimated the concentration of gold in seawater 1000–fold before pushing ahead with the research and development, ultimately leading to its economic infeasibility (Falkner and Edmond 1990; Witschi 1997).

Hermann (2006) estimates that there may be 350–times the exergy available from oceanic uranium (U) than in terrestrial deposits, making U an attractive target for extraction from seawater. Attempts to extract uranium from seawater have been the subject of significant research. Primary challenges of these projects have been the low capacity of the adsorbents developed, as well as the challenges of deploying the process at scale (Muzzarelli 2011). More novel designs have included high surface area, braided polymers that can be anchored to the seafloor for passive collection of uranium, which would be recovered by passing ships when saturated (Rao 2011). In addition, significant work continues to focus on optimized adsorbents, including protein-based ligands and novel, U-selective copolymer materials (Lu 2014). Manufacturing and operation costs will dictate whether such technologies will ever be deployed, as most economic estimates show sea-water extraction to be roughly 10–fold more expensive with 10% of the energy returned on energy invested compared to traditional

mining (Kim et al. 2013; Rao 2011).

Extraction of natural gas from tight (low-permeability) shales is an example of a highly successful development of a "low-quality" or technologically challenging resource. The large quantities of natural gas present in shale plays, such as the Marcellus Shale in the Appalachian Basin, had been known for many years prior to their development (Harper 2008; Soeder 2010). Only with the advent of economical technologies for extraction — namely horizontal drilling coupled with staged, hydraulic fracturing — was extraction of this resource possible (Kargbo et al. 2010).

The use of this Sherwood analysis and simplified cost models allow for baseline feasibility determinations regarding separative processes and dilute resources. As will be discussed, a solid-phase extraction technology is likely the most viable for capturing the REE from aqueous sources. Using a general cost model for ion exchange (IX) technologies (k_c = \$0.12 – \$0.32 per 1000 liters in 2014 dollars; Federal Remediation Technologies Roundtable 2003) and average metal pricing (k_v = \$570 including Sc and \$132 excluding Sc; prices as of 2014-12-31, in 2014 dollars; London Metal Exchange 2015), a *minimally* viable resource stream would have total REE concentrations on the order of 100 – 1000 ppb based on Equation 3.1. These target concentrations may be biased high by the IX cost model, in that a primary cost associated with IX for groundwater treatment is pumping, which could be minimized by integration into the normal operations of an industry utilizing a high volumetric flow rate stream, such as at a seawater desalination facility (Diallo et al. 2015) or at a geothermal power plant. Alternatively, the IX cost model does not consider additional steps after REE elution (resin regeneration) that would be required to achieve a salable product (here the rare earth solids), which may increase cost.

The cost requirements (monetary or otherwise) of a mineral extraction operation can be expressed in a number of ways. Almost all expressions are a function of the target resources

concentration in the starting material (e.g. ore, aqueous sources, EOL materials). The simplest form may be the Separative Work Unit (SWU), which is agnostic to the energy and monetary requirements of the enrichment process (taking units of mass or mass per time). The SWU is used to describe the overall amount of enrichment/purification achieved by a process (De La Garza et al. 1961). For a feed stock flow F with resource assay (mass fraction) x_F, which is split to a product flow P with assay x_P and a tailings flow T with assay x_T, the separative work (W_{SWU}) is defined by Equation 3.2:

$$W_{SWU} = P \cdot V(x_P) + T \cdot V(x_T) - F \cdot V(x_F) \tag{3.2}$$

$$\text{Where, } V(x) = (1 - 2x) \ln\left(\frac{1-x}{x}\right)$$

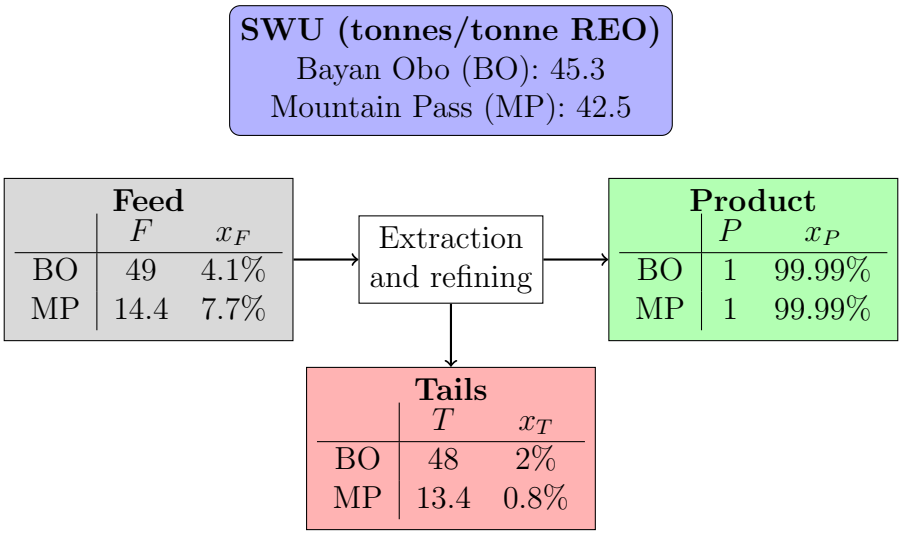

Figure 3.2: Separative work unit (Eq. 3.2) comparison of Bayan Obo and Mountain Pass REE mines. Data reproduced from Peiró and Méndez (2013), except for the product assay (x_p) which was assumed.

While highly simplified, the SWU allows for comparison of enrichment or purification configurations. For example, using data from Peiró and Méndez (2013, Table II.), we can

compare the SWU of the Bayan Obo and Mountain Pass mining operations (Figure 3.2). The Bayan Obo process produces 1 tonne of 99.99% purity REO with 45.3 tonnes SWU, while Mountain Pass produces the same 1 tonne, 99.99% pure REO with 42.5 tonnes SWU, a 6% difference.

When this small technical margin is compared to the inherently higher value of the Chinese ores, i.e. critical REE-enriched (Chakhmouradian and Wall 2012; Gupta and Krishnamurthy 1992; Peiró and Méndez 2013); Chinese federalized control over a vertically integrated industry resulting in heavy subsidies and less stringent environmental regulations (Smith Stegen 2015); and cheaper supply of the energy to achieve the noted SWU, it is apparent why a Chinese quasi-monopoly exists on the REE supply chain.

By comparison, a process taking a fluid with $x_F = 100$ ppb total REE and enriching this by a factor of 10^3 ($x_P = 100$ ppm) with 90% recovery would require ~ 2650 tonne SWU/tonne REE-enriched phase; production of the $x_P = 99.99\%$ product used for comparison of Bayan Obo and Mountain Pass would require 2.68×10^7 tonne SWU/tonne REE. This massive SWU demand would thus require nearly free "work" to be competitive with conventional approaches. Fortunately, sorptive processes are spontaneous, and thus meet this criteria, as will be discussed in depth subsequently. Moreover, Lightfoot and Cockrem (1987) note that adsorptive techniques represent the best approach for concentration from dilute solutions, given the ability to achieve rapid, large volume reductions.

A complementary approach for assessing separative technologies is the use of statistical entropy. Derived from the Boltzmann distribution and originally popularized for language analysis by Shannon (1951), statistical entropy is utilized widely within the industrial ecology community to inform choices and compare technologies in material flow analyses (Rechberger and Brunner 2002). In this context, the industrial ecologist defines a sustainable recycling process as one which decreases statistical entropy, concentrating the desired material into

a secondary raw material; conversely, a sustainable remediation technology will maximize statistical entropy, diluting risk associated with the target material (Rechberger and Brunner 2002). These approaches have been used in a variety of assessments, including (but not limited to) the lifecycles of copper (Rechberger and Graedel 2002), polymeric-carbon (Bai et al. 2015), and lead (Kaufman et al. 2008). However, to date, no such studies have approached the separation of materials from natural, dilute resources.

Alternatively, the theoretical minimum work required to achieve a separation can be determined from the second law of thermodynamics. This first principles approach sets the lower bound, below which a separation cannot be achieved with less energy. For a separation occurring at constant temperature and pressure, the theoretical minimum work $W_{\min}$ is equivalent to the change in the Gibbs free energy of the system (House et al. 2011).

For the three-stream system illustrated in Figure 3.2, the minimum work is found by Equation 3.3. The primary differences between this thermodynamic model and the SWU model are (1) precise and meaningful units (N_i is the molar flow rate of stream i and $X_{i,j}$ is the mole fraction of component j in stream i) and (2) a more rigorous treatment of the gangue (or non-target) materials in each stream. Equation 3.3 could be further modified to account for non-idealities by including the relevant activity coefficients for each component in the logarithms (i.e. $\log \gamma_{i,j} X_{i,j}$).

$$W_{\min} = -RT\left(N_F \sum_{k=1}^{n} X_{F,k} \ln X_{F,k} - N_P \sum_{k=1}^{n} X_{P,k} \ln X_{P,k} - N_T \sum_{k=1}^{n} X_{T,k} \ln X_{T,k}\right) \tag{3.3}$$

Considering a highly simplified system of the REE and water, the thermodynamic limits of

adsorptive-concentration technologies can be estimated. If the free energy change associated with the formation of the relevant sorbed species is greater than this minimum work, then the process should be (thermodynamically) feasible. The theoretical minimum work required for various feed concentrations and for a range of desired concentration factors is presented in Figure 3.3 for a process with 90% REE recovery.

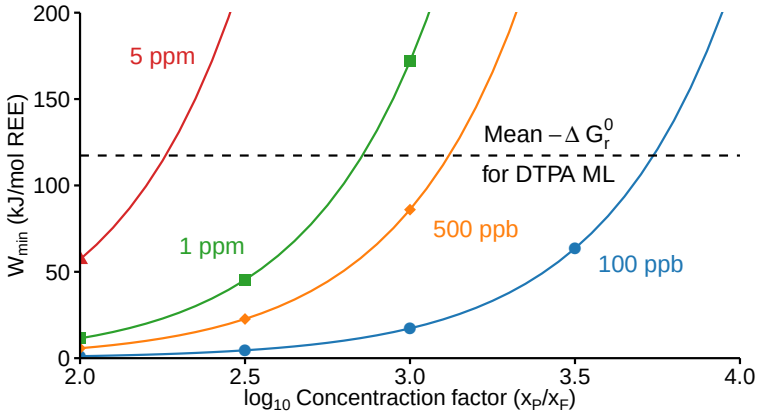

Figure 3.3: Theoretical minimum work (Equation 3.3) required to concentrate the noted feed concentration by the concentration factor (x-axis; ratio of product REE mass-fraction, x_p, to feed REE mass-fraction, x_f) for a process capturing 90% of feed REE mass. Calculations performed assuming concentration of REE from REE–H_2O binary mixtures with the average atomic mass of the REE used for mass-to-molar conversions. The dashed line denotes the work available (negative free energy change of reaction) from the formation of ML complexes between the REE^{3+} and $DTPA^{5-}$ at 298 K (data from Figure 2.1).

From this analysis it can be seen that, for low feed concentrations, large concentration factors can be achieved well within the feasible limits of a DTPA adsorbent, assuming that the free energy change for the aqueous ML complex is equivalent to the corresponding surface complex. However, as desired product concentration increases (i.e the concentration factor increases) the required work rapidly approaches unrealistic work requirements, particularly for higher feed concentrations. Moreover, these constraints limit the maximum product concentration achievable for a process ΔG_r^0. This maximum is a smooth function of the feed concentration. For the ML-DTPA data used in Figure 3.3 ($\Delta G_r^0 = 117$ kJ/mol), this relationship is show in Figure 3.4. This analysis also considers the effects of irreversibility,

denoted as the second-law efficiency η (House et al. 2011).

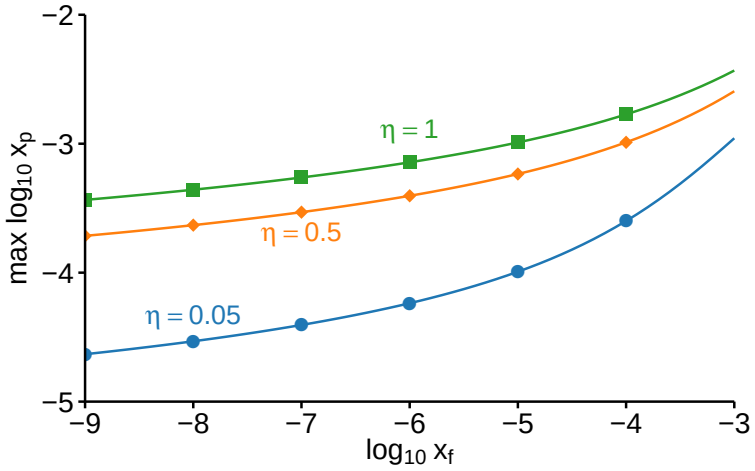

Figure 3.4: Theoretical-maximum REE mass fraction in product stream (x_p) for adsorption-based concentration process ($W_{\text{min}} = 117$ kJ/mol; assumed 90% capture of feed REE mass) as a function of feed mass fraction (x_f) for three different second-law efficiencies ($W_{eff} = \eta \cdot W_{\text{min}}$). Untransformed units for x_p and x_f are mass fractions (e.g. $10^{-9} = 1$ ppb, $10^{-2} = 1\%$). Calculations performed assuming concentration of REE from REE–H_2O binary mixtures with the average atomic mass of the REE used for mass-to-molar conversions. Maximum value found through minimization of the loss function, $L(x_p, x_f) = \big(G(x_p, x_f) - W_{eff}\big)^2$, using the `optimize` function in `R` (R Core Team 2014).

For very dilute feed-stocks, $x_f < 10^{-6}$, a near linear trend is observed between the maximum product mass fraction and the feed mass fraction. This behavior matches a Sherwood-type process, where the cost or overall efficiency is governed by the amount of non-target material being handled. Figure 3.4 also highlights the need to strive for maximal thermodynamic efficiency, as the maximum product quality is strongly a function of this variable. Fortunately, adsorptive processes are highly thermodynamically efficient and the external energy inputs into the system are limited to the pumping of fluids. The thermodynamic efficiency of the adsorption process can be effectively lowered when REE complexes are considered as the sorbing species (e.g. LnCO_3^+ or $\text{Ln}(\text{CO}_3)_2^-$). Since these species dominate REE speciation at mid-ranged pH (Figure 2.2 or 2.3), the exchange of ligands results in a decrease in the available work of $\sim 33 - 67\%$, depending on the solution chemistry (i.e. $\eta \approx 33 - 67\%$).

For the minimally viable feed mass fractions (100 ppb – 1 ppm from Equation 3.1), a final product mass fraction of 550 – 700 ppm is achieved ($\eta = 1$). At these concentrations, recovery by precipitation may be feasible. However, these concentration factors are unlikely to be realized in a single stage in practice, as noted by Lightfoot and Cockrem (1987), even for highly selective, high-capacity adsorbents. Thus, as with conventional approaches of REE production (discussed subsequently), the production of a high-purity REE product from a dilute aqueous source will likely require many stages of separation/purification. Overall though, these simplified calculations seem to indicate a first-order feasibility from first principles.

3.2 Conventional REE mining operations

Conventional mining and refining of the REE effectively constitutes 100% of primary REE production globally. Those mining activities focus exclusively on three minerals — bastnäsite ($LnCO_3F$), monazite ($LnPO_4$), and to a lesser extent xenotime ($LnPO_4$) — and ion-adsorbed clays (Gupta and Krishnamurthy 1992; Peiró and Méndez 2013). While bastnäsite ores are dominated by the LREE (primarily La and Ce), monazite, xenotime, and ion-adsorbed clays contain significantly higher HREE+Y fractions (Chakhmouradian and Wall 2012; Gupta and Krishnamurthy 1992; Peiró and Méndez 2013). A "standard" treatment train, from crude ore to finished rare earth oxide (REO) product, is depicted in Figure 3.5. Each of these stages will be addressed in detail.

Rare earth-bearing minerals are primarily mined in open pits (also referred to as open cast mining), and comingled with a variety of other products. At the largest REE mine in the world, the Bayan Obo mine in China, the REE were once a waste product, discarded during iron mining (Sprecher et al. 2014). Following mining, the choices for physical beneficia-

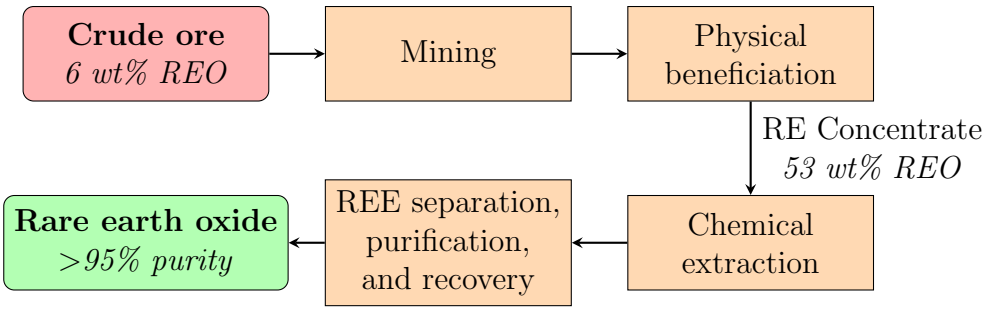

Figure 3.5: A conventional REE extraction and refining flowsheet. Figure and REO wt% values adapted from Zaimes et al. (2015)

tion (that is the enrichment of the REE-bearing phases through exploitation of differences in density, magnetisability, conductivity, or other physical attributes of the mineral) are largely driven by the REE-minerals present (Gupta and Krishnamurthy 1992; Jordens et al. 2013).

Figure 3.6 compares, at a high level, the physical beneficiation steps involved at the Mountain Pass, CA and Bayan Obo facilities. The flow sheets are very similar, except that the high iron-content ores of Bayan Obo require magnetic separation steps to remove magentite, fluorite, and hematite (Gupta and Krishnamurthy 1992). The chemical conditioner, or collector, chosen is a function of the mineral hosts of the REE. In Figure 3.6, the "rougher, cleaner, scavengers" step refers to a series of froth floatations with recycle (rougher → scavenger → cleaner). Sprecher et al. (2014) note that physical beneficiation represents the least efficient operation (in terms of REE recovery) in this process flow, estimating that 50% of the REE containing minerals are lost to tailings at Bayan Obo, though Peiró and Méndez (2013) argue that this recovery rate is mine-specific and increasing. Jordens et al. (2013) provide a thorough review of all current REE-mineral beneficiation techniques. Once a sufficient concentrate material has been produced, chemical treatments are used to solubilize the REE and subsequently purify the individual elements.

As with physical beneficiation, the techniques for chemical extraction of the REE from ore

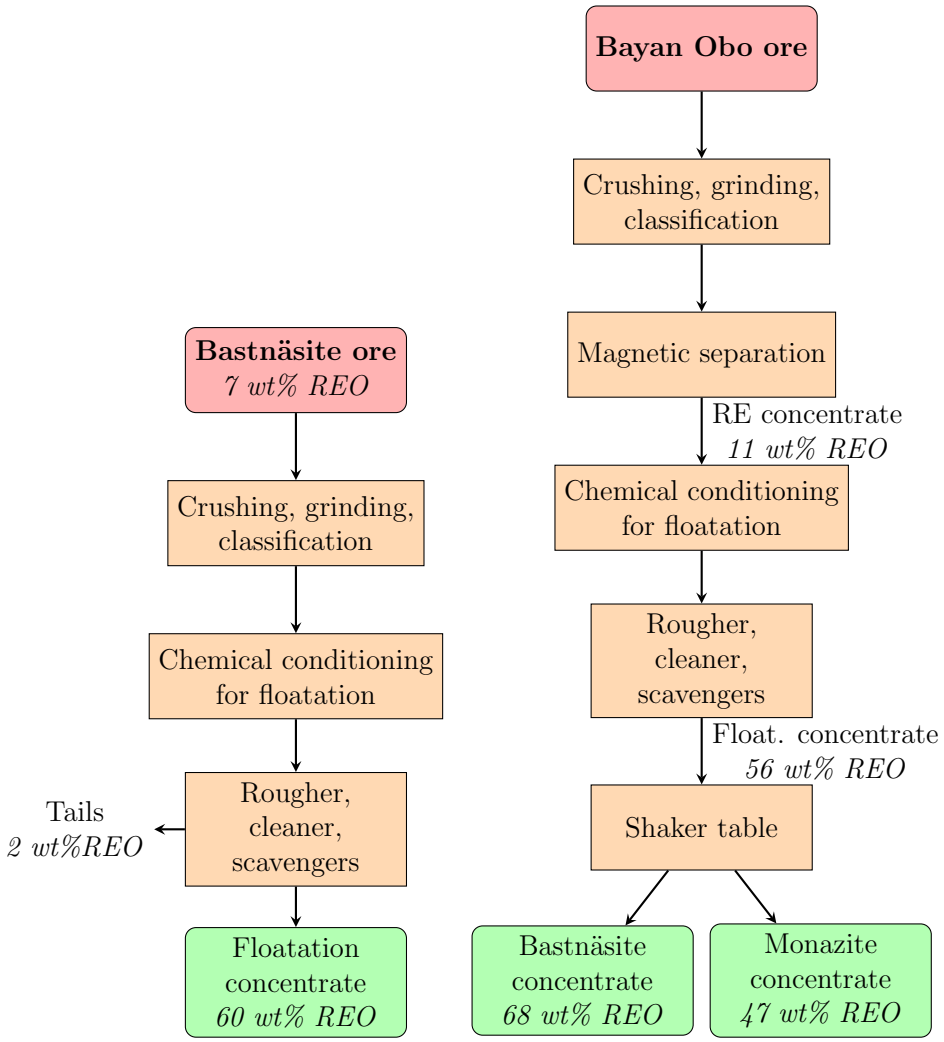

Figure 3.6: Comparison of physical beneficiation steps for processing of Mountain Pass (basnäsite) and Bayan Obo ores. Figure and REO wt% values adapted from Gupta and Krishnamurthy (1992).

concentrates are varied and chosen to balance cost along with the target REE product (e.g. chlorides vs. oxides). For monazite, exposure to either H_2SO_4 or NaOH at high temperatures (200°C or 140°C respectively) yields an REE-rich leachate (acid) or hydroxide cake (alkali) which are further processed (Gupta and Krishnamurthy 1992). The chemical extraction may result from sequential stages of alternating acid-base decompositions, as is the case at Mountain Pass where the bastnäsite concentrate is first digested with HCl, then NaOH, and finally neutralized with HCl again (Peiró and Méndez 2013).

Purification processes are chosen based on the desired end product (Figure 3.7). Many of the final, REE recovery steps described by Gupta and Krishnamurthy (1992) produce mixed-REE materials (i.e. do not include intra-REE separations). While the direct utilization of REE mixtures (mischmetal) is diminished, these materials can be further processed to yield higher purity products (e.g. by a separate entity). However, driven by the Chinese dominance of the supply chain, most REE production is vertically integrated (i.e. mining through finished REE product), necessitating solvent extraction processes to achieve a high-purity product (Peiró and Méndez 2013; Sprecher et al. 2014; Zaimes et al. 2015).

The most widely applied organic solution for solvent extraction is di-(2-ethylhexyl)phosphoric acid (DEPHA; alternatively HDEHP) in kerosene (Gupta and Krishnamurthy 1992; Xie et al. 2014). The structure of HDEHP and a proposed complex structure with the REE is shown in Figure 3.8. However, this extractant offers little intra-REE selectivity (separation factors for adjacent elements, $S^{M}_{M'} = D^{M}/D^{M'}$, typically between 1 – 2.5; Kimura 1960; Nash 1993). If an extractant has a separation factor of 1 for M and M', it cannot be used to separate these elements. Thus, these small separation factors require a large number of solvent extraction stages in series to achieve a satisfactory single element purity. The purity of element M after n stages of separation, using a process with separation factor $S^{M}_{M'}$, from a mixture with in initial concentrations $[M]_0$ and $[M']_0$ is defined by Equation 3.4. Figure 3.9 demonstrates

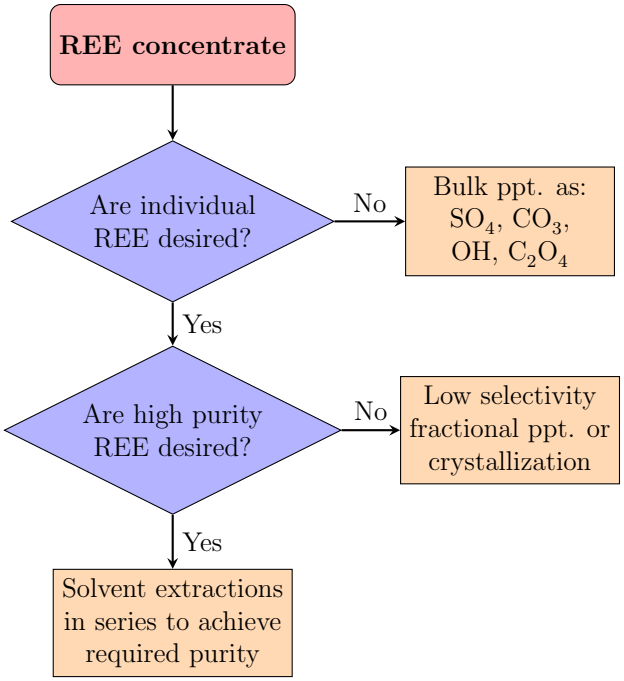

Figure 3.7: Influence of material needs on the choice of REE separation and purification technologies. Decision tree based on Figures 11–16 of Gupta and Krishnamurthy (1992).

the purity of M as a function of sequential extraction stages for a range of separation factors. More efficient designs, such as counter-current extractors (Xie et al. 2014; Yan et al. 2006), are typically applied, however a large number of stages is unavoidable for low-selectivity extractants.

Ignoring differential complexation in the aqueous phase:

$$R_n = \frac{[M]_n}{[M']_n} = \left(\frac{[M]_0}{[M']_0}\right) \cdot \left(S^M_{M'}\right)^n \tag{3.4a}$$

$$\text{Purity of M after } n \text{ stages} = P^M_n = \frac{R_n}{R_n + 1} \tag{3.4b}$$

The combined effect of these numerous and varied industrial production activities yields a substantial lifecycle environmental impact. On a per-kg basis, REO production consumes $> 10\times$ more energy and results in $> 10\times$ more green house gas emissions than does steel

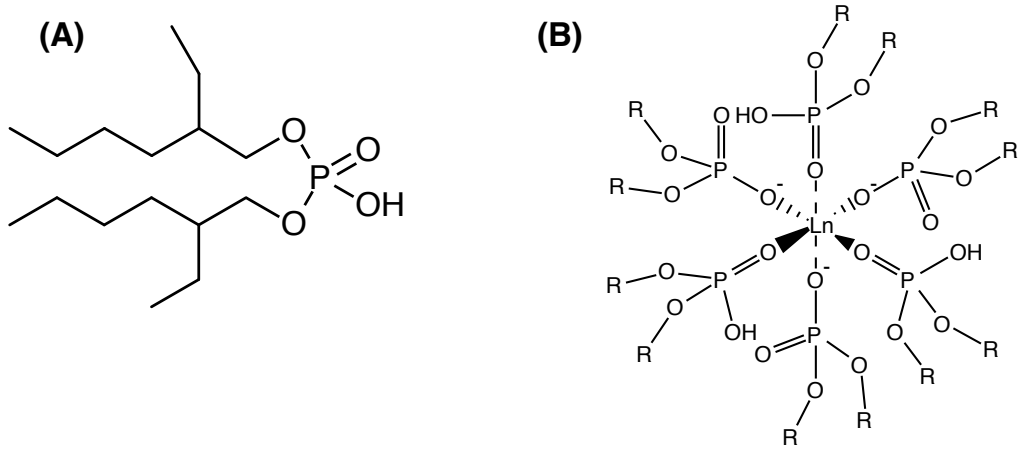

Figure 3.8: Chemical structure of HDEHP (A) and proposed structure of REE complex with the protonated HDEHP dimer (B). Complex structure adapted from Marie et al. (2012), who describe the complex with a HDEHP-dimer (formed by hydrogen bonding between adjacent P=O and P−OH groups) as the ligand.

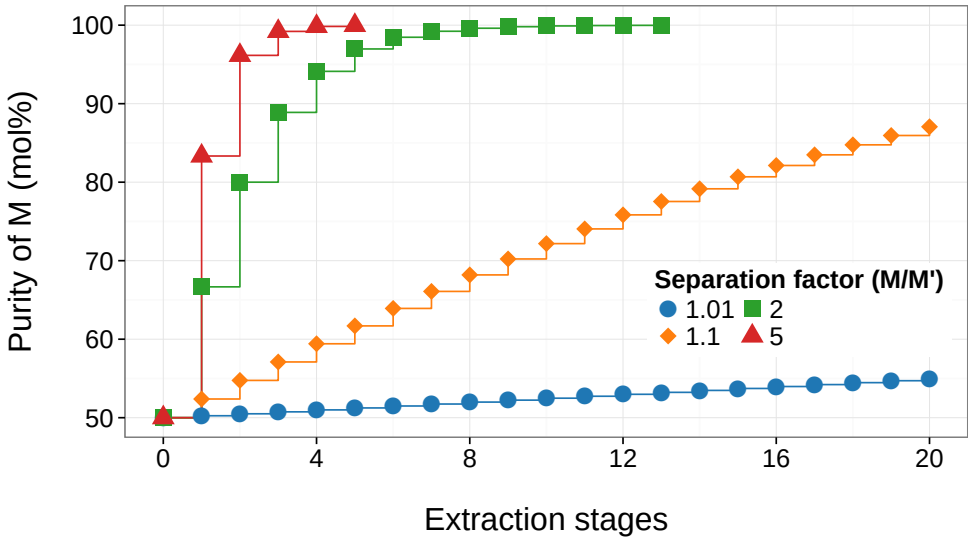

Figure 3.9: Purity of metal M as a function of sequential extraction stages from a 50:50 M:M' binary mixture for four different separation factors, $S^{M}_{M'} = D^{M}/D^{M'}$. Values for $S^{M}_{M'}$ of 2 and 5 truncated for purity $> 99.99\%$.

production (Zaimes et al. 2015). While this comparison will undoubtedly be different on a functional basis (i.e. per kg finished product, where REE make up $< 100\%$), Zaimes et al. (2015) have not considered further, downstream refining processes beyond REO production in determining this lifecycle impact. Such considerations would only increase the environmental burden of the REE.

3.3 REE recycling efforts

As discussed in Chapter 1, the usage of the REE falls into either high-volume or high-value applications. Chemical catalysts for catalytic cracking of petroleum or in vehicular catalytic conveters represent high-volume, but low-value, uses of the REE. Moreover, these applications are among the highest in-use REE dissipation of all REE applications (Ciacci et al. 2015). Alternatively, permanent magnets and metal-hydride batteries represent high-value REE applications where a significant portion of the REE content may be recoverable or recyclable. A brief review of studies of REE recycling from these products is presented here to illustrate the similarities among approaches: namely, the need for selective, high-capacity separation technologies. Binnemans et al. (2013) and Tunsu et al. (2015) provide critical reviews of REE recycling opportunities and technologies, and should be referenced for greater detail.

As with traditional mineral processing, a variety of unit operations are required for any recycling scheme (in a traditional, hydrometallurgical sense). Thus, Figure 3.5 closely approximates a recycling flowsheet. Using batteries as an example, the REE are only used in the anode, thus physical beneficiation may include the mechanical separation of the anode from the remainder of the battery components. Following the separation from the bulk, the anode must be milled or ground and dissolved in a solvent (chemical extraction). Next,

the REE must be separated from the resulting leachate and its various other components through some form of selective extraction.Tunsu et al. (2015) reasonably offer solvent extraction, ion exchange (or solid phase extraction), and precipitation as the viable options for this extraction. Finally, and depending on the choice of separation processes, the REE must be recovered as a salable product (e.g. oxide, carbonate, or mineral salt). Thus, the only true difference between the flowsheet of Figure 3.5 and a recycling flowsheet is the mining stage, which can be approximated as the collection of the waste material. The recycling flowsheet is summarized in Figure 3.10.

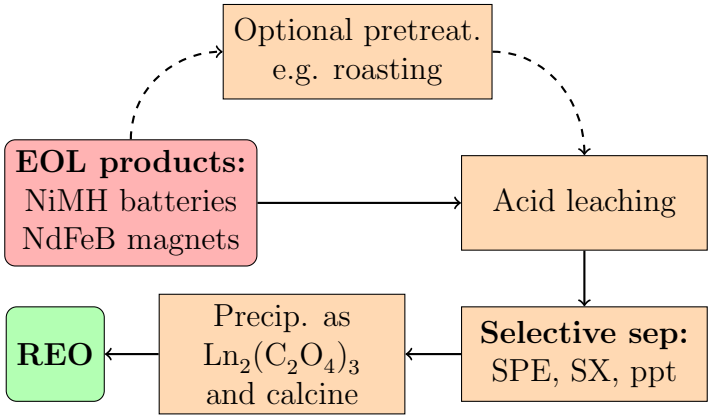

Figure 3.10: End-of-life (EOL) recycling flowsheet for the extraction and recovery of the REE.

3.3.1 Recycling permanent magnets

Around the year 2000, rare earth-based permanent magnets surpassed ferrite magnets in global magnet sales revenue (Dent 2012). As a result, Du and Graedel (2011) estimated global in-use stocks of Nd, Pr, Dy, and Tb from NdFeB batteries at 62, 15.7, 15.7, and 3.1 kilotonnes respectively, or roughly four times the annual extraction of each element (in 2007). Obviously representing a large, untapped resource, significant efforts have been devoted towards the recycling of manufacturing wastes (swarf), small magnets from electronic waste (e.g. hard disk drives), and large magnets in hybrid vehicles or wind turbines (Du and

Graedel 2011). Rademaker et al. (2013) project recycling from NdFeB magnets (from wind turbines, hybrid/electric vehicles, and hard disk drives) to constitute between 10 and 30% of global Nd supply and 5–25% of Dy supply by 2030.

REE metals can be directly regenerated from off-specification scrap magnets through the use of a molten fluoride flux (Takeda et al. 2014). However, this technique does not provide for substantial control over the composition of the regenerated alloys.

Vander Hoogerstraete et al. (2014) describe a process for the dissolution of NdFeB magnets following roasting at 950°C. Following roasting, the REE were more readily leachable, while the Fe and Co components were minimally dissolved. An ionic liquid (IL) was used for solvent exchange separation of the REE from the Fe and Co that was liberated. Finally the REE were recovered from IL through salting out with NH_4Cl and precipitated as oxalate solids.

After dissolution of scrap NdFeB magnets in 6 M HNO_3, Kim et al. (2015) employed membrane assisted solvent extraction to effectively separate the Nd (as well as Pr and Dy) from the Fe and B bulk. Here, the dissolution and extraction chemistries are not unique, but instead the engineering of the system (i.e. hollow-fiber membrane solvent extraction) maintains high, non-equilibrium driving forces for rapid and efficient extraction. Moreover, the enclosed systems allowed for facile regeneration, limiting chemical consumption.

3.3.2 Recycling metal-hydride batteries

Zhang et al. (1998) dissolved Ni metal hydride battery electrodes in HCl at 95°C and separated the REE using HDEHP. Following stripping of the organic phase with HCl, the REE were precipitated as oxalates after pH adjustment through ammonia addition. Non-REE impurities (Co, Mn, Zn, Fe, and Al) accounted for < 1wt% of the precipitate. However, the

calcined final product was an impure mixture of the REE. Larsson and Binnemans (2014) applied a series of solvent extractions, utilizing ILs, to accomplish separations with superior efficiencies than solvent extraction utilizing HDEHP.

Bertuol et al. (2009) leached finely powdered anodes from AB_5 Ni metal hydride batteries in 2 N H_2SO_4, 2 N HNO_3, 2 N HCl, and 2 N aqua regia. The resulting leachates were subsequently dosed with NaOH until precipitates formed, with the precipitate being analyzed by x-ray fluorescence. For H_2SO_4, precipitates formed at pH 1, while precipitates were not noticed for the other lixiviant acids until pH 7. At this low pH, Bertuol et al. (2009) confirmed the formation of Na-REE-$(SO_4)_2$ or $REE_2(SO_4)_3$ salts, which effectively excluded the unwanted components of the anode material (e.g. Ni, Co, Mg, Fe, and Zn), with 98% recovery of the dissolved REE. Precipitates obtained from the other leachates at pH 7 were heavily contaminated by these undesireable components (e.g. for HNO_3, precipitate was 56wt% Ni and 29wt% Fe). While this approach appears promising, Bertuol et al. (2009) note that care must be taken during the mechanical separation of the anodic material to avoid rapid oxidation and potential ignition. Additionally, while effective for separation from non-REE elements, this approach provides no intra-REE separation.

Similar results (efficient liberation with H_2SO_4 and bulk-REE selective precipitation at pH $\sim$ 1.5) were achieved by Nan et al. (2006) (with anode isolation) and Innocenzi and Vegliò (2012) (without anode isolation). However, as before, no intra-REE separation was achieved in either of these studies. Provazi et al. (2011) offer a contrasting result, wherein H_2SO_4 leaching followed by precipitation at pH 1.5 yielded an impure precipitate. However, in this case, the starting material was significantly different than Bertuol et al. (2009), Nan et al. (2006), Innocenzi and Vegliò (2012), consisting of a mixture of batteries (only 1.4wt% NiMH) and having undergone significant pretreatment (roasting at 1000°C under an inert atmosphere),

As an alternative to H_2SO_4 leaching and REE-SO_4 precipitation, Fernandes et al. (2013) utilized a multi-stage process to recover REE-oxalates. Oxalate precipitation is an attractive process choice because the resulting solids can be oxidatively roasted to yield REE oxides. As with Innocenzi and Vegliò (2012), Fernandes et al. (2013) performed no separation of the active battery components (cathode, anode, electrolyte), leaching the ground, mixed materials with 12 N HCl. Following leaching Zn and Fe were extracted using tributyl phosphate (TBP). Ammonium oxalate was added to raise the solution pH to 0.5, at which point $La_2(C_2O_4)_3$ was recovered (98.5% of dissolved La precipitated) without precipitation of Ni. However, Fernandes et al. (2013) found that a series of solvent extractions (using different extractants and organic phases) performed better for La recovery (on a mass yield basis) than did selective precipitation. Since La was the only element, no assessment of intra-REE selectivity can be made, however, as with SO_4 precipitation, it is unlikely to achieve significant selectivity.

Contrary to many of the other processes described here, an adsorbent, prepared by Gasser and Aly (2013) showed significant selectivity among the REE. The layered double-hydroxide (LDH), loaded with a phosphinic acid carrier showed both kinetic and equilibrium selectivity between La and Nd ($S_{Nd}^{La} = 4$). The inter-layer spacing of the LDH enhances the small thermodynamic selectivities afforded by the HDEHP.

3.4 Alternative resources

Given the technical and societal challenges associated with recycling processes (Reck and Graedel 2012), there is renewed interest in critical material mining of non-traditional resources. These non-traditional sources include: seawater and other aqueous sources, REE-containing industrial wastes, coal combustion residuals, and landfilled or incinerated munic-

ipal solid waste.

3.4.1 Natural aqueous sources

While an average freshwater stream may not contain a viable quantity of the REE for extraction (based on calculations in Section 3.1), Johnson et al. (2012) document a wide variety of adsorbents with high capacity and selectivity for the REE. These high-affinity adsorbents could potentially be used for the passive collection of the REE from promising dilute waters similar to proposed routes of U extraction from seawater (Seko et al. 2003). A more active process could make use of magentic particles, such as those described by Tu et al. (2015), which could be introduced to a flow and easily removed *via* magentic separation and regenerated.

The U.S. Department of Energy Office of Energy Efficiency and Renewable Energy, has funded several projects focused on the extraction and recovery of the REE (and other critical materials) from geothermal brines (Thomas et al. 2015). These technologies include many distinct embodiments of capture and recovery processes, spanning the use of microbial-, nanoparticle-, and membrane driven processes. The common thread to each project is the engineering of a technology with selective-extraction of targeted elements.

3.4.2 REE-containing process wastes

Because of their ubiquitous occurrence, the REE are commonly found in the tailings of mining operations for other minerals or in other process wastes. The foremost example of this was the unexploited REE content in iron ore tailings at Bayan Obo, which would subsequently become the single largest REE mine in the world (Sprecher et al. 2014). Hence, waste streams that are enriched in REE are promising alternative resources for the REE.

Binnemans et al. (2015) provides a thorough review of published studies of valorization of REE-containing wastes, and should be referenced for greater detail.

As previously mentioned, a large portion of the primary REE supply are mined from phosphate minerals (monazite and xenotime). In general, phosphate minerals tend to accumulate REE disproportionately compared to other minerals. Chen and Graedel (2015) propose that the 176 megatonnes of phosphate rock (2010 production) mined annually represents a large, untapped trace-metal resource stream, particularly for the REE, which typically occur at concentrations 10× that of the Earth's crust. In the processing chain of phosphate rock, the REE tend to accumulate in phosphogypsum, a waste product of phosphoric acid production (Chen and Graedel 2015). A patented process claims 85% recovery of the REE from phosphogypsum using acid leaching and cation exchange (Abramov et al. 2013).

While many other process wastes of interest exist , bauxite residue is particularly promising (economically) given elevated Sc concentrations (Binnemans et al. 2015). Scandium is the most valuable of the REE, valued roughly an order of magnitude higher than the rest of the REE (London Metal Exchange 2015). Overall, REE concentrations greater than 0.1wt% have been described in bauxite residues (also known as "red mud"), depending on its source (Ochsenkühn-Petropulu et al. 1996; Wagh and Pinnock 1987). While the mineral associations of the REE are not well defined for bauxite residues (Binnemans et al. 2015), the REE are easily liberated by dilute mineral acids (Ochsenkühn-Petropulu et al. 1996; Wang et al. 2011). As with many other processes detailed here, the REE (and Sc) are separated from the undesirable metals by solvent extraction with HDEHP as the extractant (Wang et al. 2013). However, given the high stability between Sc and HDEHP, Sc is not able to be eluted with strong acids in contrast to the other REE (Kimura 1960). Wang et al. (2013) recovered Sc from the organic phase by stripping with NaOH, followed by neutralization and precipitation as an oxalate.

3.4.3 Coal combustion products

Organic-rich sedimentary formations are known to be strong accumulators of heavy metals (Ketris and Yudovich 2009). The mode of occurrence varies depending on the metal, however the primary mechanisms of this accumulation are the association with organic complexes or the precipitation of sulfides in a highly reducing environment (Chermak and Schreiber 2014; Dai et al. 2014; Ketris and Yudovich 2009). As a result of these elevated concentrations, researchers have speculated as to the mineral value of such deposits, with significant attention being paid to coal (Seredin et al. 2013).

Given the low volatility of the REE (Lide 2012), these elements are further concentrated in the ash fraction of coal upon combustion. The current (and projected) utilization of coal for electricity generation produces enormous quantities of fly ash domestically as well as globally (ACAA 2014). Researchers have speculated that this ash could meet a significant portion of REE demand (Franus et al. 2015), given the appropriate extractive technologies (Zhang et al. 2015). Moreover, the valorization of such a large-tonnage process waste, by extraction of valuable mineral contents, is of great interest to regulatory bodies (Blissett and Rowson 2012).

Zhang et al. (2015) note that while the chemical mineralogy of the REE could make traditional, physical beneficiation possible from ashes and coals, the fine particle sizes of the REE minerals, as well as the ash, are limiting factors. Thus the prevailing design strategy for REE extraction from coals and coal ash includes minimal physical beneficiation, followed by strong acid leaching and solvent extraction (Joshi et al. 2015). Liberation of the REE from ashes may be enhanced with a roasting procedure prior to leaching. For example roasting of fluoro-carbonate and phosphate ores with Na_2CO_3 at $T \approx 350 - 650°C$ has been demonstrated to convert the REE to oxides for significantly more effective leaching with HNO_3

(Zhang et al. 2015).

3.4.4 Municipal solid waste

Most modern consumer electronics contain some amount of REE in their componentry. When these materials are discarded, they accumulate in landfills or (where incineration occurs) in waste incinerator ashes. While the techniques used to extract the REE from incinerator ashes is essentially the same as coal combustion products, mining of landfills presents unique challenges worth noting. Gutiérrez-Gutiérrez et al. (2015) found the REE to be uniformly distributed with depth in 55 samples from 4 distinct landfills; concentrations in this waste averaged 40 ppb – 25 ppm depending on the metal and the location. Gutiérrez-Gutiérrez et al. (2015) concluded that mining of landfill material explicitly for REE content is likely not economically viable, but could be accomplished via co-production of other valuable metals.

3.5 References

Abramov, Y., Veselov, V., Zalevsky, V., Argunov, N., Bogdanova, L., Gukasov, N., Evdokimov, V., Tamurka, V., and Motovilova, L. Method for extracting rare earth elements from phosphogypsum, 2013.

ACAA. 2013 Coal Combustion Product (CCP) Production & Use Survey Report. Report, American Coal Ash Association, 2014.

Bai, L., Qiao, Q., Li, Y., Wan, S., Xie, M., and Chai, F. Statistical entropy analysis of substance flows in a lead smelting process. *Resources, Conservation and Recycling*, 94: 118–128, 2015.

Bertuol, D. A., Bernardes, A. M., and Tenório, J. A. S. Spent nimh batteries—the role of selective precipitation in the recovery of valuable metals. *Journal of Power Sources*, 193 (2):914–923, 2009.

Binnemans, K., Jones, P. T., Blanpain, B., Van Gerven, T., Yang, Y., Walton, A., and Buchert, M. Recycling of rare earths: a critical review. *Journal of Cleaner Production*, 51:1–22, 2013.

Binnemans, K., Jones, P. T., Blanpain, B., Van Gerven, T., and Pontikes, Y. Towards zero-waste valorisation of rare-earth-containing industrial process residues: a critical review. *Journal of Cleaner Production*, 99(0):17–38, 2015.

Blissett, R. S. and Rowson, N. A. A review of the multi-component utilisation of coal fly ash. *Fuel*, 97:1–23, 2012.

Chakhmouradian, A. R. and Wall, F. Rare earth elements: Minerals, mines, magnets (and more). *Elements*, 8(5):333–340, 2012.

Chen, M. and Graedel, T. E. The potential for mining trace elements from phosphate rock. *Journal of Cleaner Production*, 91:337–346, 2015.

Chermak, J. A. and Schreiber, M. E. Mineralogy and trace element geochemistry of gas shales in the United States: Environmental implications. *International Journal of Coal Geology*, 126(1):32–44, 2014.

Ciacci, L., Reck, B. K., Nassar, N. T., and Graedel, T. E. Lost by design. *Environmental Science & Technology*, 49(16):9443–51, 2015.

Dahmus, J. B. and Gutowski, T. G. What gets recycled: an information theory based model for product recycling. *Environmental Science & Technology*, 41(21):7543–7550, 2007.

Dai, S., Seredin, V. V., Ward, C. R., Jiang, J., Hower, J. C., Song, X., Jiang, Y., Wang, X., Gornostaeva, T., Li, X., Liu, H., Zhao, L., and Zhao, C. Composition and modes of occurrence of minerals and elements in coal combustion products derived from high-Ge coals. *International Journal of Coal Geology*, 121:79–97, 2014.

De La Garza, A., Garrett, G., and Murphy, J. Multicomponent isotope separation in cascades. *Chemical Engineering Science*, 15(3):188–209, 1961.

Dent, P. C. Rare earth elements and permanent magnets. *Journal of Applied Physics*, 111 (7), 2012.

Diallo, M. S., Kotte, M. R., and Cho, M. Mining critical metals and elements from seawater: Opportunities and challenges. *Environmental Science & Technology*, 49(16):9390–9399, 2015.

Du, X. and Graedel, T. Global rare earth inuse stocks in NdFeB permanent magnets. *Journal of Industrial Ecology*, 15(6):836–843, 2011.

Falkner, K. K. and Edmond, J. Gold in seawater. *Earth and Planetary Science Letters*, 98 (2):208–221, 1990.

Federal Remediation Technologies Roundtable. *FRTR cost and performance remediation case studies and related information.* U.S. Environmental Protection Agency, Solid Waste and Emergency Response, 2003.

Fernandes, A., Afonso, J. C., and Dutra, A. J. B. Separation of nickel (ii), cobalt (ii) and lanthanides from spent ni-mh batteries by hydrochloric acid leaching, solvent extraction and precipitation. *Hydrometallurgy*, 133:37–43, 2013.

Franus, W., Wiatros-Motyka, M. M., and Wdowin, M. Coal fly ash as a resource for rare earth elements. *Environmental Science and Pollution Research*, 22(12):9464–9474, 2015.

Gasser, M. and Aly, M. Separation and recovery of rare earth elements from spent nickel–metal-hydride batteries using synthetic adsorbent. *International Journal of Mineral Processing*, 121:31–38, 2013.

Gupta, C. and Krishnamurthy, N. Extractive metallurgy of rare earths. *International Materials Reviews*, 37(1):197–248, 1992.

Gutiérrez-Gutiérrez, S. C., Coulon, F., Jiang, Y., and Wagland, S. Rare earth elements and critical metal content of extracted landfilled material and potential recovery opportunities. *Waste Management*, 42:128–136, 2015.

Haber, F. Das gold im Meerwasser. *Angewandte Chemie*, 40(11):303–314, 1927.

Harper, J. The Marcellus Shale - an old "new" gas reservoir. *Pennsylvania Geology*, 38(1): 2–13, 2008.

Hermann, W. A. Quantifying global exergy resources. *Energy*, 31(12):1685–1702, 2006.

House, K. Z., Baclig, A. C., Ranjan, M., van Nierop, E. A., Wilcox, J., and Herzog, H. J. Economic and energetic analysis of capturing CO_2 from ambient air. *Proceedings of the National Academy of Sciences*, 108(51):20428–20433, 2011.

Innocenzi, V. and Vegliò, F. Recovery of rare earths and base metals from spent nickel-metal hydride batteries by sequential sulphuric acid leaching and selective precipitations. *Journal of Power Sources*, 211:184–191, 2012.

Johnson, B. E., Santschi, P. H., Chuang, C.-Y., Otosaka, S., Addleman, R. S., Douglas, M., Rutledge, R. D., Chouyyok, W., Davidson, J. D., Fryxell, G. E., and Schwantes, J. M. Collection of lanthanides and actinides from natural waters with conventional and nanoporous sorbents. *Environmental Science & Technology*, 46(20):11251–11258, 2012.

Jordens, A., Cheng, Y. P., and Waters, K. E. A review of the beneficiation of rare earth element bearing minerals. *Minerals Engineering*, 41:97–114, 2013.

Joshi, P. B., Preda, D. V., Skyler, D. A., Tsinberg, A., Green, B. D., and Marinelli, W. J. Recovery of rare earth elements and compounds from coal ash, 2015.

Kargbo, D. M., Wilhelm, R. G., and Campbell, D. J. Natural gas plays in the Marcellus shale: Challenges and potential opportunities. *Environmental Science & Technology*, 44 (15):5679–5684, 2010.

Kaufman, S., Krishnan, N., Kwon, E., Castaldi, M., Themelis, N., and Rechberger, H. Examination of the fate of carbon in waste management systems through statistical entropy and life cycle analysis. *Environmental science & technology*, 42(22):8558–8563, 2008.

Ketris, M. and Yudovich, Y. E. Estimations of Clarkes for carbonaceous biolithes: World averages for trace element contents in black shales and coals. *International Journal of Coal Geology*, 78(2):135–148, 2009. ISSN 0166-5162.

Kim, D., Powell, L. E., Delmau, L. H., Peterson, E. S., Herchenroeder, J., and Bhave, R. R. Selective extraction of rare earth elements from permanent magnet scraps with membrane solvent extraction. *Environmental Science & Technology*, 49(16):9452–9459, 2015.

Kim, J., Tsouris, C., Mayes, R. T., Oyola, Y., Saito, T., Janke, C. J., Dai, S., Schneider, E., and Sachde, D. Recovery of uranium from seawater: A review of current status and future research needs. *Separation Science and Technology*, 48(3):367–387, 2013.

Kimura, K. Inorganic extraction studies on the system between bis (2-ethyl hexyl)-orthophosphoric acid and hydrochloric acid (I). *Bulletin of the Chemical Society of Japan*, 33(8):1038–1046, 1960. ISSN 0009-2673.

Larsson, K. and Binnemans, K. Selective extraction of metals using ionic liquids for nickel metal hydride battery recycling. *Green Chemistry*, 16(10):4595–4603, 2014.

Lide, D. R. *CRC handbook of chemistry and physics*. CRC press, 2012. ISBN 1439880492.

Lightfoot, E. and Cockrem, M. What are dilute solutions? *Separation Science and Technology*, 22(2-3):165–189, 1987.

London Metal Exchange. Rare earth element prices, 2015. URL http://mineralprices.com/default.aspx#rar.

Lu, Y. Uranium extraction: Coordination chemistry in the ocean. *Nature chemistry*, 6(3): 175–177, 2014.

Marie, C., Hiscox, B., and Nash, K. L. Characterization of HDEHPlanthanide complexes formed in a non-polar organic phase using ^{31}P NMR and ESI-MS. *Dalton Transactions*, 41(3):1054–1064, 2012.

Muzzarelli, R. A. Potential of chitin/chitosan-bearing materials for uranium recovery: An interdisciplinary review. *Carbohydrate Polymers*, 84(1):54–63, 2011.

Nan, J., Han, D., Yang, M., Cui, M., and Hou, X. Recovery of metal values from a mixture of spent lithium-ion batteries and nickel-metal hydride batteries. *Hydrometallurgy*, 84(1): 75–80, 2006.

Nash, K. L. A review of the basic chemistry and recent developments in trivalent f-elements separations. *Solvent Extraction and Ion Exchange*, 11(4):729–768, 1993.

Ochsenkühn-Petropulu, M., Lyberopulu, T., Ochsenkühn, K., and Parissakis, G. Recovery of lanthanides and yttrium from red mud by selective leaching. *Analytica Chimica Acta*, 319(1):249–254, 1996.

Peiró, L. T. and Méndez, G. V. Material and energy requirement for rare earth production. *JOM*, 65(10):1327–1340, 2013.

Provazi, K., Campos, B. A., Espinosa, D. C. R., and Tenório, J. A. S. Metal separation from mixed types of batteries using selective precipitation and liquid–liquid extraction techniques. *Waste Management*, 31(1):59–64, 2011.

R Core Team. *R: A Language and Environment for Statistical Computing*. R Foundation for Statistical Computing, Vienna, Austria, 2014. URL http://www.R-project.org/.

Rademaker, J. H., Kleijn, R., and Yang, Y. Recycling as a strategy against rare earth element criticality: A systemic evaluation of the potential yield of ndfeb magnet recycling. *Environmental Science & Technology*, 47(18):10129–10136, 2013.

Rao, L. Recent international r&d activities in the extraction of uranium from seawater. Report, Lawrence Berkeley National Laboratory, 2011.

Rechberger, H. and Graedel, T. The contemporary european copper cycle: statistical entropy analysis. *Ecological Economics*, 42(1):59–72, 2002.

Rechberger, H. and Brunner, P. H. A new, entropy based method to support waste and resource management decisions. *Environmental Science & Technology*, 36(4):809–816, 2002.

Reck, B. K. and Graedel, T. E. Challenges in metal recycling. *Science*, 337(6095):690–695, 2012.

Seko, N., Katakai, A., Hasegawa, S., Tamada, M., Kasai, N., Takeda, H., Sugo, T., and

Saito, K. Aquaculture of uranium in seawater by a fabric-adsorbent submerged system. *Nuclear Technology*, 144(2):274–278, 2003.

Seredin, V. V., Dai, S., Sun, Y., and Chekryzhov, I. Y. Coal deposits as promising sources of rare metals for alternative power and energy-efficient technologies. *Applied Geochemistry*, 31(0):1–11, 2013.

Shannon, C. E. Prediction and entropy of printed english. *Bell system technical journal*, 30 (1):50–64, 1951.

Smith Stegen, K. Heavy rare earths, permanent magnets, and renewable energies: An imminent crisis. *Energy Policy*, 79:1–8, 2015.

Soeder, D. J. The Marcellus Shale: Resources and reservations. *Eos Trans. AGU*, 91(32), 2010.

Sprecher, B., Xiao, Y., Walton, A., Speight, J., Harris, R., Kleijn, R., Visser, G., and Kramer, G. J. Life cycle inventory of the production of rare earths and the subsequent production of NdFeB rare earth permanent magnets. *Environmental Science & Technology*, 48(7): 3951–3958, 2014.

Takeda, O., Nakano, K., and Sato, Y. Recycling of rare earth magnet waste by removing rare earth oxide with molten fluoride. *Materials Transactions*, 55(2):334–341, 2014.

Thomas, H., Reinhardt, T. P., and Segneri, B. Low temperature geothermal mineral recovery program. In *Proceedings of the Fortieth Workshop on Geothermal Reservoir Engineering*, Stanford, CA, January 26–28 2015.

Tu, Y.-J., Lo, S.-C., and You, C.-F. Selective and fast recovery of neodymium from seawater by magnetic iron oxide Fe_3O_4. *Chemical Engineering Journal*, 262:966–972, 2015.

Tunsu, C., Petranikova, M., Gergorić, M., Ekberg, C., and Retegan, T. Reclaiming rare earth elements from end-of-life products: A review of the perspectives for urban mining using hydrometallurgical unit operations. *Hydrometallurgy*, In press., 2015.

Vander Hoogerstraete, T., Blanpain, B., Van Gerven, T., and Binnemans, K. From NdFeB magnets towards the rare-earth oxides: a recycling process consuming only oxalic acid. *RSC Advances*, 4(109):64099–64111, 2014.

Wagh, A. S. and Pinnock, W. R. Occurrence of scandium and rare earth elements in Jamaican bauxite waste. *Economic Geology*, 82(3):757–761, 1987.

Wang, W., Pranolo, Y., and Cheng, C. Y. Metallurgical processes for scandium recovery from various resources: A review. *Hydrometallurgy*, 108(1):100–108, 2011.

Wang, W., Pranolo, Y., and Cheng, C. Y. Recovery of scandium from synthetic red mud leach solutions by solvent extraction with d2ehpa. *Separation and Purification Technology*, 108:96–102, 2013.

Witschi, H. The story of the man who gave us" haber's law". *Inhalation toxicology*, 9(3): 201–209, 1997.

Xie, F., Zhang, T. A., Dreisinger, D., and Doyle, F. A critical review on solvent extraction of rare earths from aqueous solutions. *Minerals Engineering*, 56:10–28, 2014.

Yan, C., Jia, J., Liao, C., Wu, S., and Xu, G. Rare earth separation in China. *Tsinghua Science & Technology*, 11(2):241–247, 2006.

Zaimes, G. G., Hubler, B. J., Wang, S., and Khanna, V. Environmental life cycle perspective on rare earth oxide production. *ACS Sustainable Chemistry & Engineering*, 3(2):237–244, 2015.

Zhang, P., Yokoyama, T., Itabashi, O., Wakui, Y., Suzuki, T. M., and Inoue, K. Hydrometallurgical process for recovery of metal values from spent nickel-metal hydride secondary batteries. *Hydrometallurgy*, 50(1):61–75, 1998.

Zhang, W., Rezaee, M., Bhagavatula, A., Li, Y., Groppo, J., and Honaker, R. A review of the occurrence and promising recovery methods of rare earth elements from coal and coal by-products. *International Journal of Coal Preparation and Utilization*, 35(6):295–330, 2015.

Chapter 4

Rare earth element distributions and trends in natural waters with a focus on groundwater

This chapter is adapted from a publication by the same name, co-authored by David A. Dzombak and Athanasios K. Karamalidis. This paper is citable as:

Noack, C. W.; Dzombak, D. A.; Karamalidis, A. K., Rare Earth Element Distributions and Trends in Natural Waters with a Focus on Groundwater. *Environ. Sci. Technol.* **2014**, *48*, (8), 4317-4326.

The accumulated database of reported REE concentrations is freely accessible from the CMU Research Showcase.

My contributions to this work were the collection, analysis, and visualization of the data; development of `R` scripts; interpretation of results; and drafting of the manuscript.

Abstract

Systematically varying properties and reactivities have led to focused research of the environmental forensics capabilities of the rare earth elements (REE). Increasing anthropogenic inputs to natural systems may permanently alter the natural signatures of REEs, motivating characterization of natural REE variability. We compiled and analyzed reported dissolved REE concentration data over a wide range of natural water types (groundwater, ocean-, river-, and lake water) and groundwater chemistries (e.g. fresh, brine, and acidic) with the goal of quantifying the extent of natural REE variability, especially for groundwater systems. Quantitative challenges presented by censored data were addressed with non-parametric distributions and regressions. Reported measurements of rare earth elements in natural waters range over nearly ten orders of magnitude, though the majority of measurements are within two to four orders of magnitude, and are highly correlated with one another. Few global correlations exist among dissolved abundance and bulk solution properties in groundwaters indicating the complex nature of source-sink terms and the need for care when comparing results between studies. This collection, homogenization, and analysis of a disparate literature facilitates inter-study comparison and provides insight into the wide range of variables that influence REE geochemistry.

4.1 Introduction

In the natural sciences, predictable thermodynamic differences between the rare earth elements (REE) allow for interpretation of natural geologic and chemical processes (Laveuf and Cornu 2009; Murray et al. 1990). Rare earth lithogeochemistries have long been used to infer depositional environments of geologic strata (Hanson 1980; Murray et al. 1990; Nance

and Taylor 1976). Similarly, REE serve as benign analogs to the transuranic actinides for nuclear waste disposal studies (Krauskopf 1986; Millero 1992) and for studying mixing and metal cycling in the oceans (De Baar et al. 1983; Elderfield et al. 1988). These characteristics make REE attractive tools for environmental forensic applications such as pollutant source identification and apportionment (Kulkarni et al. 2006; 2007).

Based on atomic number, the REE are segregated into light and heavy REE (LREE and HREE, respectively) with the division occurring between Eu and Gd (Castor and Hedrick 2006); some studies also distinguish middle REE (MREE), though the specific elements are inconsistently defined between authors (Brookins 1989; Choi et al. 2009; Hannigan and Sholkovitz 2001; Tang and Johannesson 2010). These "weight" distinctions allow for simplified description and quantification of the inter-element relationships, typically ratios of normalized concentrations, which are exploited in REE analysis. Similarly, anomalies of certain REE – due to redox lability for Ce and Eu (Brookins 1989) and large anthropogenic emissions for Gd (Bau and Dulski 1996) – are used to interpret geochemical processes. Y and Sc exhibit similar properties to the lanthanides and are thus included in the suite of REE with Y being most similar to HREE and Sc being most similar to LREE in solution (Brookins 1989).

Aquatic geochemists apply the same principles used by geologists, the inter-element ratios and anomalies described previously, to infer water-rock interactions, hydrologic connectivity between geologic units, and groundwater mixing members (Bwire Ojiambo et al. 2003; Johannesson et al. 1997a;b; Siebert et al. 2012). Interactions with different mineral phases have been shown to alter REE patterns predictably. For example, an MREE enrichment is observed for fresh waters in contact with phosphate-rich minerals (Hannigan and Sholkovitz 2001) while HREE enrichment is found in carbonate-rich waters (Johannesson et al. 1996b). Tester et al. (Tesmer et al. 2007) showed that groundwater end-members, es-

pecially at shallow depths, could be established by interpretation of REE patterns. Similarly, REE concentrations have been used to calculate end-member contributions to groundwater (Bwire Ojiambo et al. 2003; Johannesson et al. 1997a).

The capabilities of REE to serve as tracers of groundwater migration and mixing have potential applications to the study of hydrology and geochemistry of shale gas development or the capture and sequestration of carbon dioxide (CO_2) gas in geologic formations. For example, characteristic REE profiles could possibly enable detection of brines displaced from shale or CO_2 storage zones and into overlying groundwater aquifers (Benson and Cole 2008; Chaudhuri et al. 2011; Cheung et al. 2009; Karamalidis et al. 2012). Capable tools for contaminant detection, as well as contaminant source apportionment, are critical to the long-term environmental feasibility of these technologies. Increasing anthropogenic inputs of REE to the environment threaten to obfuscate natural signals, which would complicate these applications (Kulaksiz and Bau 2013; Kulaksız and Bau 2011).

A primary challenge in analyzing REE data, like other geochemical compositional data (Palarea-Albaladejo et al. 2011), is the prevalence of censored observations, defined as values below the analytical method detection limit (MDL) or a value excluded due to excessive analytical interferences. Appropriate statistical methodologies, largely borrowed from survival analysis (or reliability analysis), allow for analysis of these data without relying on substitution or interpolation (Helsel 1990). Utilizing these techniques removes the bias of left-censored data and of uneven sample sizes from summary statistics and statistical inference (Helsel 1990; 2005).

Significant contributions to the understanding of REE geochemistry in natural waters have been made through critical review of thermodynamics (Brookins 1989; Wood 1990), catchment-scale case studies (Dia et al. 2000; Gruau et al. 2004; Ma et al. 2011; Pourret et al. 2010), and groundwater flow system studies (Johannesson et al. 1997a; 1999; 2000; Tang and Jo-

hannesson 2006; Willis and Johannesson 2011) among others. Lacking thus far in the REE literature is the aggregation and analysis of the numerous and disparate studies of the REE and the origin of their concentrations. Such a compilation would enhance inter-study comparison through internal consistency, allow for investigation of broader trends, and enhance statistical analysis by increasing sample sizes.

In this work, a compilation and analysis of data from independent studies of REE in natural waters was performed, focusing on trends in groundwaters. The study focused on shallow groundwaters well as some deeper groundwaters capable of impacting surface water or shallow groundwater. The compiled data were used to develop a consistent database of REE concentrations and their associated major solute chemistry and to explore interelement relationships, examine trends in REE abundance, and test hypotheses related to REE abundance as functions of major solution chemistry parameters. The objectives of this work were: (1) to ascertain an expected range of dissolved REE concentrations in waters of variable chemistries, deriving unbiased estimates of REE distributions and (2) to investigate trends in REE abundance in groundwater in relation to other available chemical parameters (e.g. pH, ionic strength, and major solution species).

4.2 Methods

4.2.1 Data assimilation and criteria

The low-temperature, aqueous REE systematics were investigated by extracting available REE concentration data in reported studies of ground-, sea-, river-, and lake waters. Data were gathered from these studies for dissolved REE concentrations (defined here as constituents passing through a 0.45 µm filter). Many studies filter at finer pore sizes in order to

study colloidal association (Dia et al. 2000; Pourret et al. 2007b; Stolpe et al. 2013), however 0.45 µm was chosen because it is a common size for groundwater analysis and maximized the number of samples available. While REE are commonly defined to include Y and Sc, very few studies measured Y and almost none examined Sc. Therefore, our analyses of REE focused on the 14 naturally abundant lanthanides (excluding the short-lived, radioactive Pm). In total, 31 studies with 619 samples were collected for groundwater (Bwire Ojiambo et al. 2003; Choi et al. 2009; de Boer et al. 1996; Dia et al. 2000; Duncan and Shaw 2003; Esmaeili-Vardanjani et al. 2012; Gosselin et al. 1992; Gruau et al. 2004; Guo et al. 2010; Janssen and Verweij 2003; Johannesson and Hendry 2000; Johannesson et al. 1995; 1996a; 1999; 2000; Leybourne et al. 2000; Michard et al. 1987; Miekeley et al. 1992; Möller et al. 1998; Nelson et al. 2004; Négrel et al. 2000; Otsuka and Terakado 2003; Pourret et al. 2010; Siebert et al. 2012; Smedley 1991; Tang and Johannesson 2006; Tricca et al. 1999; Tweed et al. 2006; Willis and Johannesson 2011; Worrall and Pearson 2001b; Yan et al. 2001), 16 studies with 178 samples for seawater (Alibo and Nozaki 1999; Bau et al. 1997; De Baar et al. 1983; Duncan and Shaw 2003; Elderfield et al. 1990; Elderfield and Greaves 1982; Fu et al. 2007; Haley and Klinkhammer 2003; Hirata et al. 2002; Nozaki et al. 1999; 2000; Piepgras and Jacobsen 1992; Schijf et al. 1995; Sholkovitz et al. 1994; Vicente et al. 1998; Zhu et al. 2006), 16 studies with 259 samples for river water (Biddau et al. 2002; Bwire Ojiambo et al. 2003; Centeno et al. 2004; Elderfield et al. 1990; Gammons et al. 2005a;b; Han and Liu 2007; Hannigan and Sholkovitz 2001; Ingri et al. 2000; Johannesson et al. 2004; Lawrence et al. 2006; Nozaki et al. 1999; Sholkovitz 1992; Tang and Johannesson 2003; Tricca et al. 1999; Zhang et al. 1998; Åström and Corin 2003), and 8 studies with 74 samples for lake water (Bwire Ojiambo et al. 2003; De Carlo and Green 2002; Gammons et al. 2005b; Johannesson and Lyons 1994; Johannesson et al. 2004; Johannesson and Lyons 1995; Johannesson et al. 1995; Leybourne et al. 2000).

A significant literature exists for other water types, for example mine drainage (Borrego et al. 2012; Bozau et al. 2004; Doulati Ardejanii et al. 2013; Romero et al. 2010; Verplanck et al. 2004; Worrall and Pearson 2001a; Zhao et al. 2007) and hydrothermal waters/hot springs (Haas et al. 1995; Lepel et al. 1988; Lewis et al. 1998; 1997; Michard 1989; Sanada et al. 2006). However, these water types have been excluded from this study in order to focus on waters minimally impacted by anthropogenic activity (in the case of mine drainage) and that occur broadly with chemistry dominated by near-surface pressure, temperature, and mineralogical conditions (in the case of hydrothermal waters/hot springs).

4.2.2 Analysis of censored data

In the accumulated data set, 18% of all REE measurements were either below detection or missing. For individual elements in different waters, up to 52% of measurements were censored (Tm in groundwater). The censoring rates of each element, in each water type, are given in Figure 4.1. Given this high frequency, it was necessary to employ modified statistical methods to handle this type of information and avoid creating a false data signal either by substitution (i.e., one-half MDL) or interpolation (Helsel 2005).

An additional complexity of this data set was the uneven distribution of data points between data sets (Figure 4.2). For example, some data sets included more than seventy samples, while other contained fewer than ten. This uneven distribution can bias calculated statistics towards studies with a higher number of samples, giving larger studies more weight than smaller studies (Singh et al. 2013).

Censored data were stored at the study-specific MDL with a separate binary variable indicating that the data were censored. Missing data – that is where REE were either not measured, not reported, or where an MDL was not specified – were excluded from calculations because

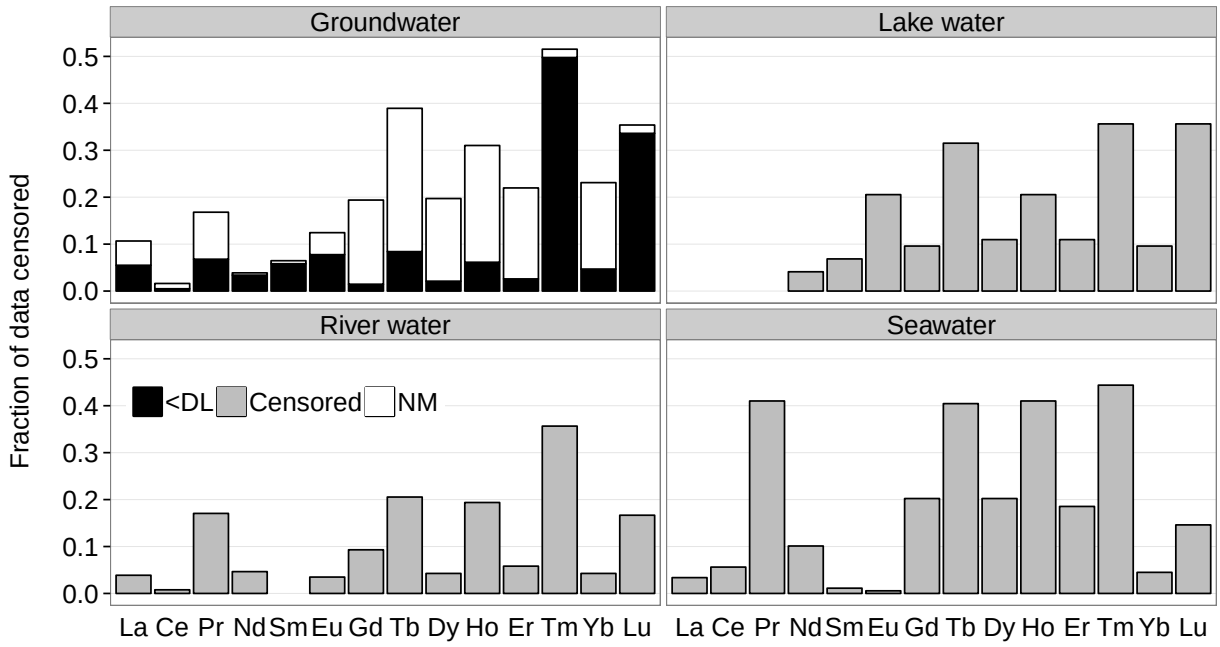

Figure 4.1: Fraction of below detection limit (<DL) or missing data (NM) for 14 REE in data sets for water types studied. For water types other than groundwater, censored data were not differentiated as below detection or missing, and are lumped together as "censored".

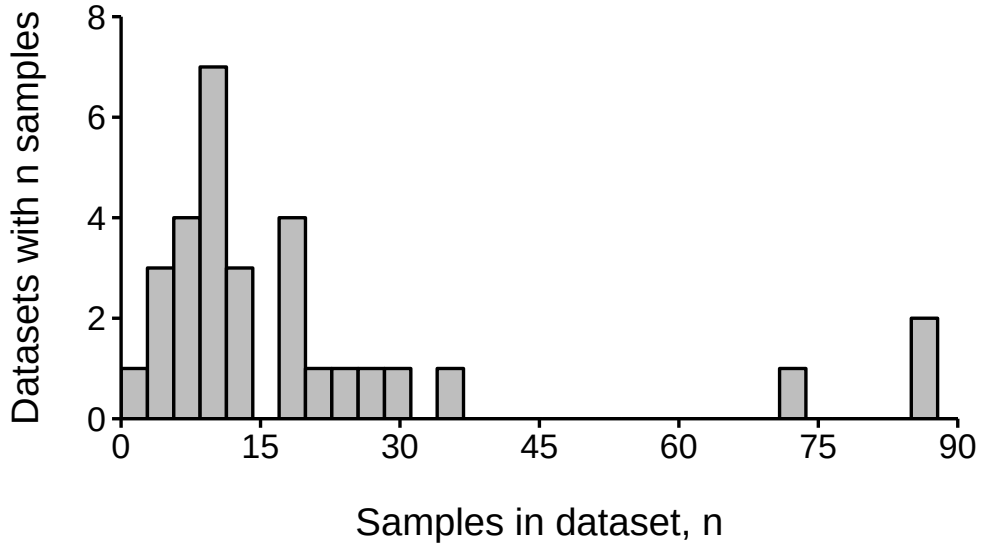

Figure 4.2: Histogram of sample distribution in groundwater data set (compiled from 31 articles).

nothing was known about the data point in relation to the rest of the data.

Summary statistics were calculated using a weighted Kaplan-Meier (KM) estimator of the survival function accounting for both left-censored and source-size bias. A routine based on the methodology of Singh, et al. (Singh et al. 2013) was written in `R` (R Core Team 2014) to perform the necessary calculations. Distribution percentiles were estimated as the first value with a calculated percentile less than the percentile of interest; stated differently, if the calculated survival quantiles, $S(x)$, for adjacent observations were $S(x_1) = 0.94$ and $S(x_2) = 0.96$, then x_1 would be noted as the 95^{th} percentile. For data sets with a limited number of samples (e.g. brines) where the sample size or censoring frequency limited the number of calculable percentiles, a log-normal distribution was fit to the KM survival curve by regression on order statistics (ROS) and was used to estimate those percentiles. Mean values, μ_{KM}, were calculated from the area under the survival curve and standard deviations, σ_{KM}, from the variance of the mean (Helsel 2012).

The survival curve was approximated using a weighted KM estimator, which considers non-detect data and provides robustness to the uneven distribution of samples from the reviewed literature. Equation 4.1 represents the weighted KM estimator, where $\hat{S}(x_i)$ is the probability any observation from the data set will be *less than* the measured concentration, x_i. In this equation d_i^w represents the weighted count of uncensored observations at concentration x_i and Y_i^w represents the weighted count of all (censored and uncensored) observed concentrations less than x_i. The weight, w_i, of each observation is the inverse of the number of samples from the data source (n_i), or: $w_i = n_i^{-1}$. In the absence of weighting or censoring, this formula reduces to the empirical cumulative distribution function. These calculations, and the relevant `R` code, are discussed algorithmically in Appendix B.

$$\hat{S}(x_i) = \prod_{x \geq x_i} \left(1 - \frac{d_i^w}{Y_i^w}\right) \tag{4.1}$$

Total dissolved REE concentrations were calculated with consideration of censored data. Rather than calculating the KM survival curve and μ_{KM} for an individual element (where each sample is an observation) the survival curve was calculated for individual samples (where each REE is an observation). The sum was determined as follows (Helsel 2012):

$$\sum[REE] = 14 \times \mu_{KM} \tag{4.2}$$

In addition to univariate summary statistics, inter-element correlations are significantly influenced by the high degree of censoring within the REE data. Using Pearson's r (linear, least-squares correlation) as an estimate of the correlation would require substitution for censored or missing values (Helsel 1990), while also making assumptions about the relationship between the variables. Instead, the Kendall's τ statistic enabled incorporation of censored data, diminished the influence of outliers (by being robust to log-transformation), and assessed monotonic relationships beyond simple linear relationships. Thus Kendall's τ was used for assessing relationships between any variables with multiple censoring levels (detection limits). Similar to more common measures of correlation, τ takes values between -1 and 1 with a value of -1 indicating perfect, negative correlation and a value of 1 indicating perfect, positive correlation between the data. The Kendall's τ method will typically produce lower numeric values (often 0.2 units lower for the same strength of correlation) than other measures, which may make interpretation difficult (Helsel 2012); however, Kendall's τ

is the only technique that allows for inclusion of multiple detection limits non-parametrically without substitution or imputation. Correlations between variables without censoring were evaluated non-parametrically with Spearman's ρ.

4.2.3 Reference-normalized element anomalies and ratios

Several reduced dimension variables (RDVs) are calculated from reference normalized data including ratios of the LREE to MREE and HREE, the Ce anomaly, and the Eu anomaly. RDVs provide a simplified, univariate presentation of multivariate REE data, quantitatively capturing key features of the REE profile, the plot of reference-normalized concentrations versus atomic number. The Post Archaean Average Shale (PAAS) of Nance and Taylor (Nance and Taylor 1976) was used for normalization.

The Ce anomaly (Ce^*_N), the ratio of the normalized Ce concentration to an expected normalized value from interpolation of normalized La and Pr concentrations (calculated in this work with Equation 4.3), is commonly discussed in the REE literature.

$$Ce^*_N = \frac{2 \cdot [Ce]_N}{[La]_N + [Pr]_N} \tag{4.3}$$

The Eu anomaly (Eu^*_N) is calculated similarly using measured Eu concentrations and the concentrations of directly neighboring REE (Sm and Gd). Both anomalies are commonly log-transformed, a convention that was applied throughout this work.

The ratios of reference normalized REE concentrations were here taken to be an average over multiple elements as opposed to single weight group representatives (Stolpe et al. 2013). The LREE included in ratio analyses were La, Pr, Nd, and Sm; the MREE were Gd, Tb, and

Dy; and the HREE were Ho, Er, Tm, Yb, and Lu. Both Ce and Eu were excluded from calculation of ratios.

These anomalies and interelement ratios cannot be reliably calculated for missing or censored data, thus our analyses of RDVs pertain only to the portion of the data set where all necessary REE have been reported. This excludes many data sets utilizing isotope dilution mass spectrometry, which cannot measure mono-isotopic elements, and many studies with higher detection limits or poor analytical precision.

4.2.4 Geochemical modelling

A primary goal was to examine the relationship of REE abundance with various bulk solution chemistries in groundwater. The REE abundance and concentration data from the literature varied by their sample chemical characterization, water sample origin, sampling location, as well as the nomenclature used to classify geologic environments. To overcome this heterogeneity we employed a quantitative criterion for the classification of data before any statistical analysis was performed. For groundwater samples, the total data set ($N = 619$ samples) was screened under the criterion that the samples were fully characterized for major ions (Na^+, K^+, Ca^{2+}, Mg^{2+}, Cl^-, SO_4^{2-}, and HCO_3^-/CO_3^{2-}) and pH. These major solution chemistry data were used to calculate ionic strength and activity of the carbonate ion (CO_3^{2-}) using the geochemical equilibrium model PHREEQC with the Pitzer database (pitzer.dat) (Parkhurst and Appelo 1999; Pitzer 1973). Considering the wide range of unique systems represented by this data set we have not pursued modeling of REE solubility limiting reactions. While such analyses are useful in well-defined systems, and REE speciation is commonly used to investigate mechanisms of REE abundance (Johannesson et al. 1995; 1996a; Willis and Johannesson 2011), significantly more information than was reported for most studies

would be needed to conduct the analyses and moreover this type of modeling was deemed beyond the scope of the study.

4.3 Results and discussion

4.3.1 Occurrence of REE in aqueous media

Measured concentrations of REE in natural waters are summarized in Figure 4.3. Reported concentrations of REE in surface- and groundwater spanned ten orders of magnitude, while individual elements fluctuate with atomic number (i.e., the observed "zig-zag" pattern). This fluctuation of abundance is attributable to the Oddo-Harkins rule, which stipulates that, other than hydrogen, elements with even atomic numbers are more abundant than adjacent elements having odd atomic numbers (Harkins 1917); this fluctuation gives rise to the common practice of normalizing REE data to a reference standard, for example an average shale or chondritic meteorite, which also exhibits the Oddo-Harkins effect (McLennan 1994). Individual REE are distributed log normally (Figure REF) and are highly correlated with one-another (Figure 4.4).

Groundwater

In groundwater, the KM-calculated interquartile ranges (KM-IQR, first and third quartile) of overall REE concentrations vary between 5.7 and 410 pmol/kg solution (pmol/kg; Figure 4.3A). The mean concentration of the groundwater data set was 3.5×10^4 pmol/kg and the median was 53 pmol/kg. As shown in the disparity between the mean and median, REE concentrations in groundwater were heavily right-tailed with many "outlier" values and a maximum of 9.7×10^6 pmol/kg (Miekeley et al. 1992). The REE profile of a groundwater is

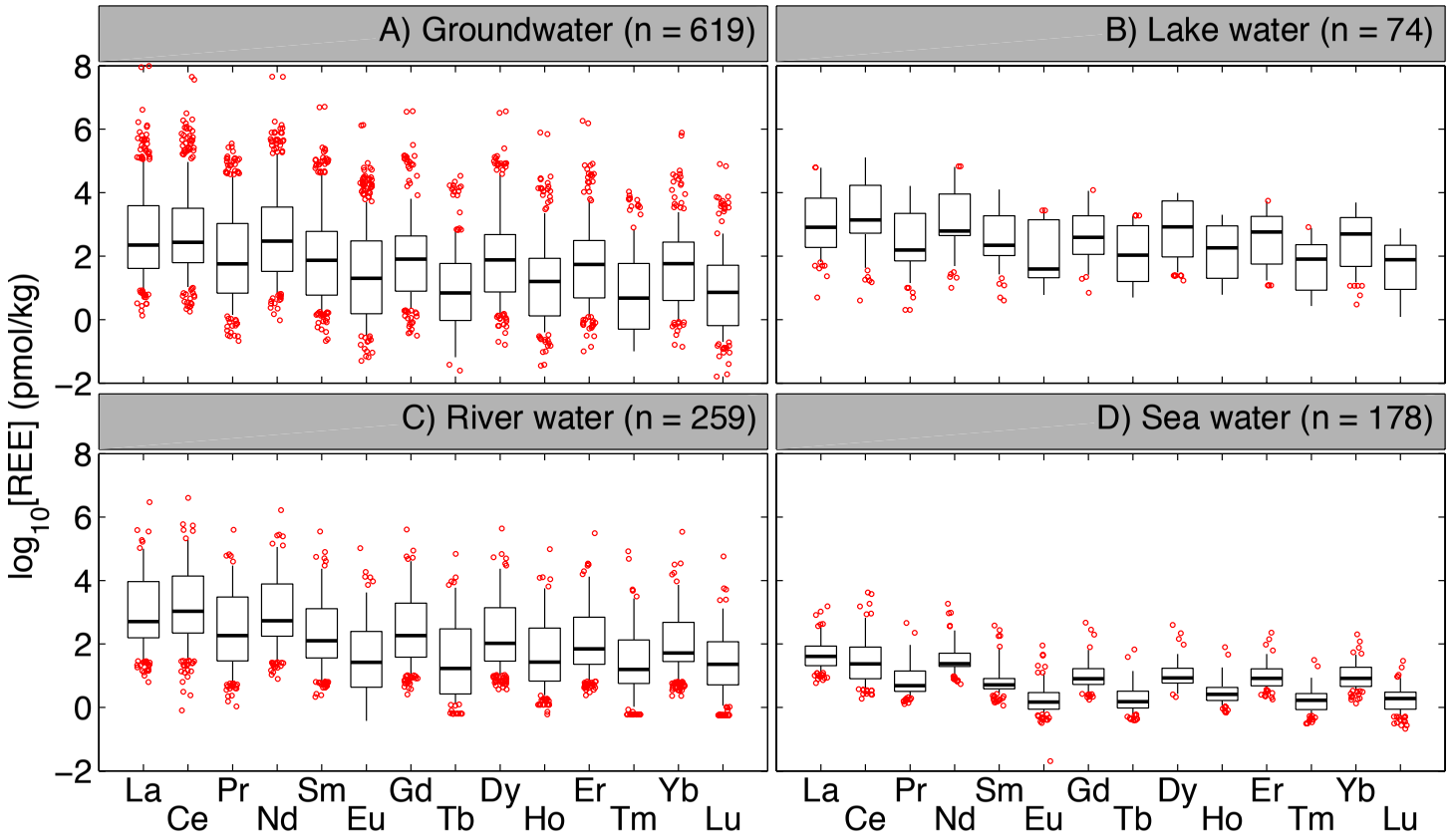

Figure 4.3: REE concentration distributions in waters of different types. Boxplots are based on source-size weighted Kaplan-Meier estimates of REE concentration percentiles and represent the median (thick, black line), inter-quartile range (IQR; first to third quartile; boxed range), 5th to 95th percentile range (whiskers), and remaining outliers (red circles). In each subfigure heading, "n" in the parenthesis denotes the total number of measurements in each water type The number of detected measurements varies between elements. These data are inclusive, representing unique water sources, spatial and temporal variations within an individual water, and any duplicate analyses.

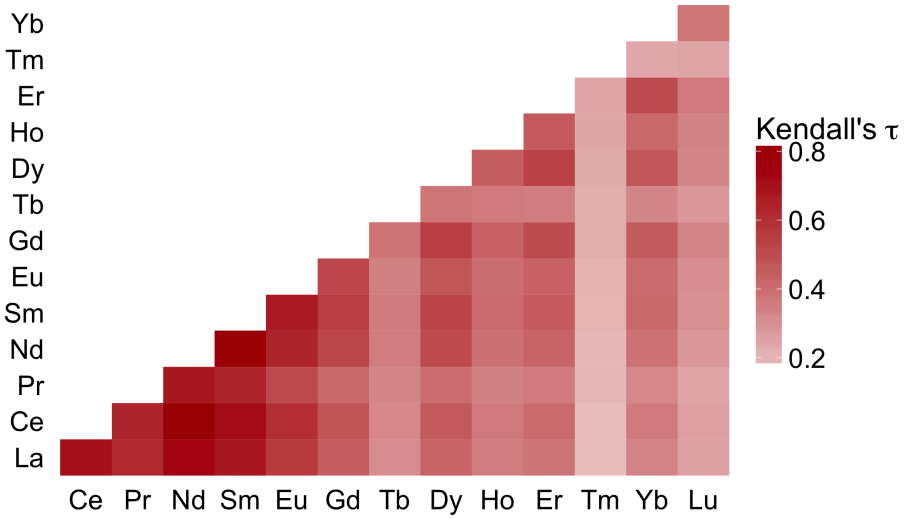

Figure 4.4: Heatmap visualization of Kendall's τ correlation coefficients among the REE in the groundwater data set. All correlations are statistically significantly positive.

thought to arise either from water-rock interactions (Smedley 1991; Willis and Johannesson 2011) or by changes in the aqueous chemistry (Dia et al. 2000), e.g., in relation to the residence time within the aquifer (Bwire Ojiambo et al. 2003; Johannesson et al. 1997b).

By comparison, substitution of censored data between 0 and 100% of the detection limit values (without source weighting) results in medians ranging from 4.4 to 13 pmol/kg and mean values ranging from 4.7×10^4 to 4.9×10^4 pmol/kg. Alternatively, deletion of below detection data roughly doubles all KM summary statistic estimates: 120 and 5.3×10^4 pmol/kg for median and mean respectively. Linear interpolation to fill in censored data also leads to significant error (Figure 4.5). This highlights the criticality of applying appropriate tools in calculating relevant summary statistics, particularly for quantitative analysis.

Terrestrial surface water

In lake water, the KM-IQR of overall REE concentrations varied between 30 and 1.4×10^3 pmol/kg (Figure 4.3B). The mean concentration of the lake water data set was 3.8×10^3

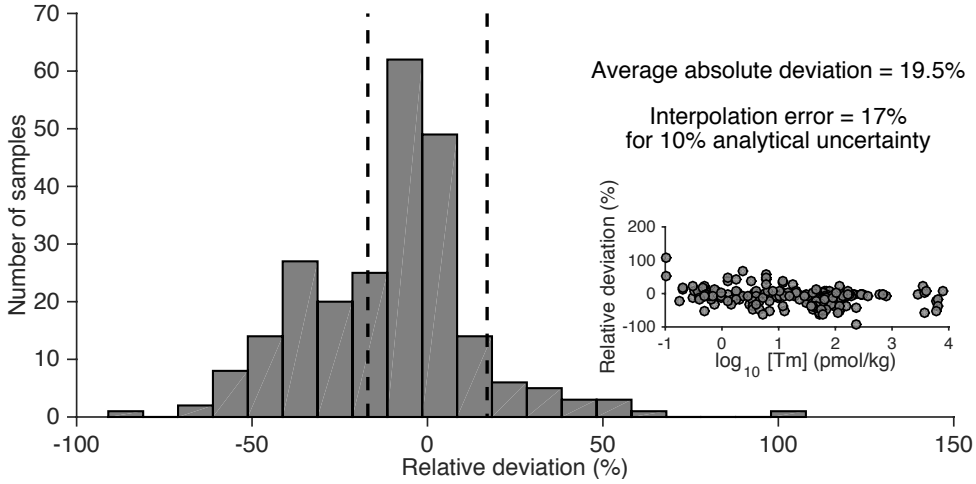

Figure 4.5: Histogram of relative Post Archaean Averaged Shale normalized interpolation error of Tm in groundwater data set and (inset) dependence of error on measured Tm values. PAAS normalized Er and Yb were used to "guess" the Tm concentration and then compared to the actual measured Tm concentrations. Dashed lines mark the bounds of 10% analytical uncertainty propagated through the interpolation. In this analysis 42% of 241 samples exhibit interpolation error outside the bounds of analytical uncertainty.

pmol/kg and the median was 170 pmol/kg.

In river water, the KM-IQRs of overall REE concentrations varied between 15 and 270 pmol/kg (Figure 4.3C). The mean concentration of the river water data set was 3.3×10^3 pmol/kg and the median was 71 pmol/kg.

Seawater

In seawater, the KM-IQR of reported REE concentrations varied between 1.6 and 13 pmol/kg (Figure 4.3D). The mean concentration of the seawater data set was 19 pmol/kg and the median was 5 pmol/kg. The disparity between the dissolved REE in seawater and its influent waters is likely attributable to particulate scavenging (Erel and Stolper 1993; Sholkovitz et al. 1994) at a rate that exceeds mass fluxes from surface- and groundwater sources. In groundwater by comparison, continuous weathering of the aquifer rock counteracts sorption

and co-precipitation loss mechanisms. Dubinin (Dubinin 2004) notes that dissolved fractions of REE increase with distance off-shore as terrigenous material settles, which removes REE mass faster than it can be replenished by other sources such as aeolian deposition or hydrothermal venting

Shale-normalized anomalies and ratios

The groundwaters in this data set primarily exhibited mild negative and positive shale-normalized anomalies for Ce and Eu respectively, though, as with abundance, these RDVs varied widely (Figure 4.6). Both terrestrial surface waters reported here exhibit similar Ce* and Eu* (Figure 4.6A and 4.6B), which are mildly negative and nearly zero respectively. The Ce* of seawater is starkly different than any of the three water types, developing consistent, negative anomalies with instances of large positive anomalies.

Nearly all waters in this study are LREE depleted (Figure 4.6C and 4.6D). As with element anomalies, the mean and IQR of interelement ratios among groundwaters and terrestrial surface waters are similar while seawater exhibits distinctly lower ratios. Both anomalies in groundwater exhibit large outlier values, similar to REE abundance, which underscores the extreme variability in groundwater systems.

The anomalies of Ce and Eu are of interest because they are the two REE with redox lability within the Eh-pH regime of water stability (Brookins 1983). Upon oxidation – Ce(III) to Ce(IV) – cerium readily precipitates as CeO_2(s); alternatively, europium becomes less soluble when reduced from Eu(III) to Eu(II) based on preferential incorporation into other minerals due to the lower valency and higher ionic radius of the reduced state (similar to Sr) (Brookins 1989). Where anomalies in rock samples have been used to infer paleo-redox conditions, the anomalies in aqueous samples are often used to analyze water-rock interactions (Smedley

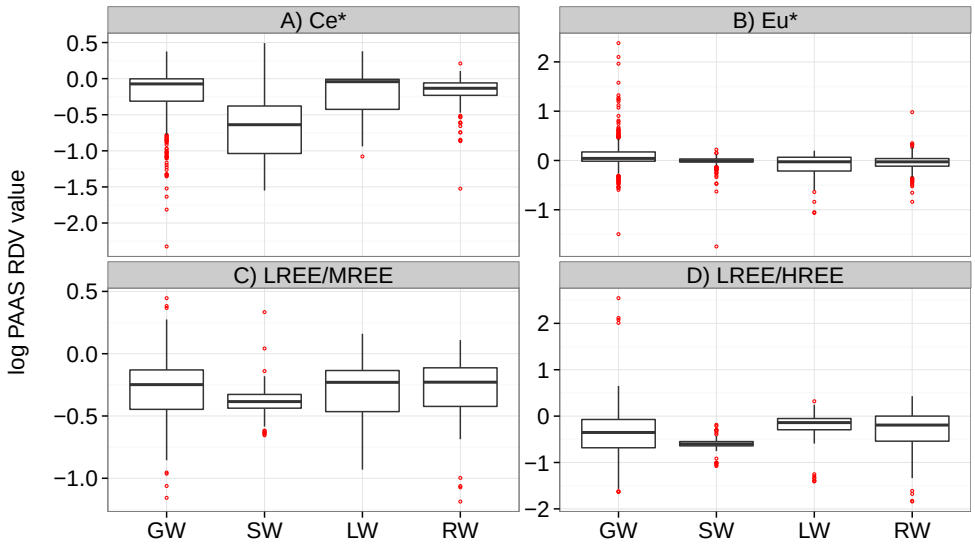

Figure 4.6: Log-transformed, Post-Archaean Average Shale (PAAS)- normalized, reduced dimension variables (RDVs) calculated for groundwater (GW), seawater (SW), lake water (LW), and river water (RW) data. RDVs are the cerium anomaly (Ce*), europium anomaly (Eu*), LREE / MREE ratio, and LREE / HREE ratio. Boxplots represent the median (thick, black line), interquartile range (IQR; first to third quartile; boxed range), ±1.5 times the IQR (whiskers), and remaining outliers (red circles).

1991; Willis and Johannesson 2011).

Divalent europium is energetically favorable under extremely reducing conditions or at high temperatures. Reduced Eu(II) exhibits strong partitioning to various minerals during crystallization from magmatic fluids. Thus many source rocks are either highly enriched (e.g. plagioclase (Nash and Crecraft 1985)) or highly depleted (e.g. olivine (Foley and Jenner 2004) and pyroxene (Hanson 1980)) in Eu, enhancing or limiting availability during weathering (Sverjensky 1984). In hot, reduced, alkaline waters fracture filling calcite commonly contains notable Eu enrichments indicating that the source fluids developed negative Eu* (Cai et al. 2008; Lee et al. 2003). However, such environments are representative of hydrothermal waters (Sverjensky 1984), which were specifically excluded from this analysis. Thus the Eu* in this data set are thought to result from mineral weathering (Sverjensky 1984).

While aquatic redox couples are commonly in disequilibrium for measured redox potential (Eh) (Linberg and Runnels 1984), Figure 4.7A illustrates a negative correlation ($\rho = -0.33$; $P < 1 \times 10^{-6}$) between Ce^*_N and Eh in groundwater, as expected for oxidative scavenging. However, the low strength of the correlation reflects the mechanism being a function of both source composition and aqueous chemistry. Europium anomalies do not exhibit the expected positive trend with redox potential in groundwater, though a weak negative correlation is observed ($\rho = -0.18$, $P = 0.006$; Figure 4.7B). Stability diagrams with measure Ce* and Eu* are included in Figure 4.8 and show the lack of agreement between measured and thermodynamically predicted anomalies.

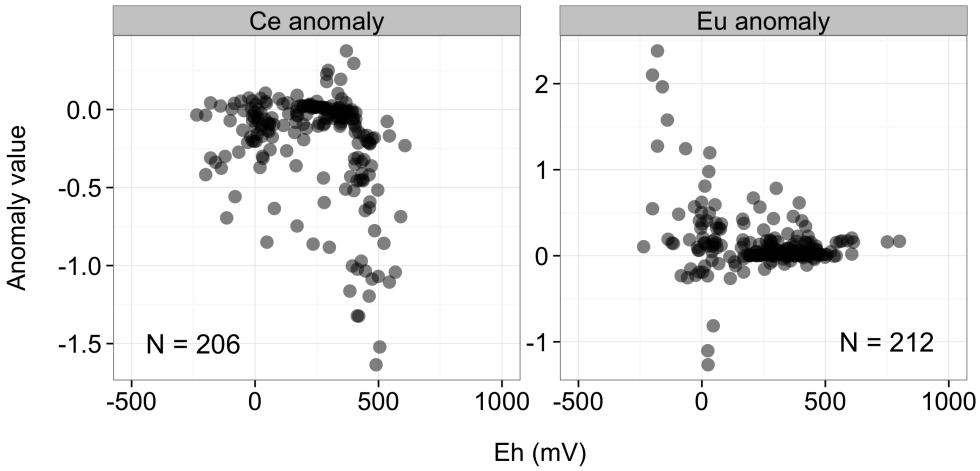

Figure 4.7: Groundwater Post-Archaean Average Shale Ce anomaly (left, Eq. 4.3) and Eu anomaly (right) as a function of reported redox potential (Eh). Sample size denoted by "N". Plot markers are semitransparent to illustrate data density.

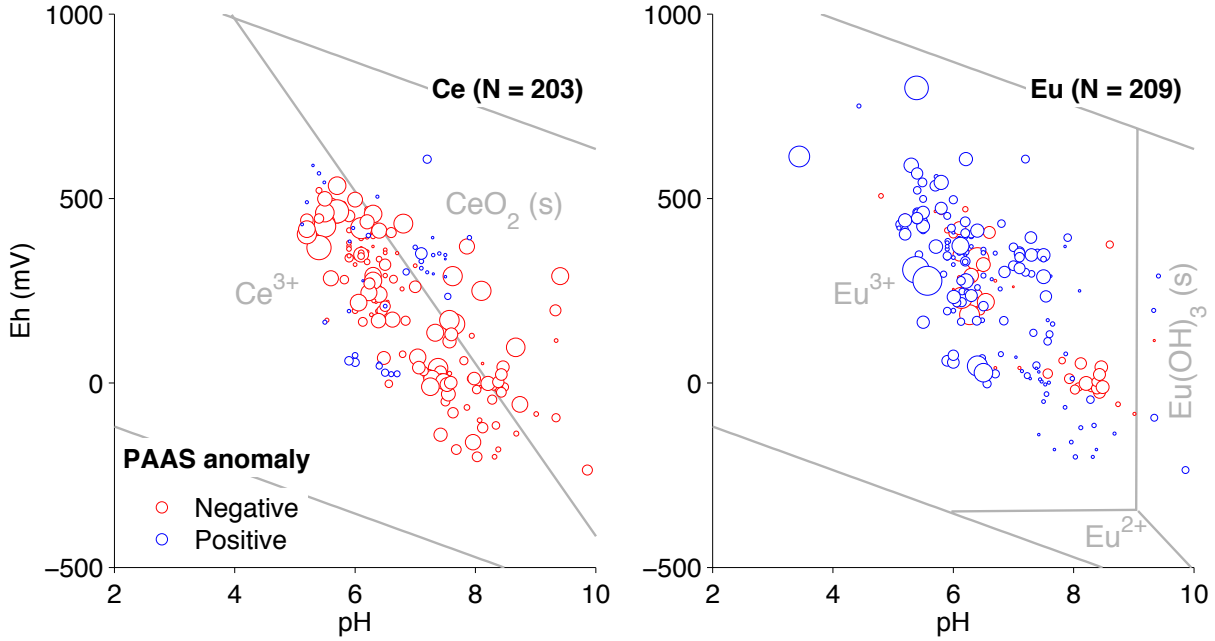

Figure 4.8: Post-Archaean Average Shale (PAAS) Cerium (Ce; left) and Europium (Eu; right) anomalies in groundwater data set as functions of reported redox potential (Eh) and pH. Marker color corresponds to the sign of the anomaly and marker size corresponds to the magnitude of the anomaly. Theoretical stability fields, reproduced from Brookins (Brookins 1989), for relevant species in the REE-H_2O system underlie the reported data for TOTCe=TOTEu = 10^{-11} M at 298 K.

4.3.2 REE abundance trends in groundwater

Of all the bulk solution chemistry parameters for groundwater, pH exerted the greatest control as an independent variable over dissolved REE abundance (Figure 4.9). Generally, more acidic waters contained the most REE, either via acidification-enhanced weathering or from an enrichment of REE in the acid source (Dia et al. 2000; Gosselin et al. 1992; Janssen and Verweij 2003; Leybourne et al. 2000; Miekeley et al. 1992; Smedley 1991; Worrall and Pearson 2001b). REE are effectively scavenged from more neutral and basic waters via sorption onto oxides and clays or co-precipitation with carbonates and phosphates by replacing calcium, which has a comparable atomic radius (Bradbury and Baeyens 2002; Coppin et al. 2002; Johannesson and Lyons 1994; Lide 2012; Quinn et al. 2006; Terakado and Masuda 1988). Over the pH range 4-8, dissolved REE abundance follows an approximate -1 slope with increasing pH (95% confidence interval of -1.02 ± 0.1), indicative of a single-proton (i.e. mono-dentate) surface complexation reaction or calcite precipitation when carbonate far exceeds calcium (Morel and Hering 1993). Geochemical modeling showed that nearly all samples were significantly undersaturated with respect to either pure-phase REE hydroxides or carbonates (Figure 4.10).

Strong complexation with carbonate, particularly as a dicarbonato complex ($REE(CO_3)_2^-$) is thought to account for the apparent amphoteric behavior as pH becomes more basic (Johannesson et al. 1995; Millero 1992; Wood 1990). The REE form progressively stronger carbonate and dicarbonato complexes with increasing atomic number (Millero 1992; Wood 1990), which would suggest an increase of MREE or HREE relative to LREE as a function of pH or carbonate ion activity. However, such a trend is not observed within the current data set (Figure 4.11) though the breadth of the current data set may simply obscure such trends seen in individual studies (e.g. Ref. Choi et al. 2009).

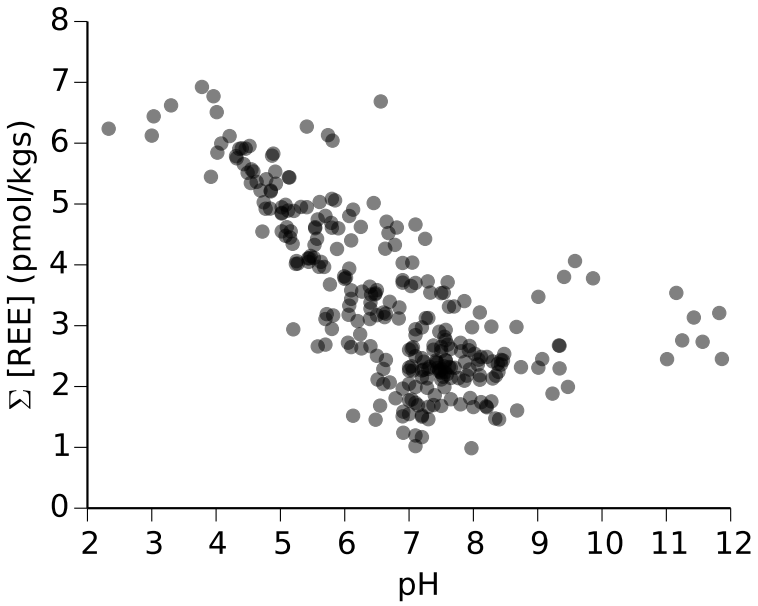

Figure 4.9: Sum of dissolved REE vs pH for groundwater data from Kaplan-Meier estimates (Eq 4.2). Markers are semitransparent to illustrate data density. Data presented for 281 samples.

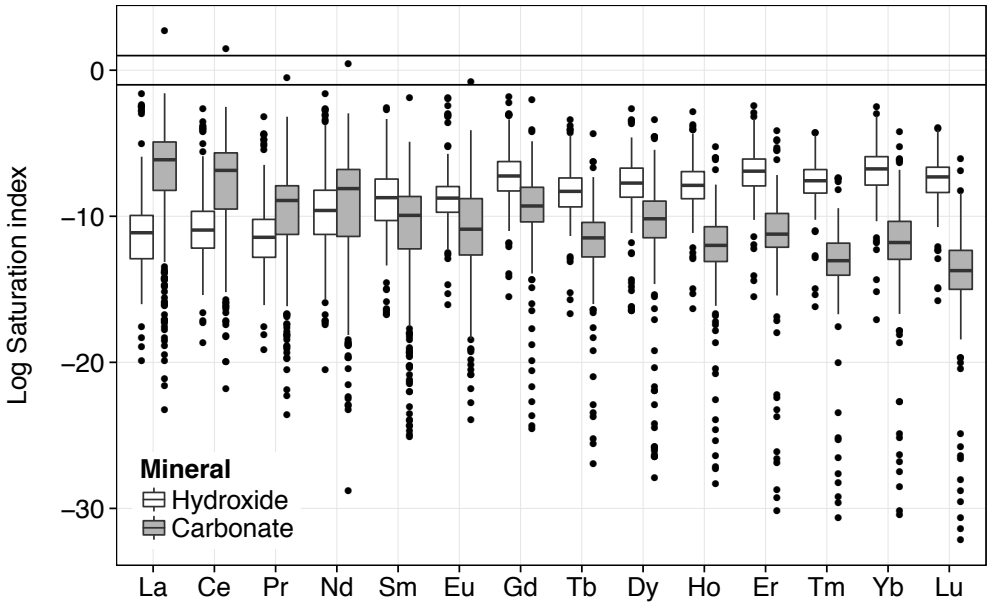

Figure 4.10: Modeled, log-transformed saturation indices of pure phase REE hydroxides and carbonates for groundwater data. Saturation indices calculated using PHREEQC and the LLNL database. Solid lines at −1 and 1 indicate range of potentially solubility controlling phases (Meima and Comans 1997).

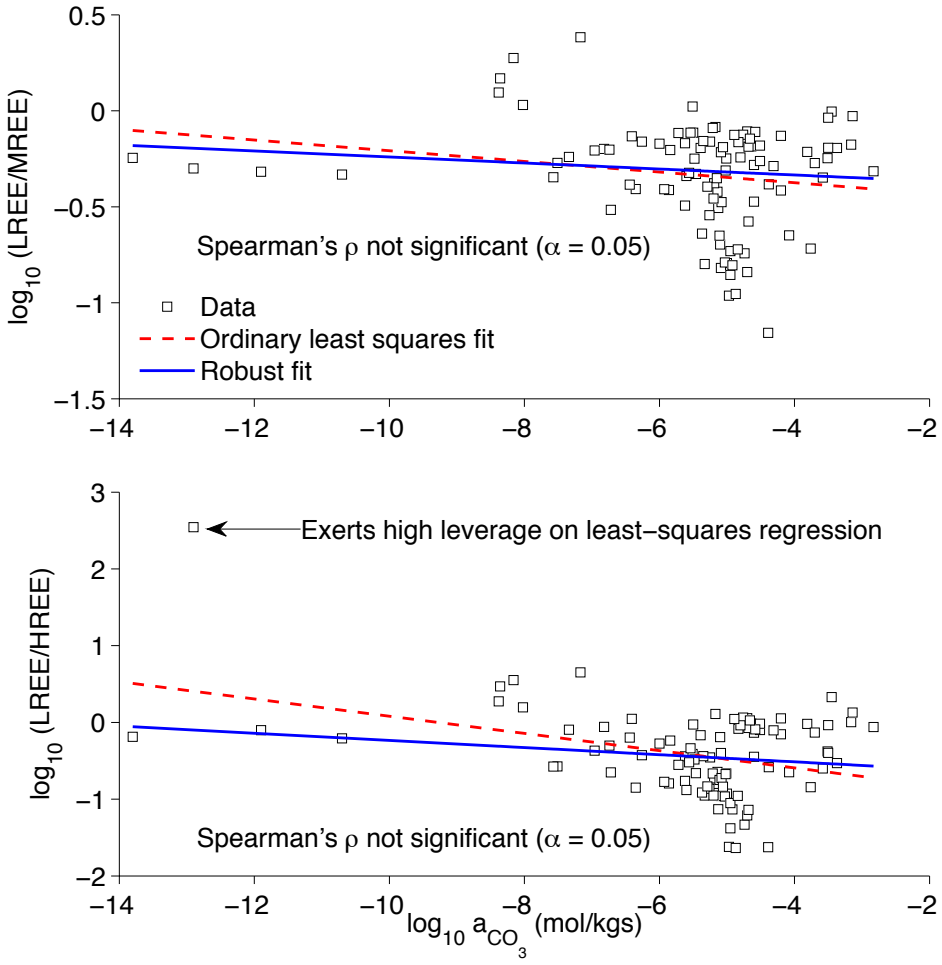

Figure 4.11: Light-middle REE fractionation (top) and light-heavy REE fractionation (bottom) as a function of modeled carbonate ion activity (a_{CO_3}). For L/M fractionation neither regression is significant, while L/H ordinary least squares regression is significant due to a high outlier value. Each plot contains 99 data points.

Kendall's τ correlation analysis of REE with bulk solutes shows inconsistent trends, however most of the meaningful relationships are between the solutes and the LREE and are weakly negative (Figure 4.12). This behavior is contrary to many other metals that correlate positively with dissolved solids. This likely highlights the heterogeneity of the data set and the importance of surface reactions in controlling dissolved REE abundance.

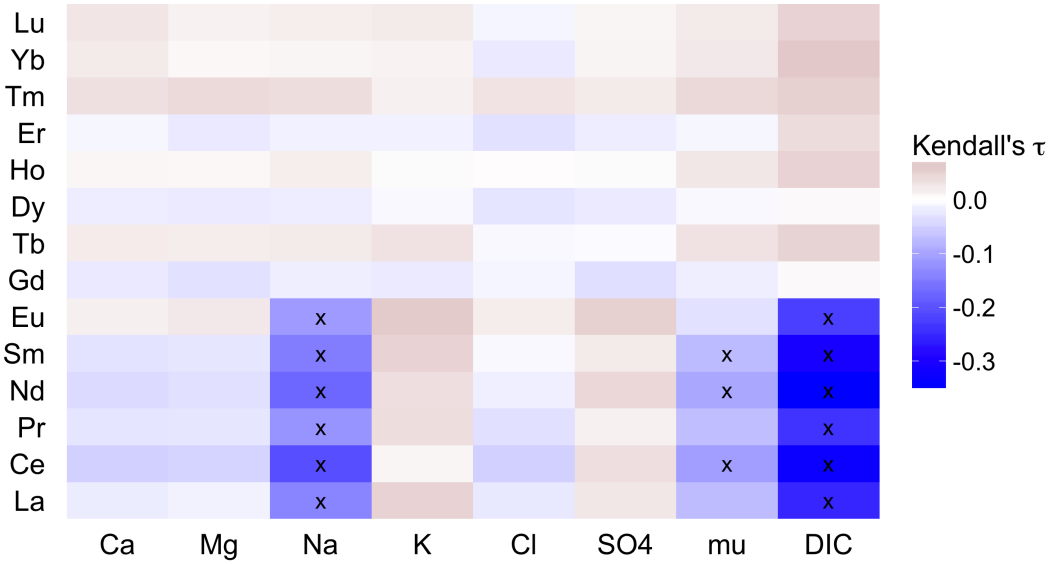

Figure 4.12: Heatmap visualization of Kendall's τ coefficients between REE abundance and total bulk solutes and calculated ionic strength ("mu") in groundwater. Statistically significant correlations ($\alpha = 0.05$) are noted with an "x".

Major element chemistry of the groundwater data

For the groundwater data, the screening process reduced the total number of samples from 619 to 328. The representative chemistries of the screened data set samples varied widely, with several orders of magnitude range in the major ion concentrations (Figure 4.13). Plotting the major ion concentrations using a Piper diagram (Piper 1944) showed that the major anions were predominantly Cl/SO_4, while the predominant cations varied between monovalent and divalent (Figure 4.14).

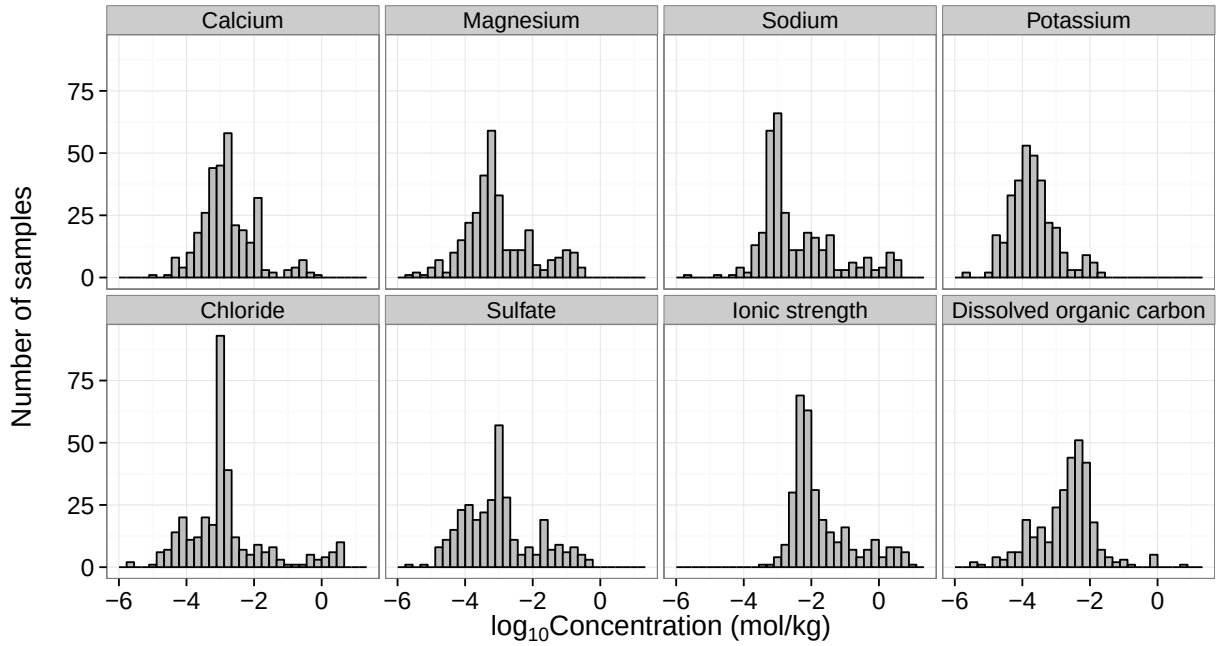

Figure 4.13: Major solution chemistry histograms for groundwater data set. Total dissolved inorganic carbon was either given or estimated from alkalinity data using PHREEQC. Ionic strength was calculated using PHREEQC.

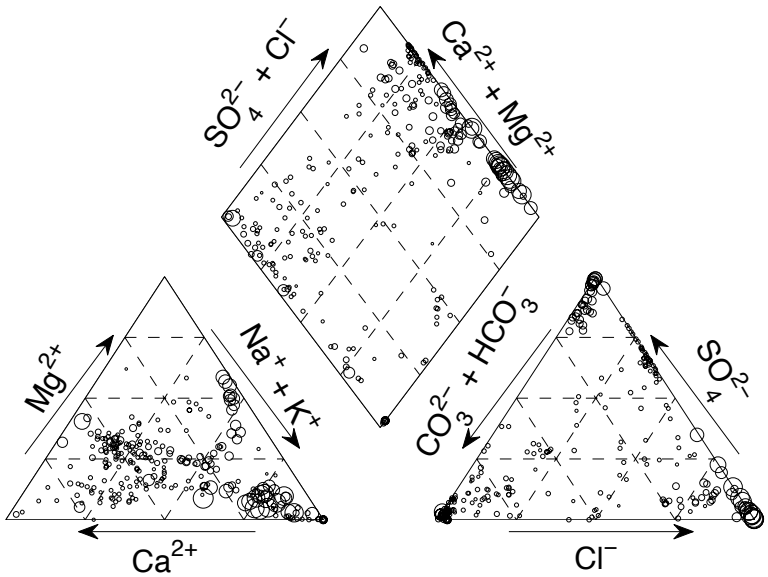

Figure 4.14: Piper diagram of ground water chemistry for circumneutral ($5.5 < \text{pH} < 8.5$) groundwater. Points scaled based on total dissolved solids. All plots range from 0 – 100%.

Based on the available data three qualitative, rule-based water types were classified: fresh water ($N = 122$; $6.5 \leq$ pH ≤ 8.5; I ≤ 0.1 mol/kg), brines ($N = 20$; $5.3 \leq$ pH ≤ 8.0; I ≥ 1.0 mol/kg), and acidic waters ($N = 63$; pH < 5.3); ionic strength and pH values were chosen to maximize data points within the various water classes while maintaining a reasonable bound on parameters. Further subdivision of the freshwater data was possible (e.g. based on relative cation/anion composition) but was not pursued in favor of retaining a larger sample size. The medians of the REE distributions of the classified groundwaters are shown in Figure 4.15.

Utility of REE as tracers is reliant on identifying distinctive trends in different water types. Of note in Figure 4.15 is the markedly higher concentrations of REE in acidic waters than either fresh water or brines, which supports the observations from Figure 4.9, but also a deviation from the standard Oddo-Harkins effect pattern where Er and Yb are both less concentrated than their odd-numbered neighbors. This effect was attributed to high degrees of censored or missing data for these elements (87% for both Er and Yb in the acidic data set) which leads to low-biased percentile estimates (as with Er and Yb) and large uncertainty (seen in all the HREE). Despite showing little or no correlation with ionic strength (Figure 4.12) the REE, in particular the LREE and MREE, were more concentrated in brines than freshwater.

Understanding of the aqueous systematics of the REE is dominated by studies of fresh groundwaters, surface waters, and seawater. Only 14% of the groundwater data gathered had a calculated ionic strength of 1.0 mol/kg or greater (Figure 4.16). While thermodynamic models have been developed to predict REE aqueous speciation in brines (Millero 1992), the energetics of precipitation-dissolution and sorption-desorption in the REE system are not well defined for high ionic strength, chemically complex brines (Quinn et al. 2006). Moreover, increased utilization of groundwater (Chen et al. 2013) in response to population growth,

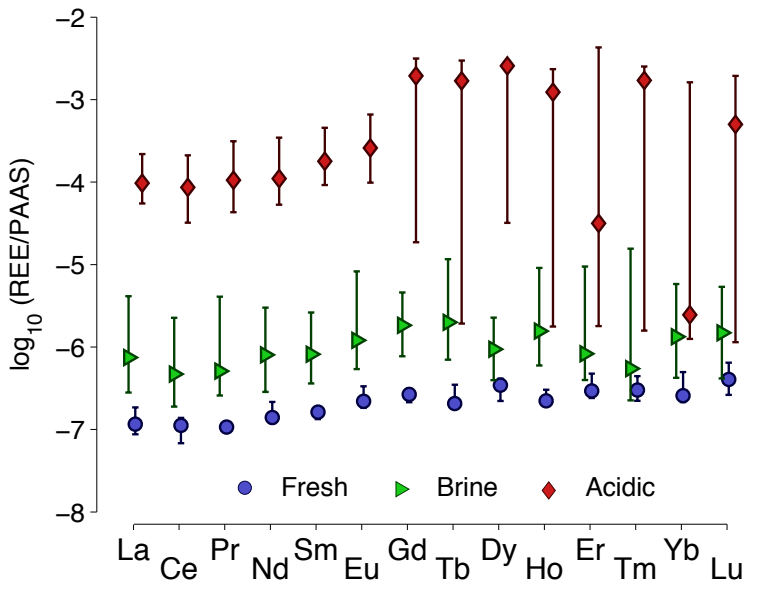

Figure 4.15: Source-size weighted Kaplan-Meier estimates of median dissolved REE concentrations, normalized to Post-Archaean Average Shale (PAAS) values, in three characteristic groundwater types. Error bars represent the 95% confidence interval of the median. Definitions of water classes are found in the text. Estimates were made for individual elements, thus results do not represent a "typical" water sample across the REE suite.

economic development, and climate change and the potential to exploit saline aquifers (Benko and Drewes 2008) underscores the need to better understand the trace metal chemistry of brines.

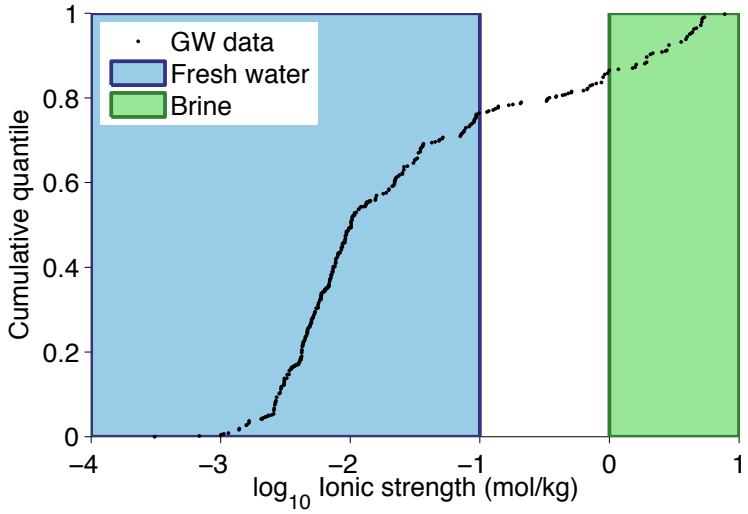

Figure 4.16: Source-size weighted, empirical cumulative distribution of calculated ionic strength in groundwater data set. Ionic strength calculated using PHREEQC (Parkhurst and Appelo 1999).

Comparison of the HREE/MREE ratio to the MREE/LREE ratio succinctly captures the general shape of the REE profile of a sample, greatly simplifying visual comparison of samples. Figure 4.17 plots this scatter for classified groundwater data where all 14 REE were detected (39% of the data set). For freshwater, more than 90% of the samples exhibited MREE/LREE ratios greater than 1, with a median ratio of 1.74 and an IQR from 1.36 to 2.64. HREE-MREE fractionation was more balanced with 53% of samples having HREE/MREE ratios greater than 1, with a median ratio of 1.25 and an IQR from 0.64 to 1.6. These data closely resemble the trends observed in the unclassified data set (not pictured), likely because freshwaters account for a large portion of the total data. Fewer brine and acidic samples are available to plot, however brines appear to cluster with HREE enrichment, with all samples having MREE/LREE ratios greater than 1.0 and only 1 sample having HREE/MREE ratio less than 1.0, while acid samples exhibit convex-down profiles (MREE/LREE $>$ 1 and

HREE/MREE < 1). However, it is difficult to ensure these are representative patterns given the small sample size for these water classes.

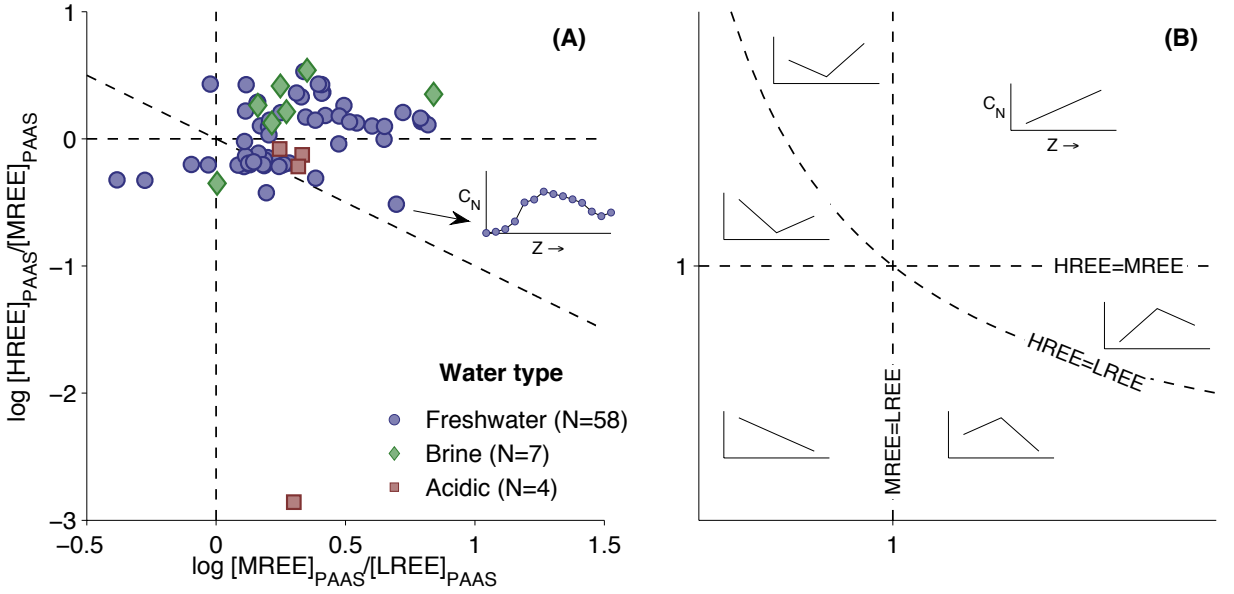

Figure 4.17: (A) Averaged Post-Archaean Average Shale (PAAS) element ratio biplot for chemistry-classified groundwater data with no censoring, and (B) a schematic intended for interpretation, illustrating the general shape of the REE profile for a given sample. Because each marker in (A) is a summary of the REE profile for an individual sample, an inset has been included to show the raw data (PAAS-normalized concentration, C_N, vs. elements in order of increasing atomic number, Z) for one sample. The schematic in (B) is modified from Stolpe et al. (Stolpe et al. 2013) with permission. Copyright 2013 Elsevier. Note that the values in (A) have been log-transformed while the axes of the schematic are linear.

4.3.3 Limitations of assembled data set

The primary goal of this analysis was to understand large-scale REE variability and trends. However, researchers have understood that, because of complex geologies and watershed characteristics, there is significant merit in studying local, small-scale REE systematics. This leads to specialized studies, for example, on the importance of colloids (Dia et al. 2000; Ingri et al. 2000; Pourret et al. 2010; Sholkovitz 1992; Stolpe et al. 2013), phosphate

complexation (Hannigan and Sholkovitz 2001; Johannesson and Lyons 1994; Johannesson et al. 1996b), or organic compounds (Johannesson et al. 2000; Marsac et al. 2011; Pourret et al. 2007a;b; Stern et al. 2007). While this approach yields crucial understanding of these processes, it also leads to a paucity of consistent data for inter-study comparison. Moreover, it could motivate spurious extrapolation of thermodynamic or case study data to unique systems.

4.4 References

Alibo, D. S. and Nozaki, Y. Rare earth elements in seawater: particle association, shale-normalization, and Ce oxidation. *Geochimica et Cosmochimica Acta*, 63(3–4):363–372, 1999.

Bau, M. and Dulski, P. Anthropogenic origin of positive gadolinium anomalies in river waters. *Earth and Planetary Science Letters*, 143(1):245–255, 1996.

Bau, M., Möller, P., and Dulski, P. Yttrium and lanthanides in eastern mediterranean seawater and their fractionation during redox-cycling. *Marine Chemistry*, 56(1–2):123–131, 1997.

Benko, K. L. and Drewes, J. E. Produced water in the western united states: geographical distribution, occurrence, and composition. *Environmental Engineering Science*, 25(2): 239–246, 2008.

Benson, S. M. and Cole, D. R. Co_2 sequestration in deep sedimentary formations. *Elements*, 4(5):325–331, 2008.

Biddau, R., Cidu, R., and Frau, F. Rare earth elements in waters from the albitite-bearing granodiorites of Central Sardinia, Italy. *Chemical Geology*, 182(1):1–14, 2002.

Borrego, J., Carro, B., Lopez-Gonzalez, N., de la Rosa, J., Grande, J., Gomez, T., and de la Torre, M. Effect of acid mine drainage on dissolved rare earth elements geochemistry along a fluvial-estuarine system: the tinto-odiel estuary (sw spain). *Hydrology Research*, 43(3): 262–274, 2012.

Bozau, E., Leblanc, M., Seidel, J. L., and Stärk, H.-J. Light rare earth elements enrichment in an acidic mine lake (lusatia, germany). *Applied Geochemistry*, 19(3):261–271, 2004.

Bradbury, M. H. and Baeyens, B. Sorption of Eu on Na- and Ca-montmorillonites: experimental investigations and modelling with cation exchange and surface complexation. *Geochimica et Cosmochimica Acta*, 66(13):2325–2334, 2002.

Brookins, D. G. Aqueous geochemistry of rare earth elements. *Reviews in Mineralogy and Geochemistry*, 21(1):201–225, 1989.

Brookins, D. G. Eh-pH diagrams for the rare earth elements at 25 °c and one bar pressure. *Geochem. J*, 17(5):223–229, 1983.

Bwire Ojiambo, S., Berry Lyons, W., Welch, K. A., Poreda, R. J., and Johannesson, K. H. Strontium isotopes and rare earth elements as tracers of groundwater–lake water interactions, Lake Naivasha, Kenya. *Applied Geochemistry*, 18(11):1789–1805, 2003.

Cai, C., Li, K., Li, H., and Zhang, B. Evidence for cross formational hot brine flow from integrated ^{87}sr / ^{8}6sr, REE and fluid inclusions of the Ordovician veins in Central Tarim, China. *Applied Geochemistry*, 23(8):2226–2235, 2008.

Castor, S. B. and Hedrick, J. B. *Rare Earth Elements*, pages 769–792. SME, 7 edition, 2006.

Centeno, L. M., Faure, G., Lee, G., and Talnagi, J. Fractionation of chemical elements including the REEs and ^{226}Ra in stream contaminated with coal-mine effluent. *Applied Geochemistry*, 19(7):1085–1095, 2004.

Chaudhuri, S., Totten, M., Clauer, N., Miesse, J., Riepl, G., Massie, S., and Semhi, K. A study yielding the first demonstration that rare-earth elements could be a useful geochemical tracer in formation hydraulic fracturing schemes for enhanced gas and oil production. *The Journal of the Oklahoma City Geological Society*, pages 214–223, 2011.

Chen, Y. W., Chang, L. C., Huang, C. W., and Chu, H. J. Applying genetic algorithm and neural network to the conjunctive use of surface and subsurface water. *Water resources management*, 27(14):4731–4757, 2013.

Cheung, K., Sanei, H., Klassen, P., Mayer, B., and Goodarzi, F. Produced fluids and shallow groundwater in coalbed methane (cbm) producing regions of alberta, canada: Trace element and rare earth element geochemistry. *International Journal of Coal Geology*, 77(3–4):338–349, 2009.

Choi, H.-S., Yun, S.-T., Koh, Y.-K., Mayer, B., Park, S.-S., and Hutcheon, I. Geochemical behavior of rare earth elements during the evolution of co2-rich groundwater: A study from the kangwon district, south korea. *Chemical Geology*, 262(3–4):318–327, 2009.

Coppin, F., Berger, G., Bauer, A., Castet, S., and Loubet, M. Sorption of lanthanides on smectite and kaolinite. *Chemical Geology*, 182(1):57–68, 2002.

De Baar, H. J. W., Bacon, M. P., and Brewer, P. G. Rare-earth distributions with a positive Ce anomaly in the western North-Atlantic ocean. *Nature*, 301(5898):324–327, 1983.

de Boer, J. L. M., Verweij, W., van der Velde-Koerts, T., and Mennes, W. Levels of rare earth elements in Dutch drinking water and its sources. Determination by inductively coupled plasma mass spectrometry and toxicological implications. A pilot study. *Water Research*, 30(1):190–198, 1996.

De Carlo, E. H. and Green, W. J. Rare earth elements in the water column of Lake Vanda, McMurdo Dry Valleys, Antarctica. *Geochimica et Cosmochimica Acta*, 66(8):1323–1333, 2002.

Dia, A., Gruau, G., Olivé-Lauquet, G., Riou, C., Molénat, J., and Curmi, P. The distribution of rare earth elements in groundwaters: assessing the role of source-rock composition, redox changes and colloidal particles. *Geochimica et Cosmochimica Acta*, 64(24):4131–4151, 2000.

Doulati Ardejanii, F., Rooki, R., Jodieri Shokri, B., Eslam Kish, T., Aryafar, A., and Tourani, P. Prediction of rare earth elements in neutral alkaline mine drainage from razi coal mine, golestan province, northeast iran, using general regression neural network. *Journal of Environmental Engineering*, 139(6):896–907, 2013.

Dubinin, A. V. Geochemistry of rare earth elements in the ocean. *Lithology and Mineral Resources*, 39(4):289–307, 2004.

Duncan, T. and Shaw, T. J. The mobility of rare earth elements and redox sensitive elements in the groundwater/seawater mixing zone of a shallow coastal aquifer. *Aquatic Geochemistry*, 9(3):233–255, 2003.

Elderfield, H., Whitfield, M., Burton, J. D., Bacon, M. P., and Liss, P. S. The oceanic chemistry of the rare-earth elements [and discussion]. *Philosophical Transactions of the Royal Society of London. Series A, Mathematical and Physical Sciences*, 325(1583):105–126, 1988.

Elderfield, H., Upstill-Goddard, R., and Sholkovitz, E. R. The rare earth elements in rivers, estuaries, and coastal seas and their significance to the composition of ocean waters. *Geochimica et Cosmochimica Acta*, 54(4):971–991, 1990.

Elderfield, H. and Greaves, M. J. The rare earth elements in seawater. *Nature*, 296(5854): 214–219, 1982.

Erel, Y. and Stolper, E. M. Modeling of rare-earth element partitioning between particles and solution in aquatic environments. *Geochimica et Cosmochimica Acta*, 57(3):513–518, 1993.

Esmaeili-Vardanjani, M., Shamsipour-Dehkordi, R., Eslami, A., Moosaei, F., and Pazand, K. A study of differentiation pattern and rare earth elements migration in geochemical and hydrogeochemical environments of airekan and cheshmeh shotori areas (central iran). *Environmental Earth Sciences*, pages 1–14, 2012.

Foley, S. F. and Jenner, G. A. Trace element partitioning in lamproitic magmas - the Gaussberg olivine leucitite. *Lithos*, 75(1–2):19–38, 2004.

Fu, Q., Yang, L., and Wang, Q. On-line preconcentration with a novel alkyl phosphinic acid extraction resin coupled with inductively coupled plasma mass spectrometry for determination of trace rare earth elements in seawater. *Talanta*, 72(4):1248–1254, 2007.

Gammons, C. H., Wood, S. A., and Nimick, D. A. Diel behavior of rare earth elements in a mountain stream with acidic to neutral pH. *Geochimica et Cosmochimica Acta*, 69(15): 3747–3758, 2005a.

Gammons, C. H., Wood, S. A., Pedrozo, F., Varekamp, J. C., Nelson, B. J., Shope, C. L., and Baffico, G. Hydrogeochemistry and rare earth element behavior in a volcanically acidified watershed in Patagonia, Argentina. *Chemical Geology*, 222(3–4):249–267, 2005b.

Gosselin, D. C., Smith, M. R., Lepel, E. A., and Laul, J. C. Rare earth elements in chloride-rich groundwater, Palo Duro Basin, Texas, USA. *Geochimica et Cosmochimica Acta*, 56 (4):1495–1505, 1992.

Gruau, G., Dia, A., Olivié-Lauquet, G., Davranche, M., and Pinay, G. Controls on the

distribution of rare earth elements in shallow groundwaters. *Water Research*, 38(16): 3576–3586, 2004.

Guo, H., Zhang, B., Wang, G., and Shen, Z. Geochemical controls on arsenic and rare earth elements approximately along a groundwater flow path in the shallow aquifer of the Hetao Basin, Inner Mongolia. *Chemical Geology*, 270(1):117–125, 2010.

Haas, J. R., Shock, E. L., and Sassani, D. C. Rare earth elements in hydrothermal systems: Estimates of standard partial molal thermodynamic properties of aqueous complexes of the rare earth elements at high pressures and temperatures. *Geochimica et Cosmochimica Acta*, 59(21):4329–4350, 1995.

Haley, B. A. and Klinkhammer, G. P. Complete separation of rare earth elements from small volume seawater samples by automated ion chromatography: method development and application to benthic flux. *Marine Chemistry*, 82(3–4):197–220, 2003.

Han, G. and Liu, C.-Q. Dissolved rare earth elements in river waters draining karst terrains in Guizhou Province, China. *Aquatic Geochemistry*, 13(1):95–107, 2007.

Hannigan, R. E. and Sholkovitz, E. R. The development of middle rare earth element enrichments in freshwaters: weathering of phosphate minerals. *Chemical Geology*, 175 (3–4):495–508, 2001.

Hanson, G. N. Rare-earth elements in petrogenetic studies of igneous systems. *Annual Review of Earth and Planetary Sciences*, 8:371–406, 1980.

Harkins, W. D. The evolution of the elements and the stability of complex atoms. I. A new periodic system which shows a relation between the abundance of the elements and the structure of the nuclei of atoms. *Journal of the American Chemical Society*, 39(5):856–879, 1917.

Helsel, D. R. Less than obvious-statistical treatment of data below the detection limit. *Environmental Science & Technology*, 24(12):1766–1774, 1990.

Helsel, D. R. More than obvious: better methods for interpreting nondetect data. *Environmental Science & Technology*, 39(20):419–423, 2005.

Helsel, D. *Statistics for Censored Environmental Data Using Minitab and R*. Wiley, 2 edition, 2012.

Hirata, S., Kajiya, T., Aihara, M., Honda, K., and Shikino, O. Determination of rare earth elements in seawater by on-line column preconcentration inductively coupled plasma mass spectrometry. *Talanta*, 58(6):1185–1194, 2002.

Ingri, J., Widerlund, A., Land, M., Gustafsson, , Andersson, P., and Öhlander, B. Temporal variations in the fractionation of the rare earth elements in a boreal river; the role of colloidal particles. *Chemical Geology*, 166(1–2):23–45, 2000.

Janssen, R. P. T. and Verweij, W. Geochemistry of some rare earth elements in groundwater, Vierlingsbeek, The Netherlands. *Water Research*, 37(6):1320–1350, 2003.

Johannesson, K. H. and Lyons, W. B. The rare-earth element geochemistry of Mono Lake water and the importance of carbonate complexing. *Limnology and Oceanography*, 39(5): 1141–1154, 1994.

Johannesson, K. H., Tang, J., Daniels, J. M., Bounds, W. J., and Burdige, D. J. Rare earth element concentrations and speciation in organic-rich blackwaters of the Great Dismal Swamp, Virginia, USA. *Chemical Geology*, 209(3–4):271–294, 2004.

Johannesson, K. H. and Hendry, M. J. Rare earth element geochemistry of groundwaters from a thick till and clay-rich aquitard sequence, Saskatchewan, Canada. *Geochimica et Cosmochimica Acta*, 64(9):1493–1509, 2000.

Johannesson, K. H. and Lyons, W. B. Rare-earth element geochemistry of Colour lake, an acidic freshwater lake on Axel Heiberg Island, Northwest Territories, Canada. *Chemical Geology*, 119(1–4):209–223, 1995.

Johannesson, K. H., Lyons, W. B., Stetzenbach, K. J., and Byrne, R. H. The solubility control of rare earth elements in natural terrestrial waters and the significance of PO_4^{3-} and CO_3^{2-} in limiting dissolved rare earth concentrations: A review of recent information. *Aquatic Geochemistry*, 1(2):157–173, 1995.

Johannesson, K. H., Lyons, W. B., Yelken, M. A., Gaudette, H. E., and Stetzenbach, K. J. Geochemistry of the rare-earth elements in hypersaline and dilute acidic natural terrestrial waters: Complexation behavior and middle rare-earth element enrichments. *Chemical Geology*, 133(1–4):125–144, 1996a.

Johannesson, K. H., Stetzenbach, K. J., Hodge, V. F., and Berry Lyons, W. Rare earth element complexation behavior in circumneutral pH groundwaters: Assessing the role of carbonate and phosphate ions. *Earth and Planetary Science Letters*, 139(1–2):305–319, 1996b.

Johannesson, K. H., Stetzenbach, K. J., and Hodge, V. F. Rare earth elements as geochemical tracers of regional groundwater mixing. *Geochimica et Cosmochimica Acta*, 61(17):3605–3618, 1997a.

Johannesson, K. H., Stetzenbach, K. J., Hodge, V. F., Kreamer, D. K., and Zhou, X. Delineation of ground-water flow systems in the Southern Great Basin using aqueous rare earth element distributions. *Ground Water*, 35(5):807–819, 1997b.

Johannesson, K. H., Farnham, I. M., Guo, C., and Stetzenbach, K. J. Rare earth element fractionation and concentration variations along a groundwater flow path within a shallow, basin-fill aquifer, southern Nevada, USA. *Geochimica et Cosmochimica Acta*, 63(18):2697–2708, 1999.

Johannesson, K. H., Zhou, X., Guo, C., Stetzenbach, K. J., and Hodge, V. F. Origin of rare earth element signatures in groundwaters of circumneutral pH from southern Nevada and eastern California, USA. *Chemical Geology*, 164(3–4):239–257, 2000.

Karamalidis, A. K., Torres, S. G., Hakala, J. A., Shao, H., Cantrell, K. J., and Carroll, S. Trace metal source terms in carbon sequestration environments. *Environmental Science & Technology*, 47(1):322–329, 2012.

Krauskopf, K. B. Thorium and rare-earth metals as analogs for actinide elements. *Chemical Geology*, 55(3–4):323–335, 1986.

Kulaksiz, S. and Bau, M. Anthropogenic dissolved and colloid/nanoparticle-bound samarium, lanthanum and gadolinium in the rhine river and the impending destruction of the natural rare earth element distribution in rivers. *Earth and Planetary Science Letters*, 362:43–50, 2013.

Kulaksız, S. and Bau, M. Rare earth elements in the rhine river, germany: First case of anthropogenic lanthanum as a dissolved microcontaminant in the hydrosphere. *Environment International*, 37(5):973–979, 2011.

Kulkarni, P., Chellam, S., and Fraser, M. P. Lanthanum and lanthanides in atmospheric fine particles and their apportionment to refinery and petrochemical operations in Houston, TX. *Atmospheric Environment*, 40(3):508–520, 2006.

Kulkarni, P., Chellam, S., and Fraser, M. P. Tracking petroleum refinery emission events using lanthanum and lanthanides as elemental markers for $pm_{2.5}$. *Environmental Science & Technology*, 41(19):6748–6754, 2007.

Laveuf, C. and Cornu, S. A review on the potentiality of rare earth elements to trace pedogenetic processes. *Geoderma*, 154(1):1–12, 2009.

Lawrence, M., Greig, A., Collerson, K., and Kamber, B. Rare earth element and yttrium variability in south east Queensland waterways. *Aquatic Geochemistry*, 12(1):39–72, 2006.

Lee, S.-G., Lee, D.-H., Kim, Y., Chae, B.-G., Kim, W.-Y., and Woo, N.-C. Rare earth elements as indicators of groundwater environment changes in a fractured rock system: evidence from fracture-filling calcite. *Applied Geochemistry*, 18(1):135–143, 2003.

Lepel, E., Laul, J. C., and Smith, M. Rare-earth elements in hot brines (165 to 190°c) from the salton sea geothermal field, 1988.

Lewis, A., Komninou, A., Yardley, B., and Palmer, M. Rare earth element speciation in geothermal fluids from yellowstone national park, wyoming, usa. *Geochimica et Cosmochimica Acta*, 62(4):657–663, 1998.

Lewis, A. J., Palmer, M. R., Sturchio, N. C., and Kemp, A. J. The rare earth element geochemistry of acid-sulphate and acid-sulphate-chloride geothermal systems from Yellow-

stone National Park, Wyoming, USA. *Geochimica et Cosmochimica Acta*, 61(4):695–706, 1997.

Leybourne, M. I., Goodfellow, W. D., Boyle, D. R., and Hall, G. M. Rapid development of negative Ce anomalies in surface waters and contrasting REE patterns in groundwaters associated with Zn—Pb massive sulphide deposits. *Applied Geochemistry*, 15(6):695–723, 2000.

Lide, D. R. *CRC handbook of chemistry and physics*. CRC press, 2012. ISBN 1439880492.

Linberg, R. and Runnels, D. Ground water redox reactions: an analysis of equilibrium state applied to Eh measurements and geochemical modeling. *Science*, 225:925–927, 1984.

Ma, L., Jin, L., and Brantley, S. L. How mineralogy and slope aspect affect REE release and fractionation during shale weathering in the Susquehanna/Shale Hills Critical Zone Observatory. *Chemical Geology*, 290(1):31–49, 2011.

Marsac, R., Davranche, M., Gruau, G., Bouhnik-Le Coz, M., and Dia, A. An improved description of the interactions between rare earth elements and humic acids by modeling: PHREEQC-Model vi coupling. *Geochimica et Cosmochimica Acta*, 75(19):5625–5637, 2011.

McLennan, S. M. Rare earth element geochemistry and the "tetrad" effect. *Geochimica et Cosmochimica Acta*, 58(9):2025–2033, 1994.

Meima, J. A. and Comans, R. N. Geochemical modeling of weathering reactions in municipal solid waste incinerator bottom ash. *Environmental science & technology*, 31(5):1269–1276, 1997.

Michard, A. Rare earth element systematics in hydrothermal fluids. *Geochimica et Cosmochimica Acta*, 53(3):745–750, 1989.

Michard, A., Beaucaire, C., and Michard, G. Uranium and rare earth elements in CO_2-rich waters from Vals-les-Bains (France). *Geochimica et Cosmochimica Acta*, 51(4):901–909, 1987.

Miekeley, N., Coutinho de Jesus, H., Porto da Silveira, C. L., Linsalata, P., and Morse, R. Rare-earth elements in groundwaters from the Osamu Utsumi mine and Morro do Ferro analogue study sites, Poços de Caldas, Brazil. *Journal of Geochemical Exploration*, 45 (1–3):365–387, 1992.

Millero, F. J. Stability constants for the formation of rare earth-inorganic complexes as a function of ionic strength. *Geochimica et Cosmochimica Acta*, 56(8):3123–3132, 1992.

Morel, F. M. and Hering, J. G. *Principles and Applications of Aquatic Chemistry*. John Wiley & Sons, Inc., 1993.

Murray, R. W., Buchholtz ten Brink, M. R., Jones, D. L., Gerlach, D. C., and Russ, G.

Rare earth elements as indicators of different marine depositional environments in chert and shale. *Geology*, 18(3):268–271, 1990.

Möller, P., Dulski, P., Gerstenberger, H., Morteani, G., and Fuganti, A. Rare earth elements, yttrium and H, O, C, Sr, Nd and Pb isotope studies in mineral waters and corresponding rocks from NW-Bohemia, Czech Republic. *Applied Geochemistry*, 13(8):975–994, 1998.

Nance, W. B. and Taylor, S. R. Rare earth element patterns and crustal evolution—i. australian post-archean sedimentary rocks. *Geochimica et Cosmochimica Acta*, 40(12): 1539–1551, 1976.

Nash, W. and Crecraft, H. Partition coefficients for trace elements in silicic magmas. *Geochimica et Cosmochimica Acta*, 49(11):2309–2322, 1985.

Nelson, B. J., Wood, S. A., and Osiensky, J. L. Rare earth element geochemistry of groundwater in the Palouse Basin, northern Idaho–eastern Washington. *Geochemistry: Exploration, Environment, Analysis*, 4(3):227–241, 2004.

Nozaki, Y., Alibo, D.-S., Amakawa, H., Gamo, T., and Hasumoto, H. Dissolved rare earth elements and hydrography in the Sulu Sea. *Geochimica et Cosmochimica Acta*, 63(15): 2171–2181, 1999.

Nozaki, Y., Lerche, D., Alibo, D. S., and Tsutsumi, M. Dissolved indium and rare earth elements in three Japanese rivers and Tokyo Bay: Evidence for anthropogenic Gd and In. *Geochimica et Cosmochimica Acta*, 64(23):3975–3982, 2000.

Négrel, P., Guerrot, C., Cocherie, A., Azaroual, M., Brach, M., and Fouillac, C. Rare earth elements, neodymium and strontium isotopic systematics in mineral waters: evidence from the Massif Central, France. *Applied Geochemistry*, 15(9):1345–1367, 2000.

Otsuka, M. and Terakado, Y. Rare earth element abundances in high phosphorus and low iron groundwaters from the Nishinomiya district, Japan: Variations in Ce anomaly, redox state and heavy rare earth enrichment. *Geochemical Journal*, 37(1):1–19, 2003.

Palarea-Albaladejo, J., Martín-Fernández, J., and Olea, R. Non-detect bootstrap method for estimating distributional parameters of compositional samples revisited: a multivariate approach. In *Proceedings of the 4th international workshop on compositional data analysis, San Feliu de Guixols, Spain*, pages 1–9, 2011.

Parkhurst, D. L. and Appelo, C. PHREEQC, 1999.

Piepgras, D. J. and Jacobsen, S. B. The behavior of rare earth elements in seawater: Precise determination of variations in the north pacific water column. *Geochimica et Cosmochimica Acta*, 56(5):1851–1862, 1992.

Piper, A. M. A graphic procedure in the geochemical interpretation of water-analyses. *Transactions, American Geophysical Union*, 25:914–928, 1944.

Pitzer, K. S. Thermodynamics of electrolytes. i. theoretical basis and general equations. *The Journal of Physical Chemistry*, 77(2):268–277, 1973.

Pourret, O., Davranche, M., Gruau, G., and Dia, A. Rare earth elements complexation with humic acid. *Chemical Geology*, 243(1–2):128–141, 2007a.

Pourret, O., Davranche, M., Gruau, G., and Dia, A. Competition between humic acid and carbonates for rare earth elements complexation. *Journal of Colloid and Interface Science*, 305(1):25–31, 2007b.

Pourret, O., Gruau, G., Dia, A., Davranche, M., and Molénat, J. Colloidal control on the distribution of rare earth elements in shallow groundwaters. *Aquatic Geochemistry*, 16(1): 31–59, 2010.

Quinn, K. A., Byrne, R. H., and Schijf, J. Sorption of yttrium and rare earth elements by amorphous ferric hydroxide: Influence of ph and ionic strength. *Marine Chemistry*, 99 (1–4):128–150, 2006.

R Core Team. *R: A Language and Environment for Statistical Computing*. R Foundation for Statistical Computing, Vienna, Austria, 2014. URL http://www.R-project.org/.

Romero, F. M., Prol-Ledesma, R. M., Canet, C., Alvares, L. N., and Pérez-Vázquez, R. Acid drainage at the inactive santa lucia mine, western cuba: Natural attenuation of arsenic, barium and lead, and geochemical behavior of rare earth elements. *Applied Geochemistry*, 25(5):716–727, 2010.

Sanada, T., Takamatsu, N., and Yoshiike, Y. Geochemical interpretation of long-term variations in rare earth element concentrations in acidic hot spring waters from the Tamagawa geothermal area, Japan. *Geothermics*, 35(2):141–155, 2006.

Schijf, J., De Baar, H. J. W., and Millero, F. J. Vertical distributions and speciation of dissolved rare earth elements in the anoxic brines of Bannock Basin, eastern Mediterranean Sea. *Geochimica et Cosmochimica Acta*, 59(16):3285–3299, 1995.

Sholkovitz, E. R. Chemical evolution of rare earth elements: fractionation between colloidal and solution phases of filtered river water. *Earth and Planetary Science Letters*, 114(1): 77–84, 1992.

Sholkovitz, E. R., Landing, W. M., and Lewis, B. L. Ocean particle chemistry: The fractionation of rare earth elements between suspended particles and seawater. *Geochimica et Cosmochimica Acta*, 58(6):1567–1579, 1994.

Siebert, C., Rosenthal, E., Möller, P., Rödiger, T., and Meiler, M. The hydrochemical identification of groundwater flowing to the bet she'an-harod multiaquifer system (lower jordan valley) by rare earth elements, yttrium, stable isotopes (h, o) and tritium. *Applied Geochemistry*, 27(3):703–714, 2012.

Singh, A., Neuhauser, E. F., Azzolina, N. A., Distler, M., Anders, K. M., Doroski, M. A.,

and Rabideau, A. J. Statistical techniques for analyzing of soil vapor intrusion data: A case study of manufactured gas plant sites. *J. Air Waste Manage. Assoc.*, 63(2), 2013.

Smedley, P. L. The geochemistry of rare earth elements in groundwater from the Carnmenellis area, southwest England. *Geochimica et Cosmochimica Acta*, 55(10):2767–2779, 1991.

Stern, J. C., Sonke, J. E., and Salters, V. J. M. A capillary electrophoresis-ICP-MS study of rare earth element complexation by humic acids. *Chemical Geology*, 246(3–4):170–180, 2007.

Stolpe, B., Guo, L., and Shiller, A. M. Binding and transport of rare earth elements by organic and iron-rich nanocolloids in Alaskan rivers, as revealed by field-flow fractionation and ICP-MS. *Geochimica et Cosmochimica Acta*, 106:446–462, 2013.

Sverjensky, D. A. Europium redox equilibria in aqueous solution. *Earth and Planetary Science Letters*, 67(1):70–78, 1984.

Tang, J. and Johannesson, K. H. Controls on the geochemistry of rare earth elements along a groundwater flow path in the Carrizo Sand aquifer, Texas, USA. *Chemical Geology*, 225 (1–2):156–171, 2006.

Tang, J. and Johannesson, K. H. Rare earth elements adsorption onto Carrizo sand: Influence of strong solution complexation. *Chemical Geology*, 279(3–4):120–133, 2010.

Tang, J. and Johannesson, K. H. Speciation of rare earth elements in natural terrestrial waters: assessing the role of dissolved organic matter from the modeling approach. *Geochimica et Cosmochimica Acta*, 67(13):2321–2339, 2003.

Terakado, Y. and Masuda, A. The coprecipitation of rare-earth elements with calcite and aragonite. *Chemical Geology*, 69(1–2):103–110, 1988.

Tesmer, M., Möller, P., Wieland, S., Jahnke, C., Voigt, H., and Pekdeger, A. Deep reaching fluid flow in the North East German Basin: origin and processes of groundwater salinisation. *Hydrogeology Journal*, 15(7):1291–1306, 2007.

Tricca, A., Stille, P., Steinmann, M., Kiefel, B., Samuel, J., and Eikenberg, J. Rare earth elements and Sr and Nd isotopic compositions of dissolved and suspended loads from small river systems in the Vosges mountains (France), the river Rhine and groundwater. *Chemical Geology*, 160(1–2):139–158, 1999.

Tweed, S. O., Weaver, T. R., Cartwright, I., and Schaefer, B. Behavior of rare earth elements in groundwater during flow and mixing in fractured rock aquifers: An example from the Dandenong Ranges, southeast Australia. *Chemical Geology*, 234(3–4):291–307, 2006.

Verplanck, P. L., Nordstrom, D. K., Taylor, H. E., and Kimball, B. A. Rare earth element partitioning between hydrous ferric oxides and acid mine water during iron oxidation. *Applied Geochemistry*, 19(8):1339–1354, 2004.

Vicente, O., Padró, A., Martinez, L., Olsina, R., and Marchevsky, E. Determination of some rare earth elements in seawater by inductively coupled plasma mass spectrometry using flow injection preconcentration. *Spectrochimica Acta Part B: Atomic Spectroscopy*, 53(9): 1281–1287, 1998.

Willis, S. S. and Johannesson, K. H. Controls on the geochemistry of rare earth elements in sediments and groundwaters of the Aquia aquifer, Maryland, USA. *Chemical Geology*, 285(1–4):32–49, 2011.

Wood, S. A. The aqueous geochemistry of the rare-earth elements and yttrium 1. Review of available low-temperature data for inorganic complexes and the inorganic REE speciation of natural waters. *Chemical Geology*, 82:159–186, 1990.

Worrall, F. and Pearson, D. G. Water-rock interaction in an acidic mine discharge as indicated by rare earth element patterns. *Geochimica et Cosmochimica Acta*, 65(18):3027–3040, 2001a.

Worrall, F. and Pearson, D. G. The development of acidic groundwaters in coal-bearing strata: Part I. Rare earth element fingerprinting. *Applied Geochemistry*, 16(13):1465–1480, 2001b.

Yan, X.-P., Kerrich, R., and Hendry, M. J. Distribution of the rare earth elements in porewaters from a clay-rich aquitard sequence, Saskatchewan, Canada. *Chemical Geology*, 176(1–4):151–172, 2001.

Zhang, C., Wang, L., Zhang, S., and Li, X. Geochemistry of rare earth elements in the mainstream of the Yangtze River, China. *Applied Geochemistry*, 13(4):451–462, 1998.

Zhao, F., Cong, Z., Sun, H., and Ren, D. The geochemistry of rare earth elements (REE) in acid mine drainage from the sitai coal mine, shanxi province, north china. *International Journal of Coal Geology*, 70(1–3):184–192, 2007.

Zhu, Y., Itoh, A., Fujimori, E., Umemura, T., and Haraguchi, H. Determination of rare earth elements in seawater by ICP-MS after preconcentration with a chelating resin-packed minicolumn. *Journal of Alloys and Compounds*, 408–412(0):985–988, 2006.

Åström, M. and Corin, N. Distribution of rare earth elements in anionic, cationic and particulate fractions in boreal humus-rich streams affected by acid sulphate soils. *Water Research*, 37(2):273–280, 2003.

Chapter 5

Determination of rare earth elements in hypersaline solutions using low-volume, liquid-liquid extraction

This chapter is adapted from a publication by the same name, co-authored by David A. Dzombak and Athanasios K. Karamalidis. This paper is citable as:

Noack, C. W.; Dzombak, D. A.; Karamalidis, A. K., Determination of Rare Earth Elements in Hypersaline Solutions Using Low-Volume, Liquid-Liquid Extraction. *Environ. Sci. Technol.* **2015**, *49*, (16) 9423-9430

My contributions to this work were the experimental design; execution of experiments including ICP-MS analysis; data analysis and visualization; interpretation of results; and drafting of the manuscript.

Abstract

Complex, hypersaline brines — including those co-produced with oil and gas, rejected from desalination technologies, or used as working fluids for geothermal electricity generation — could contain critical materials such as the rare earth elements (REE) in valuable concentrations. Accurate quantitation of these analytes in complex, aqueous matrices is necessary for evaluation and implementation of systems aimed at recovering those critical materials. However, most analytical methods for measuring trace metals have not been validated for highly saline and/or chemically complex brines. Here we modified and optimized previously published liquid-liquid extraction (LLE) techniques [Shabani et al., *Anal. Chem.* 1990, 62 (24) 2709-2714; Lawrence and Kamber, *Geostand. Geoanal. Res.* 2007, 31 (2) 95-103], using bis(2-ethylhexyl) phosphate as the extractant in a heptane diluent, and studied its efficacy for REE recovery as a function of three primary variables: background salinity (as NaCl), concentration of a competing species (here Fe), and concentration of dissolved organic carbon (DOC). Results showed that the modified LLE was robust to a range of salinity, Fe, and DOC concentrations studied as well as constant, elevated Ba concentrations. With proper characterization of the natural samples of interest, this method could be deployed for accurate analysis of REE in small volumes of hyper-saline and chemically complex brines.

5.1 Introduction

The rare earth elements (REE) are among the most frequently cited critical materials for clean energy and high-tech manufacturing (APS 2011; Bauer et al. 2010). The unique and varied properties of REE have led to their application in more consumer products than nearly any other element group (Castor and Hedrick 2006). REE are mostly obtained from mining

and processing of REE-enriched ores (Bauer et al. 2010). While economically preferred, mining is laborious with a significant environmental burden, and inexpensive alternative sources of critical materials are sought after resources.

Aqueous byproduct or waste streams, both natural and industrial, are potential sources of the REE and other critical materials. With increasing global interest in geothermal energy (Lund et al. 2011), development of unconventional oil and gas resources (e.g. hydraulic fracturing of organic rich shales) (U.S. Energy Information Administration 2013), and desalination technologies (Elimelech and Phillip 2011; Shannon et al. 2008), large volumes of waste brines are being managed and processed at great expense. Development of technologies for recovery of valuable byproducts, such as the REE, from these waste streams could improve the economics of these technologies while diversifying available critical material resources. Development of such technologies requires accurate determination of the source REE concentration in order to develop and implement recovery systems. However, precise quantitation of REE in complex matrices like brines is a significant challenge for conventional instrumentation such as inductively coupled plasma mass spectrometry (ICP-MS) (Agatemor and Beauchemin 2011).

There exists a dearth of methodologies in the analytical literature for quantitation of REE in brines by ICP-MS. Many approaches have been applied for separation and concentration of REE from aqueous media including solid-phase extraction (SPE) (Benkhedda et al. 2001; Fu et al. 2007; Haley and Klinkhammer 2003; Halicz et al. 1996; Hirata et al. 2002; Kajiya et al. 2004; Katarina et al. 2009; Kim et al. 2010; Kumar et al. 2011; Kühn and Kriews 2000; Möller et al. 1992; Stetzenbach et al. 1994; Vicente et al. 1998; Wen et al. 1999; Willie and Sturgeon 2001; Zhang et al. 1998; Zhu et al. 2009), co-precipitation (co-ppt) (Raso et al. 2013; Shannon and Wood 2005; Shaw et al. 2003), and liquid-liquid extraction (LLE) (Kimura 1960; 1961; Lawrence and Kamber 2007; Shabani et al. 1990). However, nearly all studies in the

analytical chemistry literature have focused on fresh water or seawater matrices, neglecting hypersaline waters (i.e. more concentrated than $\sim$ 0.7 M NaCl or seawater). Despite this deficiency, approximately 14% of published measurements of REE in groundwater constitute brine samples (greater than 1 eq/kg ionic strength Noack et al. 2014), with these analyses utilizing methodologies not explicitly validated for extreme salinity.

Commonly applied separation techniques such as SPE and co-ppt may lack the robustness necessary to analyze REE in hypersaline brines. For example, high dissolved organic carbon may lead to fouling of column-based SPE while high dissolved metal loads may lead to saturation of the surface sites responsible for REE binding. Oliveira et al. (2011) ascribed diminished Zn recovery in 166‰ salinity produced water to competitive sorption of matrix cations on their iminodiacetate resin. Similarly, excessive cations in hypersaline solutions may screen the REE from sorption sites during co-ppt, a phenomenon noted by Nelson et al. (2014) for Ra determination in produced waters from the Marcellus Shale by both $BaSO_4$ and MnO_2 co-ppt. Moreover, at the elevated pH necessary for SPE and co-ppt techniques, the formation of energetically favorable, neutral- or negatively-charged aqueous complexes of the REE (with both organic and inorganic ligands) can further limit REE-particle partitioning (Erel and Stolper 1993).

Liquid-liquid extractions are potentially robust to all of these conditions and represent an attractive alternative for REE separation from hypersaline solutions (Nash 1993). Since LLE of REE from highly acidic solutions has been thoroughly studied for separation of lanthanides and actinides during nuclear fuel reprocessing (e.g. Nilsson and Nash 2007; Weaver and Kappelmann 1964) elevated pH is not required of LLE techniques. Moreover, electrolyte theory dictates that increased sample salinity should enhance chemical partitioning (through salting out of neutral/micellar REE-organic ligand complexes from the aqueous feed to the organic solvent) and physical phase separation (by collapsing the electric double layer of

the organic droplets, hastening coalescence). A primary obstacle in extraction of hydrophilic metals to a hydrophobic, organic phase is the dehydration of the metal cations in the aqueous phase. However, increasing salt concentrations decrease the effective concentration of water in the solution available for hydration of the target metal cations (REE), improving the energetics of the extraction (Nash 1993).

In this work, efficiency of REE separation and concentration from synthetic brines using a LLE method for quantitative analysis was studied. The LLE method was adapted, modified, and optimized from previously published studies (Lawrence and Kamber 2007; Shabani et al. 1990). For the LLE, a common ligand used for REE complexation and extraction, bis(2-ethylhexyl) phosphate (HDEHP), was studied in a heptane diluent. The objectives of this work were to: (1) evaluate the feasibility of REE recovery from small volumes of hypersaline solutions by LLE, (2) optimize the LLE methodology for high salinity brines, and (3) study the influence of brine composition on REE recovery.

5.2 Modified liquid-liquid extraction procedure

The modified LLE method adheres to many of the physical steps of the methods originally developed by Shabani et al. (1990) and Lawrence and Kamber (2007), but following optimization, differs in the operating conditions. A schematic flowsheet of the process is shown in Figure 5.1. The process involved sample preparation, followed by three cycles of extraction, whereby the REE were complexed by the HDEHP ligand and brought into the organic phase, leaving an REE-free, waste brine. Matrix elements were rinsed from the organic phase with dilute acid, and, finally, the REE were recovered by four cycles of elution with strong acid. This REE-loaded aqueous phase was then analyzed by ICP-MS. The details of the process are described in following. Details of sample preparation, instrumentation,

analytical protocols, and data analysis methods are presented in Section 5.3.

Synthetic brine solutions were adjusted to pH 2.5 in 50 mL PP centrifuge tubes with HNO_3 and subsequently split into 10 g aliquots in 15 mL PP centrifuge tubes for replicate experiments. For each aliquot or sample, the process for REE extraction and recovery is as follows. One (1) mL of 0.25 M HDEHP in heptane was added to the aqueous solution. HDEHP was used as complexing agent for REE. The phases were emulsified and mixed end over end for 10 minutes. The phases were separated by centrifugation at 6,000×g for 10 minutes and the light organic phase was removed from the centrifuge tube via pipette and accumulated in a new centrifuge tube, retaining the aqueous phase in the original tube. This process, whereby the REE are complexed with HDEHP and partitioned into the heptane (termed forward extraction), was completed a total of three times. Following the third forward extraction, the aqueous phase was discarded.

To remove any matrix (Na, Fe, etc.) and interfering species (i.e. Ba) that partitioned during forward extraction, the accumulated organic phase (3 mL total) was rinsed with 1 mL of pH 1.5 HCl. This mixture was emulsified and separated by the same methods as the forward extraction. Once separated, the dense aqueous phase was removed via pipette and discarded.

A concentrated acid solution was used to dissociate the REE-HDEHP complexes and return the REE to an aqueous phase (termed back extraction). To decrease the REE-HDEHP complexation strength and encourage complete recovery (Shabani et al. 1990), 1 mL of 1-octanol was added to the organic phase. Back extraction was achieved with four, sequential steps of stripping with 1 mL of 6.0 N HCl (collecting the eluted REE in a total of 4 mL acid). As with the forward extraction, the sample was emulsified and mixed end over end for 10 minutes and then separated via centrifugation at 6,000×g for 10 minutes. After centrifugation the aqueous phase was removed via pipette and accumulated in a separate

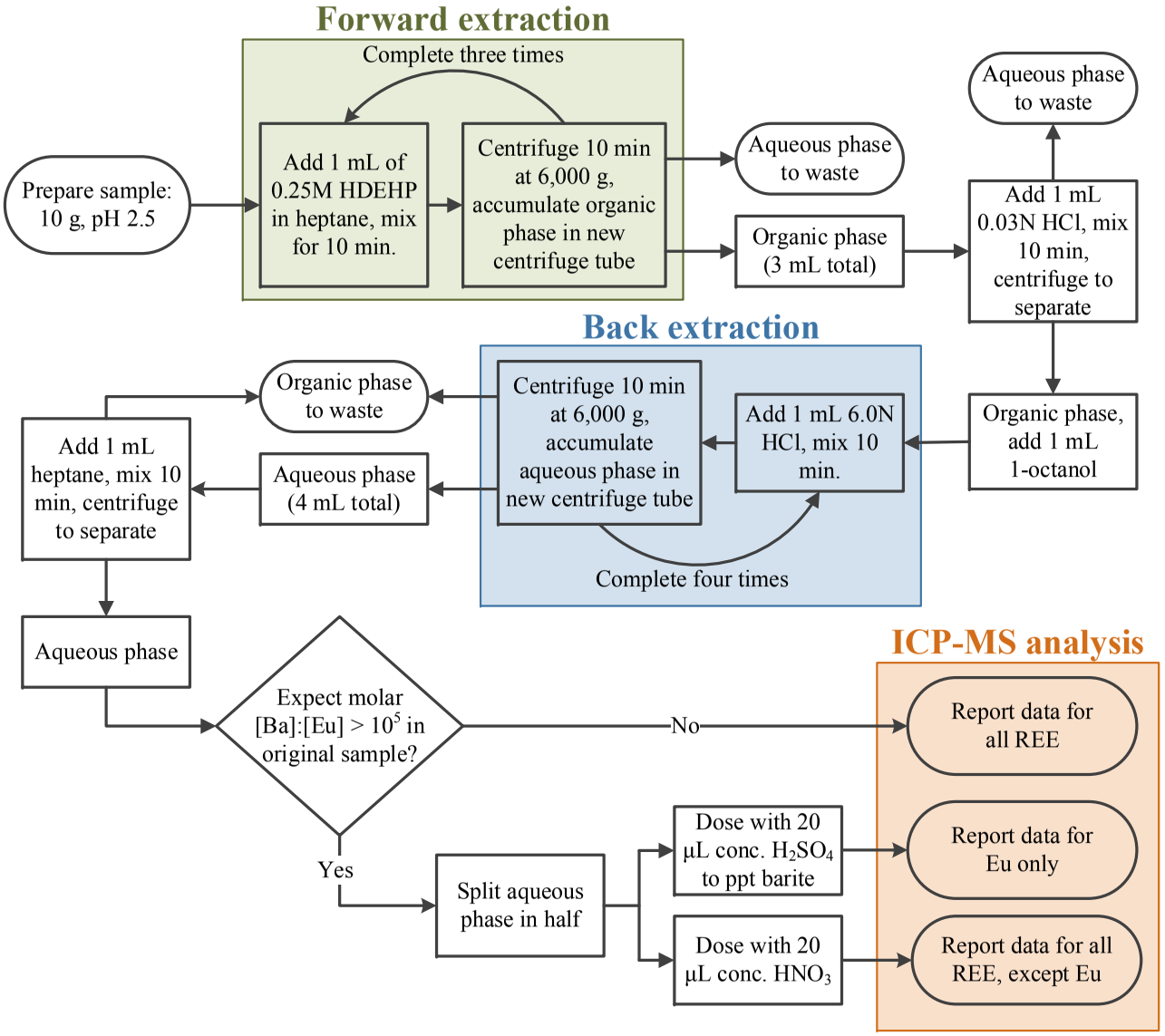

Figure 5.1: Liquid-liquid extraction method flowsheet for separation and concentration of REE from small volume, hypersaline brines. The decision node for the [Ba]:[Eu] molar ratio assumes a BaO^+ formation rate on the order of 0.1% in the ICP-MS.

centrifuge tube, retaining the organic phase in the original tube. Following the four back-extractions, the organic phase was discarded.

The collected acid volume (4 mL) was then rinsed with 1 mL of heptane to remove any dissolved organics from the aqueous phase. Phase mixing and separation were accomplished in the same manner as all other steps. Following centrifugation, the dense aqueous phase was removed and analyzed.

Preliminary experiments (Figure C.2) indicated that, while Ba was successfully removed in the course of the LLE ($>$ 99.9% average reduction) and the HEHe-mode collision cell in the ICP-MS was successfully limiting $^{135}Ba^{16}O^{+}$ interferences with $^{151}Eu^{+}$ ($^{135}Ba^{16}O^{+}$:$^{135}Ba^{+}$ $\sim$ 0.2% on average), initial Ba concentrations were so high that ppb level, background Eu concentrations were observed (Figure C.3). Thus, in order to determine Eu accurately in these synthetic brines an additional step was tested, where an aliquot of the final, collected acid volume was dosed with 20 µL concentrated sulfuric acid (H_2SO_4) to precipitate any remaining barium as barite ($BaSO_4$). Efficiency of Ba removal after H_2SO_4 addition is compared in Figure C.2B and C.2D. It should be noted that this step was unnecessary for samples without Ba.

The methodology of Jenner et al. (1990) as modified by McGinnis et al. (1997) was employed to correct for matrix effects, isobaric interferences, and instrument drift during ICP-MS analysis. For each sample a 2 mL aliquot was spiked with 2 mL of a mixed element standard (5% HNO_3 background) while a separate 2 mL aliquot was diluted with 2 mL of blank 5% HNO_3. These solutions were analyzed sequentially to examine sample-specific matrix effects and were followed by a 5% HNO_3 flush. At the beginning of each analysis run and after every third sample, two separate standard solutions and an analytical blank were analyzed to monitor instrument drift and isobaric, polyatomic interferences (e.g. $^{135}Ba^{16}O^{+}$ on $^{151}Eu^{+}$ and light REE-oxides on heavy REE). Eight, serially-diluted, multi-element standard solutions

ranging in concentration from 50 ppt to 100 ppb were analyzed at the beginning and end of each run to confirm the linearity assumed by the internal/external calibration. Typical analytical uncertainty was between 3 and 5%. Because of high backgrounds of Gd in our laboratory and high Ba in the experiments, oxide corrections for $^{137}Ba^{16}O^{+}$ interference on $^{151}Eu^{+}$ and $^{157}Gd^{16}O^{+}$ on $^{173}Yb^{+}$ were applied as in Aries et al. (Aries et al. 2000) after ICP-MS analysis. Further details on this analytical method are provided in Appendix C.

5.3 Materials and methods

5.3.1 Chemicals and equipment

For the LLE, n-heptane (Chromasolv®; Lot # SHBC0837V), 1-octanol (Chromasolv®; Lot # SHBC6245V), and HDEHP (99.7% purity; Lot # MKBK0176V) were acquired from Sigma Aldrich. Nitric acid (HNO_3; BDH ARISTAR® Plus, VWR; assay 69 wt.%; Lot # 1113050) was used for sample pH adjustment and as the solvent for all analyses. Hydrochloric acid (HCl; BDH ARISTAR® Plus, VWR; 35 wt.%; Lot # 4113083) was used for matrix rinsing and REE back-extraction in the LLE. Chloride salts of Na (Sigma Aldrich; $\geq$ 99% purity), Ba (Alfa Aesar; $\geq$ 99.998% purity), and Fe (Sigma Aldrich; $\geq$ 99.9% purity, trace metal basis) and valeric acid (Alfa Aesar; 99% purity) were used for preparation of synthetic brines. Single element standard solutions (1000 µg/L) of the REE and all elements necessary for internal and external standardization were obtained from Inorganic Ventures. Polypropylene (PP) centrifuge tubes were used in the LLE and glass volumetric flasks were used to prepare organic phases. Ultrapure water (ASTM Type I, 18.2 MΩ/cm) was used for sample preparation and was prepared using a Barnstead NANOpure® water purification system. An OrionTM 8165BNWP ROSSTM Sure-FlowTM pH electrode (Thermo Scientific), coupled

to an accumetTM XL600 meter (Fisher Scientific), was used for pH measurements of high-total dissolved solid (TDS) solutions. The pH meter was calibrated with pH 2.0, 4.0, and 7.0 standards daily. All samples were prepared gravimetrically using an analytical balance with 0.01 mg precision (Adam Equipment).

All analyses were performed on an Agilent 7700x ICP-MS with HEHe-mode octopole reaction cell. Operating parameters were optimized daily via the auto-tune function of the Agilent MassHunter software using 1000:1 diluted Agilent tuning solutions; typical operating parameters and monitored analyte masses are given in Table 5.1.

5.3.2 Recovery analysis by surrogate recovery

In the absence of a high-salinity, certified reference material for REE, the IUPAC recommended methodology of surrogate recovery (Thompson et al. 1999) was used to study the recovery of REE by this LLE method. Synthetic brine samples were either left blank or spiked with constant amounts of REE. The difference in results between these samples yielded the mass of the spiked analytes recovered by the LLE method. Additionally, indium was included in the spike solution as it is commonly employed as an internal standard for REE separation to monitor recovery (Shabani et al. 1990; Zawisza et al. 2011). Data below the instrument detection limit (DL) were assigned a value of 0.5×DL for computation; this occurred for roughly 41% of all the REE in the unspiked samples and 4% in the spiked samples.

5.3.3 Preparation of synthetic brines

In addition to optimization of operating parameters, the methodology must be validated for complex brine solutions. The complexity of the brine is a function of background salinity and interfering compounds (both inorganic and organic). This was investigated in two

Table 5.1: Typical operating conditions for ICP-MS analysis. Analysis performed on Agilent 7700x using oxygen-free argon as the carrier and dilution gas and ultra high-purity helium in the reaction cell. Conditions determined using 1000:1 diluted Agilent tuning solution. For elements where multiple mass-to-charge ratios were monitored, ^{148}Sm, ^{151}Eu, and ^{157}Gd were used in data analysis.

	Parameter	Value
Plasma		
	RF power	1600 W
	Nebulizer pump rate	0.10 rps
	Carrier argon flow rate	0.61 L/min
	Dilution argon flow rate	0.36 L/min
Lenses		
	Extract 1	0.0 V
	Extract 2	-200.0 V
	Omega bias	-110 V
	Omega lens	9.6 V
	Cell entrance	-110 V
	Cell exit	-150 V
	Deflect	-74.8 V
	Plate bias	-150 V
Octopole reaction cell		
	Octopole bias	-100.0 V
	Octopole RF	200 V
	He flow rate	10 mL/min
	Energy discrimination	7.0 V
Data aquisition		
	Replicates	5
	Integration time	0.3 s
Masses monitored		
	^{45}Sc, ^{89}Y, ^{115}In, ^{135}Ba, ^{137}Ba, ^{139}La, ^{140}Ce, ^{141}Pr, ^{145}Nd, ^{147}Sm, ^{148}Sm, ^{151}Eu, ^{153}Eu, ^{157}Gd, ^{158}Gd, ^{159}Tb, ^{163}Dy, ^{165}Ho, ^{167}Er, ^{169}Tm, ^{173}Yb, ^{175}Lu	
Oxides and doubly charged		
	$^{140}Ce^{16}O^{+}/^{140}Ce < 2.1\%$	
	$^{140}Ce^{2+}/^{140}Ce < 1.6\%$	

stages. First, simple solutions (1 m and 5 m NaCl) were used to evaluate feasibility. Second, compositional complexity was explored via a uniform shell, or Doehlert, experimental design (Doehlert 1970), varying NaCl, Fe, and dissolved organic carbon (DOC) concentrations.

The concentrations of background salinity and interfering compounds were chosen to match reported value ranges found in studies of produced waters from unconventional gas development in the Marcellus Shale (Barbot et al. 2013; Gregory et al. 2011; Haluszczak et al. 2013; Murali Mohan et al. 2013; Vidic et al. 2013), however the range of compositions studied is similar to other deep, basinal brines (Kharaka et al. 2000). Dissolved organic carbon was modeled with pentanoic (or valeric) acid, a common component of deep, saline brines (Kharaka et al. 2000), with representative metal-complexing functionality. Additionally, organic acids have been shown to be a significant component of DOC in produced waters from the Marcellus Shale (Wolford 2011). The parameters of interest — concentrations of NaCl, Fe, and DOC — were scaled linearly. Experimental conditions for variability in salinity, Fe concentration, and DOC concentration are given in Table 5.2. For all experiments the concentration of each REE (along with indium) was set at 500 ppt (parts per trillion), a value that falls between the 45th percentile (for Tm) and the 1st percentile (for La) of natural REE distributions in groundwater (Noack et al. 2014). Total dissolved Ba was held constant at 2,000 ppm, roughly the average concentration observed by Barbot, et al. (Barbot et al. 2013) for Marcellus Shale produced waters. Results of these experiments were analyzed by multiple linear regression (MLR) to determine which parameters of the synthetic brine influenced the recovery most strongly.

Table 5.2: Doehlert experimental design matrix for LLE validation in chemically complex brines. Doehlert coding for each experiment are given in parentheses next to the parameter value. All variables were varied arithmetically. Because all samples were prepared gravimetrically, units of molality (m; mol/kg solution) are used for NaCl concentrations.

Exp.	[NaCl] (m)	[Fe] (ppm)	[DOC] (ppm-C)
1	2 (0)	40 (0)	200 (0)
2	3.5 (1)	40 (0)	200 (0)
3	2.75 (0.5)	74.6 (0.866)	200 (0)
4	2.75 (0.5)	51.6 (0.289)	363 (0.817)
5	0.5 (-1)	40 (0)	200 (0)
6	1.25 (-0.5)	5.4 (-0.866)	200 (0)
7	1.25 (-0.5)	28.4 (-0.289)	37 (-0.817)
8	2.75 (0.5)	5.4 (-0.866)	200 (0)
9	2.75 (0.5)	28.4 (-0.289)	37 (-0.817)
10	1.25 (-0.5)	74.6 (0.866)	200 (0)
11	2 (0)	63.1 (0.577)	37 (-0.817)
12	1.25 (-0.5)	51.6 (0.289)	363 (0.817)
13	2 (0)	16.9 (-0.577)	363 (0.817)

5.3.4 Optimization of liquid-liquid operation parameters

Preliminary experiments utilizing LLE conditions described by Shabani et al. (1990) and Lawrence and Kamber (2007) were unable to achieve high or consistent recovery of the REE (Figure 5.2A,B). These experiments showed recovery $< 80\%$ for all elements in all replicates, with significant variability, as well as preferential recovery of the MREE over the L- and HREE. It should be noted that both Shabani et al. (1990) and Lawrence and Kamber (2007) employed a mixture of mono- and di-ester phosphonic acids as the chelating ligand. This ligand combination was also explored, however preliminary experiments provided poor results compared to the pure diester (HDEHP) under the same conditions and was not studied further.

In order to optimize method performance, a linear model (Equation 5.1) was fit by ordinary least-squares in `R` (R Core Team 2014), using the datasets of Kimura (1960) and Kimura (1961). The relationship between the response (organic-aqueous distribution coefficient, K_d)

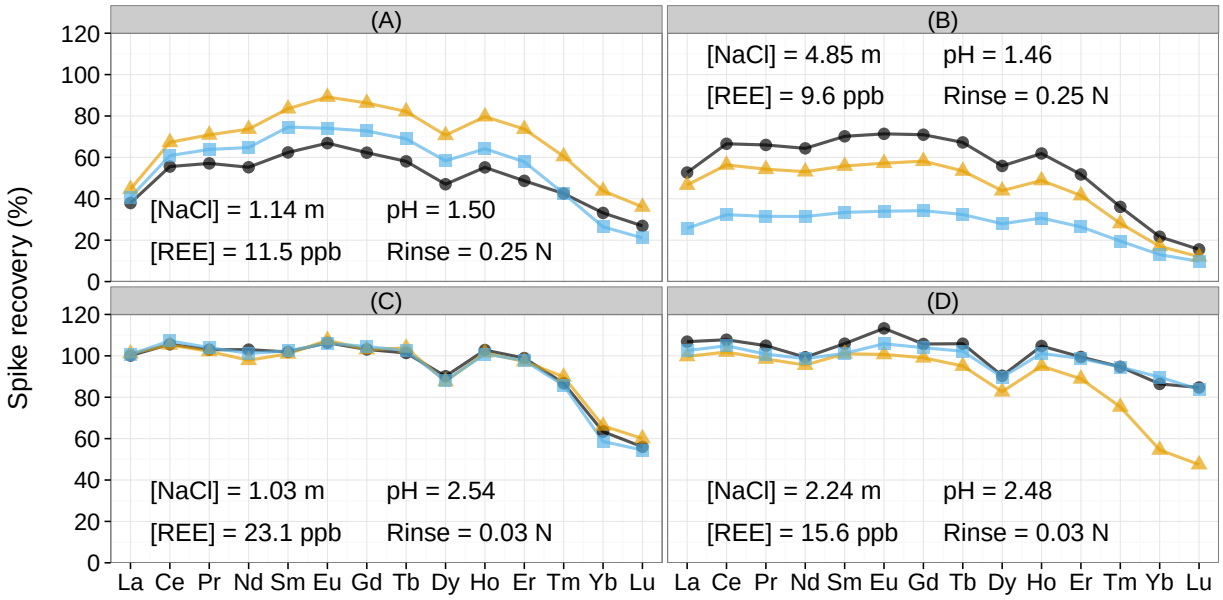

Figure 5.2: REE recovery from 10 g samples of synthetic brine solutions using LLE conditions recommended by Shabani et al. (1990) (A, B) and "optimal" conditions predicted by multiple linear regression (C, D). Each experiment was performed in triplicate (separate colors/shapes of plot) and the experimental conditions are shown in the subfigures.

and each of the predictors (solution acidity $[ACY]$, and ligand concentration $[L]$) is shown to be independently log-log linear. Therefore the variables in this model correspond to log values. Data for fitting of this model were extracted from Figure 1 of Kimura (1960) for K_d vs. $[ACY]$ at constant $[L]$ and from Figure 1 of Kimura (1961) for K_d vs. $[L]$ at constant $[ACY]$. This estimation of parameter values reflects the dependence of $\log K_d$ on $\log[ACY]$ (β_{ACY}) and on $\log[L]$ (β_L) as well as a constant intercept (β_0). Parameter estimates for Equation 5.1 with associated uncertainty are presented in Table C.1.

$$\log K_d = \beta_{ACY} \cdot \log[ACY] + \beta_L \cdot \log[L] + \beta_0 \tag{5.1}$$

The extraction of REE from the aqueous to the organic phase is calculated using the predicted K_d values based on mass balance. The fraction of REE mass in the organic phase (R_{org}) for equilibrium between an aqueous phase (with volume V_{aq}) and an organic phase (with volume V_{org}) is calculated by Equation 5.2.

$$R_{org} = \frac{1}{1 + \frac{V_{aq}}{V_{org}} \cdot K_d^{-1}} \tag{5.2}$$

The system can be represented as independent LLE in series since the phases are separated after each extraction step. Thus, the overall partitioning of REE from the brine to the organic phase (R_{tot}) in the forward extraction can be calculated for n sequential extractions with Equation 5.3. This allows for determination of the number of extractions necessary for quantitative recovery of REE. The analysis is simply reversed to examine the elution properties of REE from the organic phase back into an aqueous phase.

$$R_{tot} = \sum_{i=1}^{n} R_{org} \left(1 - R_{org}\right)^{i-1} \tag{5.3}$$

This analysis is meant to provide a "best guess" as to the optimal method parameters without requiring additional experimentation. The inherent limitation of this approach is the uncertain extensibility of the original data to both a modified methodology (i.e. small volumes, changed organic diluent, mixed analyte solutions, low initial REE concentration) and unique matrices (i.e. acidified brines vs. HCl). Therefore post hoc analysis of preliminary experiments for parameter optimization was done qualitatively and is described in Section 5.4.1. Moreover, since K_d values were not calculated as part of this study, model validation with new experimental results was not performed.

5.4 Results and discussion

5.4.1 Multiple linear-regression of organic-aqueous distribution coefficients

Fractionation of the REE observed in preliminary experiments (Figures 5.2A and 5.2B) can be qualitatively reconciled from MLR analysis. Figure 5.3 shows that the rinse step (labeled "R" in subfigures 5.3A to 5.3D) creates strong stripping conditions ($\log K_d < -1$) for the LREE (La; Figure 5.3A) while the back extraction (labeled "B") may provide inadequate acidity to recover the HREE (Tm; Figure 5.3B) once partitioned.

Using the equilibrium mass balance model (Equations 5.2 and 5.3), the K_d required to achieve the desired partitioning was matched to the results of this regression. For each step

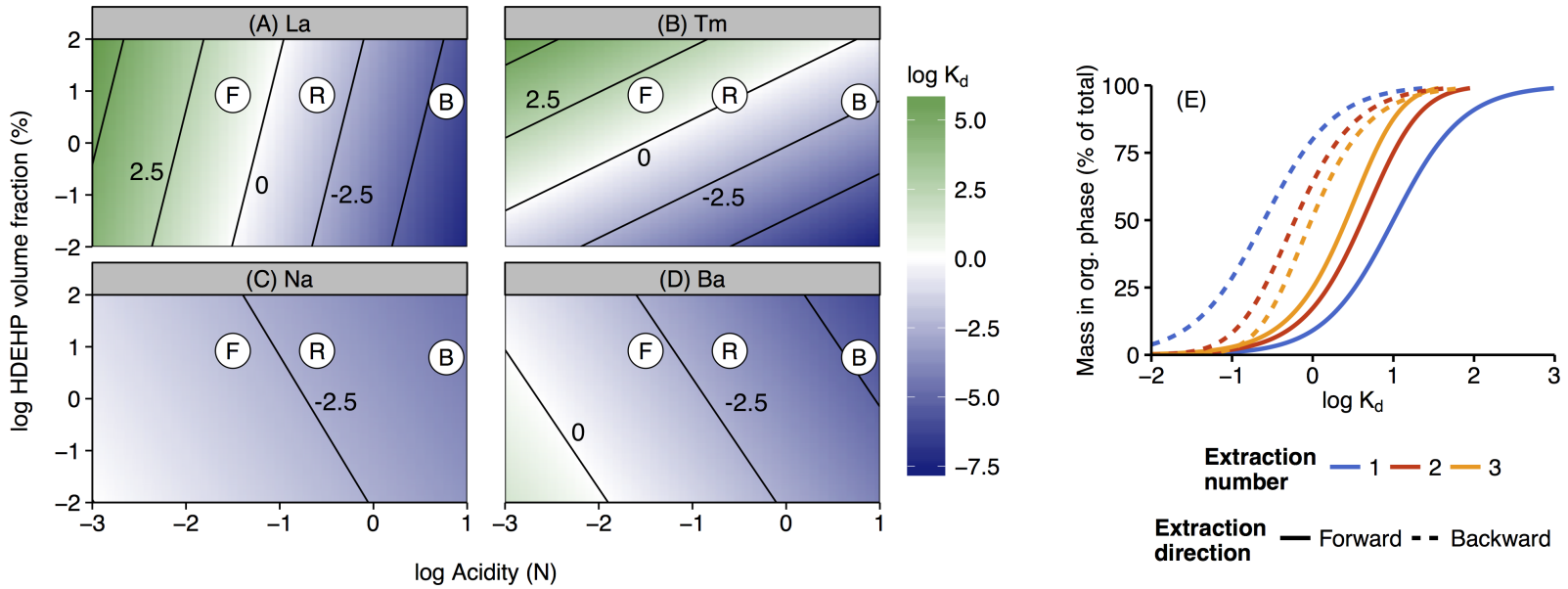

Figure 5.3: Summary of model-based optimization of LLE operating conditions. (A-D) Organic-aqueous distribution coefficient ($\log K_d$; Equation 5.1) contours as a function of acidity and HDEHP volume fraction for La, Tm, Na, and Ba calculated with data from Kimura (1960; 1961). LLE operating conditions for forward extractions (F), matrix rinse (R), and back extractions (B) suggested by Shabani et al. (1990) are noted. (E) Equilibrium partitioning for triplicate forward and backward extractions as a function of organic/aqueous distribution coefficient (K_d). Partitioning calculated by Equation 5.2 with $V_{aq}/V_{org} = 10$ for forward extraction and 0.25 for backward extraction.

of the LLE the desired partitioning is as follows:

1. Forward extraction: Achieve high ($> 99\%$) partitioning of the REE into the organic phase, while minimizing the partitioning of Ba and Na. This can be achieved in a series of forward extractions.

2. Matrix rinse: Minimize partitioning of Ba and Na (i.e. low K_d) while maintaining a high ($> 99\%$) partitioning of the REE.

3. Backward extraction: Minimize REE partitioning (i.e. leave $< 1\%$ in the organic phase). This can be achieved in a series of backward extractions.

Linear regression predicts a $\log_{10} K_d$ of 1.15 for La and 1.62 for Tm when using the conditions recommended by Shabani et al. (Shabani et al. 1990). At these values, a mass balance model would predict 93% partitioning in three forward extractions for La and exactly 99% for Tm. Similarly, in the recommended matrix rinse (0.25 N HCl) the model predicts $\log_{10} K_d$ of -1.48 for La and 0.21 for Tm, which correspond to 9% retention of La in the organic phase and 83% retention of Tm. While this simplified analysis suggests that triplicate back extraction steps should achieve quantitative recovery of all REE ($\log_{10} K_d$ of -2.18 and -5.57 for La and Tm respectively), preliminary experiments (Figure 5.2C and 5.2D) showed that the HREE were incompletely recovered. From these results an additional elution step was added to the procedure.

From this analysis, it is clear that the K_d values need to increase for forward extraction and the matrix rinse in order to achieve the desired partitioning at each step. The LLE conditions, namely the solution acidity $[ACY]$, necessary to meet these goals can be found by examining the contours of Figure 5.3A,B and E . Using Figure 5.3E it can be shown that forward extractions require $\log K_d > 1.6$ to achieve $> 99\%$ partitioning to the organic phase after triplicate extractions. Further, the conditions of the rinse phase must maintain

$\log K_d > 1.4$ to retain $> 99\%$ REE in the organic phase from one rinse step. Finally, to achieve $> 99\%$ recovery of REE during triplicate back extractions, conditions must create $\log K_d < -1.2$. By decreasing the initial acidity to $< 10^{-2}$ N (i.e. pH > 2) the initial extraction of REE can be enhanced without significantly increasing partitioning of Na or Ba. From this analysis, an initial sample pH of 2.5 was chosen. At a pH of 2.5 ($[ACY] = 10^{-2.5}$ N), forward extraction yields $\log K_d$ of 4.1 and 3.2 for La and Tm respectively. Dissolution of the organic phase, which has been shown to diminish partitioning, should be limited below pH 3 (Lee et al. 2011). Similarly, by reducing the acidity of the rinse step to $\leq 10^{-1.5}$ N (i.e. pH ≥ 1.5) salts such as Na and Ba (Figures 5.3C and 5.3D) can be eluted while retaining the REE (Figure 5.3A and 5.3B).

5.4.2 Interferences of synthetic brine constituents

Results for REE recovery from simple solutions of 1 and 5 m NaCl, are presented in Figure 5.4. In the 1 m NaCl solution, REE recovery was consistently between 90 and 110%, however, indium recovery was markedly lower: 76 and 81% in duplicate experiments. Similar results were observed in the high salinity test (5 m NaCl), except that the heaviest two lanthanides, Yb and Lu, were recovered at a much lower rate, averaging 82% for Yb and 72% for Lu. As the matrix rinse and back extraction conditions were identical between the 1 m and 5 m NaCl experiments, the diminished recovery is likely an artifact of diminished forward extraction and thus an effect of the increased salinity. Recovery of indium from the 5 m NaCl solution (mean, 76%) matched the recovery observed in the 1 m NaCl solution indicating that this diminished recovery is likely not a function of the salt concentration, and is instead endemic to indium in this extraction.

Figure 5.5 summarizes the Doehlert design matrix experimental results, while experiment-

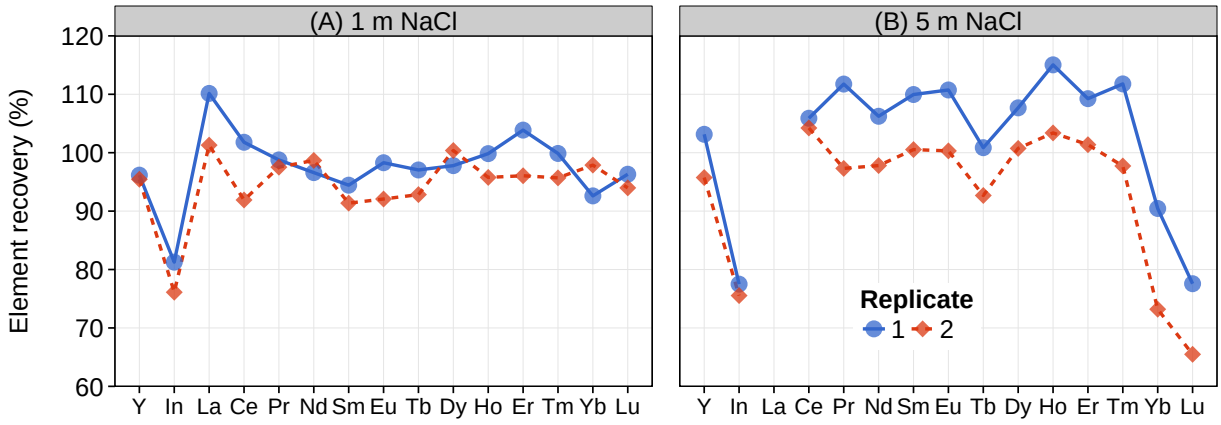

Figure 5.4: REE recovery by LLE method in simple, saline solutions. Initial REE concentrations were 500 ppt (each element) in all experiments. Duplicate experiments were conducted at each salinity and are represented by different line types, marker shapes, and colors. Data for La in the 5 m NaCl experiment and for Gd in both experiments are excluded due to excessive background concentrations ($\geq$ 250 ppt).

ordered results, with replicates, are presented in Figure C.4. Data for Sc, La, and Gd are not included because these analytes were either not recovered (Sc, which is "irreversibly bound" in the organic phase (Kimura 1960)) or contaminated by a high background (La and Gd; background $\geq$ 250 ppt in all experiments). Subsequent discussion excludes these elements. Across all analytes, median recovery, $\widehat{Q}(0.50) = 106\%$, was biased high (two-sided Wilcoxon Signed Rank test; H_1: $Q(0.5) \neq 100\%$, $P < 10^{-6}$). However, these results are well within the recommended range of mean recovery for 1 ppb analytes (40 – 120% recommended) (Taverniers et al. 2004). The absolute range of recoveries observed was 83-158% while the reference range for recoveries (i.e the values between which 95% of observations fell) was 92% – 122%. Experiments were generally reproducible (Figure C.4), with element-specific, replicate standard deviations ranging from 0.05% (Nd, experiment 4) to 21% (In, experiment 1). Finally, indium recovery was indistinguishable from any analyte (Wilcoxon, Rank-Sum test; $P > 0.05$), in contrast to recovery from the simple NaCl solutions (Figure 5.4). Since these data are not sufficient to determine the mechanism by which this disparity was over-

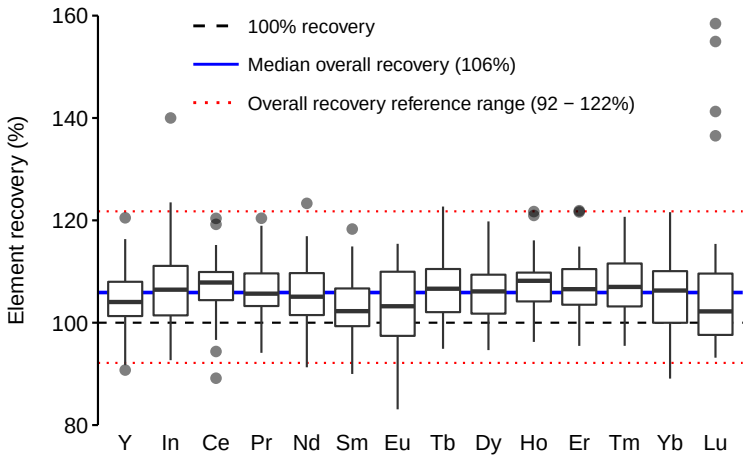

Figure 5.5: Distributions of elemental recovery in Doehlert matrix experiments by LLE methodology (see Figure C.4 for experiment-wise results). Distributions are depicted as standard box plots (McGill et al. 1978), where the thick, black line depicts the median; the boxed range represents the 25th to 75th percentile, or inter-quartile range (IQR); the thin whiskers denote all measurements within 1.5 times the IQR above or below; and the remaining observations are shown as semi-transparent grey dots. Relevant summary statistics for the overall suite of analytes are given as horizontal lines. Recovery values for Eu were determined after dosing the LLE eluent with H_2SO_4 to precipitate barite; all other recoveries were determined without barite precipitation. Data from La and Gd are not presented because the background concentration was determined to 250 ppt or greater (see Figure C.3).

come, the application of indium as a tracer of REE recovery by the LLE method in unknown samples requires further study.

The data in Figure 5.5 and Figure C.4 indicate no clear fractionation (or mass bias) of the method across the suite of REE. This result is confirmed by the Kruskal-Wallis test, which found no significant differences between any two element recoveries (H_0: No differences in element medians, $P > 0.1$). Pairwise element testing (paired sample Wilcoxon Rank-Sum test, corrected for multiple comparisons) found statistically significant differences ($P < 0.05$) between 16 element pairs. However, the differences were essentially indistinguishable from additive 3% analytical errors (Figure 5.6).

The lack of fractionation among REE in the more complex brines (i.e. with salinity, Fe,

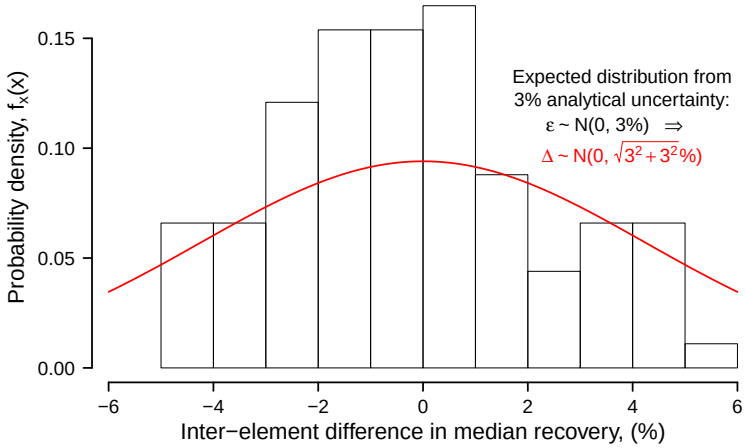

Figure 5.6: Comparison of pair-wise, inter-element differences in median recovery (Δ, estimated from the paired-sample Wilcoxon Signed Rank test) to the expected (normal) distribution based on the difference between two random variates with equal means and 3% analytical uncertainty, i.e. $\Delta = N(\mu, 3\%) - N(\mu, 3\%) = N(0, \sqrt{3^2 + 3^2}\%)$.

and DOC) differs from results obtained in experiments with simple NaCl solutions, where Yb and Lu recoveries were significantly lower at 5 m NaCl. Step-wise regression analysis of element recovery (response) against solution composition (predictors) revealed no combination of linear- or interaction-terms among the study variables that substantially influenced recovery. The results of the full-model regression are presented in Table C.5. If the solution composition did have any impact on recovery within the range of parameters explored in the Doehlert design, it was indistinguishable from replicate variability. These results give confidence to the application of the LLE methodology for natural samples with chemical characteristics within the bounds of the variables studied here, though accurate characterization of the REE concentration of unknown samples may require multiple replicates.

5.4.3 Advice regarding natural samples

Based on the results presented here, the modified LLE technique represents an attractive option for determination of REE in natural, hypersaline, and chemically complex brines.

However, it is critical to have accurate characterization of the samples of interest, as well as the oxide formation rates for the ICP-MS. For samples with low Ba (i.e. a molar [Ba]:[Eu] $< 10^5$ in raw samples), the addition of H_2SO_4 for barite precipitation is likely unnecessary if the available analytical instrumentation can maintain BaO^+ interferences on the order of 0.1% of analyte signal. Samples with salinities and/or compositions outside of the range validated here may need to be tested with synthetic brines by the user.

While this study has explored the effects of DOC on LLE performance by way of a model compound, the character of DOC in the samples of interest should be considered more explicitly. The effects of mixed organic components were not studied here. Potent REE chelators can be found in other water sources, such as municipal wastewater discharges (Bau and Dulski 1996; Kulaksiz and Bau 2013), and may have uncertain effects on the efficiency of REE recovery by this and other methods.

5.5 References

Agatemor, C. and Beauchemin, D. Matrix effects in inductively coupled plasma mass spectrometry: A review. *Analytica Chimica Acta*, 706(1):66–83, 2011.

APS. Energy critical elements: Securing materials for emerging technologies. Report, American Physical Society, 2011.

Aries, S., Valladon, M., Polvé, M., and Dupré, B. A routine method for oxide and hydroxide interference corrections in ICP-MS chemical analysis of environmental and geological samples. *Geostandards Newsletter*, 24(1):19–31, 2000.

Barbot, E., Vidic, N. S., Gregory, K. B., and Vidic, R. D. Spatial and temporal correlation of water quality parameters of produced waters from devonian-age shale following hydraulic fracturing. *Environmental Science & Technology*, 47(6):2562–2569, 2013.

Bau, M. and Dulski, P. Anthropogenic origin of positive gadolinium anomalies in river waters. *Earth and Planetary Science Letters*, 143(1):245–255, 1996.

Bauer, D., Diamond, D., Li, J., Sandalow, D., Telleen, P., and Wanner, B. US Department of Energy Critical Materials Strategy. Report, US Department of Energy, 2010.

Benkhedda, K., Infante, H. G., Ivanova, E., and Adams, F. C. Determination of sub-parts-per-trillion levels of rare earth elements in natural waters by inductively coupled plasma time-of-flight mass spectrometry after flow injection on-line sorption preconcentration in a knotted reactor. *Journal of Analytical Atomic Spectrometry*, 16(9):995–1001, 2001.

Castor, S. B. and Hedrick, J. B. *Rare Earth Elements*, pages 769–792. SME, 7 edition, 2006.

Doehlert, D. H. Uniform shell designs. *Journal of the Royal Statistical Society. Series C (Applied Statistics)*, 19(3):231–239, 1970.

Elimelech, M. and Phillip, W. A. The future of seawater desalination: Energy, technology, and the environment. *Science*, 333(6043):712–717, 2011.

Erel, Y. and Stolper, E. M. Modeling of rare-earth element partitioning between particles and solution in aquatic environments. *Geochimica et Cosmochimica Acta*, 57(3):513–518, 1993.

Fu, Q., Yang, L., and Wang, Q. On-line preconcentration with a novel alkyl phosphinic acid extraction resin coupled with inductively coupled plasma mass spectrometry for determination of trace rare earth elements in seawater. *Talanta*, 72(4):1248–1254, 2007.

Gregory, K. B., Vidic, R. D., and Dzombak, D. A. Water management challenges associated with the production of shale gas by hydraulic fracturing. *Elements*, 7(3):181–186, 2011.

Haley, B. A. and Klinkhammer, G. P. Complete separation of rare earth elements from small volume seawater samples by automated ion chromatography: method development and application to benthic flux. *Marine Chemistry*, 82(3–4):197–220, 2003.

Halicz, L., Gavrieli, I., and Dorfman, E. On-line method for inductively coupled plasma mass spectrometric determination of rare earth elements in highly saline brines. *Journal of Analytical Atomic Spectrometry*, 11(9):811–814, 1996.

Haluszczak, L. O., Rose, A. W., and Kump, L. R. Geochemical evaluation of flowback brine from Marcellus gas wells in Pennsylvania, USA. *Applied Geochemistry*, 28:55–61, 2013.

Hirata, S., Kajiya, T., Aihara, M., Honda, K., and Shikino, O. Determination of rare earth elements in seawater by on-line column preconcentration inductively coupled plasma mass spectrometry. *Talanta*, 58(6):1185–1194, 2002.

Jenner, G., Longerich, H., Jackson, S., and Fryer, B. ICP-MS - a powerful tool for high-precision trace-element analysis in earth sciences: evidence from analysis of selected USGS reference samples. *Chemical Geology*, 83(1):133–148, 1990.

Kajiya, T., Aihara, M., and Hirata, S. Determination of rare earth elements in seawater by inductively coupled plasma mass spectrometry with on-line column pre-concentration using 8-quinolinole-immobilized fluorinated metal alkoxide glass. *Spectrochimica Acta Part B: Atomic Spectroscopy*, 59(4):543–550, 2004.

Katarina, R. K., Oshima, M., and Motomizu, S. High-capacity chitosan-based chelating resin for on-line collection of transition and rare-earth metals prior to inductively coupled plasma-atomic emission spectrometry measurement. *Talanta*, 79(5):1252–1259, 2009.

Kharaka, Y. K., Lundegard, P. D., and Giordano, T. H. Distribution and origin of organic ligands in subsurface waters from sedimentary basins. *Rev. Econ. Geol*, 9:119–131, 2000.

Kim, I., Kim, S., and Kim, G. Analytical artifacts associated with the chelating resin extraction of dissolved rare earth elements in natural water samples. *Aquatic Geochemistry*, 16(4):611–620, 2010.

Kimura, K. Inorganic extraction studies on the system between bis (2-ethyl hexyl)-orthophosphoric acid and hydrochloric acid (i). *Bulletin of the Chemical Society of Japan*, 33(8):1038–1046, 1960.

Kimura, K. Inorganic extraction studies on the system between bis (2-ethyl hexyl)-orthophosphoric acid and hydrochloric acid (ii). *Bull. Chem. Soc. Japan*, 34, 1961.

Kulaksiz, S. and Bau, M. Anthropogenic dissolved and colloid/nanoparticle-bound samarium, lanthanum and gadolinium in the rhine river and the impending destruction of the natural rare earth element distribution in rivers. *Earth and Planetary Science Letters*, 362:43–50, 2013.

Kumar, S. A., Pandey, S. P., Shenoy, N. S., and Kumar, S. D. Matrix separation and preconcentration of rare earth elements from seawater by poly hydroxamic acid cartridge followed by determination using ICP-MS. *Desalination*, 281(0):49–54, 2011.

Kühn, M. and Kriews, M. Improved detection of transition and rare earth elements in

marine samples with the CETAC DSX-100 preconcentration/matrix elimination system and ICP-MS. *Fresenius' Journal of Analytical Chemistry*, 367(5):440–444, 2000.

Lawrence, M. G. and Kamber, B. S. Rare earth element concentrations in the natural water reference materials (NRCC) NASS-5, CASS-4 and SLEW-3. *Geostandards and Geoanalytical Research*, 31(2):95–103, 2007.

Lee, P.-C., Li, C.-W., Chen, J.-Y., Li, Y.-S., and Chen, S.-S. Dissolution of D2EHPA in liquid–liquid extraction process: Implication on metal removal and organic content of the treated water. *Water Research*, 45(18):5953–5958, 2011.

Lund, J. W., Freeston, D. H., and Boyd, T. L. Direct utilization of geothermal energy 2010 worldwide review. *Geothermics*, 40(3):159–180, 2011.

McGill, R., Tukey, J. W., and Larsen, W. A. Variations of box plots. *The American Statistician*, 32(1):12–16, 1978.

McGinnis, C. E., Jain, J. C., and Neal, C. R. Characterisation of memory effects and development of an effective wash protocol for the measurement of petrogenetically critical trace elements in geological samples by ICP-MS. *Geostandards Newsletter*, 21(2):289–305, 1997.

Murali Mohan, A., Hartsock, A., Bibby, K. J., Hammack, R. W., Vidic, R. D., and Gregory, K. B. Microbial community changes in hydraulic fracturing fluids and produced water from shale gas extraction. *Environmental Science & Technology*, 47(22):13141–13150, 2013.

Möller, P., Dulski, P., and Luck, J. Determination of rare earth elements in seawater by inductively coupled plasma-mass spectrometry. *Spectrochimica Acta Part B: Atomic Spectroscopy*, 47(12):1379–1387, 1992.

Nash, K. L. A review of the basic chemistry and recent developments in trivalent f-elements separations. *Solvent Extraction and Ion Exchange*, 11(4):729–768, 1993.

Nelson, A. W., May, D., Knight, A. W., Eitrheim, E. S., Mehrhoff, M., Shannon, R., Litman, R., and Schultz, M. K. Matrix complications in the determination of radium levels in hydraulic fracturing flowback water from Marcellus Shale. *Environmental Science & Technology Letters*, 1(3):204–208, 2014.

Nilsson, M. and Nash, K. L. Review article: A review of the development and operational characteristics of the TALSPEAK process. *Solvent Extraction and Ion Exchange*, 25(6): 665–701, 2007.

Noack, C. W., Dzombak, D. A., and Karamalidis, A. K. Rare earth element distributions and trends in natural waters with a focus on groundwater. *Environmental Science & Technology*, 48(8):4317–4326, 2014.

Oliveira, E. P., Yang, L., Sturgeon, R. E., Santelli, R. E., Bezerra, M. A., Willie, S. N., and Capilla, R. Determination of trace metals in high-salinity petroleum produced for-

mation water by inductively coupled plasma mass spectrometry following on-line analyte separation/preconcentration. *Journal of Analytical Atomic Spectrometry*, 26(3):578–585, 2011.

R Core Team. R: A language and environment for statistical computing, 2014.

Raso, M., Censi, P., and Saiano, F. Simultaneous determinations of zirconium, hafnium, yttrium and lanthanides in seawater according to a co-precipitation technique onto iron-hydroxide. *Talanta*, 116(0), 2013.

Shabani, M. B., Akagi, T., Shimizu, H., and Masuda, A. Determination of trace lanthanides and yttrium in seawater by inductively coupled plasma mass spectrometry after preconcentration with solvent extraction and back-extraction. *Analytical Chemistry*, 62(24): 2709–2714, 1990.

Shannon, M. A., Bohn, P. W., Elimelech, M., Georgiadis, J. G., Mariñas, B. J., and Mayes, A. M. Science and technology for water purification in the coming decades. *Nature*, 452 (7185):301–310, 2008.

Shannon, W. M. and Wood, S. A. *The Analysis of Picogram Quantities of Rare Earth Elements in Natural Waters*, page 1—37. Springer, Dordrecht, The Netherlands, 2005.

Shaw, T. J., Duncan, T., and Schnetger, B. A preconcentration/matrix reduction method for the analysis of rare earth elements in seawater and groundwaters by isotope dilution ICPMS. *Analytical Chemistry*, 75(14):3396–3403, 2003.

Stetzenbach, K. J., Amano, M., Kreamer, D. K., and Hodge, V. F. Testing the limits of ICP-MS: Determination of trace elements in ground water at the part-per-trillion level. *Ground Water*, 32(6):976–985, 1994.

Taverniers, I., De Loose, M., and Van Bockstaele, E. Trends in quality in the analytical laboratory. II. Analytical method validation and quality assurance. *TrAC Trends in Analytical Chemistry*, 23(8):535–552, 2004.

Thompson, M., Ellison, S. L., Fajgelj, A., Willetts, P., and Wood, R. Harmonized guidelines for the use of recovery information in analytical measurement. *Pure and applied chemistry*, 71(2):337–348, 1999.

U.S. Energy Information Administration. Annual energy outlook 2014 early release overview. Report, U.S. Energy Information Administration, 2013.

Vicente, O., Padró, A., Martinez, L., Olsina, R., and Marchevsky, E. Determination of some rare earth elements in seawater by inductively coupled plasma mass spectrometry using flow injection preconcentration. *Spectrochimica Acta Part B: Atomic Spectroscopy*, 53(9): 1281–1287, 1998.

Vidic, R., Brantley, S., Vandenbossche, J., Yoxtheimer, D., and Abad, J. Impact of shale gas development on regional water quality. *Science*, 340(6134), 2013. ISSN 0036-8075.

Weaver, B. and Kappelmann, F. TALSPEAK: A new method of separating americium and curium from the lanthanides by extraction from an aqueous solution of an aminopolyacetic acid complex with a monoacidic organophosphate or phosphonate. Report, Oak Ridge National Lab., Tenn., 1964.

Wen, B., Shan, X.-q., and Xu, S.-g. Preconcentration of ultratrace rare earth elements in seawater with 8-hydroxyquinoline immobilized polyacrylonitrile hollow fiber membrane for determination by inductively coupled plasma mass spectrometry. *Analyst*, 124(4):621–626, 1999.

Willie, S. N. and Sturgeon, R. E. Determination of transition and rare earth elements in seawater by flow injection inductively coupled plasma time-of-flight mass spectrometry. *Spectrochimica Acta Part B: Atomic Spectroscopy*, 56(9):1707–1716, 2001.

Wolford, R. *Characterization of organics in the Marcellus Shale flowback and produced waters*. Thesis, The Pennsylvania State University, 2011.

Zawisza, B., Pytlakowska, K., Feist, B., Polowniak, M., Kita, A., and Sitko, R. Determination of rare earth elements by spectroscopic techniques: a review. *Journal of Analytical Atomic Spectrometry*, 26(12):2373–2390, 2011.

Zhang, T.-h., Shan, X.-q., Liu, R.-x., Tang, H.-x., and Zhang, S.-z. Preconcentration of rare earth elements in seawater with poly(acrylaminophosphonic dithiocarbamate) chelating fiber prior to determination by inductively coupled plasma mass spectrometry. *Analytical Chemistry*, 70(18):3964–3968, 1998.

Zhu, Y., Umemura, T., Haraguchi, H., Inagaki, K., and Chiba, K. Determination of REEs in seawater by ICP-MS after on-line preconcentration using a syringe-driven chelating column. *Talanta*, 78(3):891–895, 2009.

Chapter 6

Effects of ligand chemistry and geometry on rare earth element partitioning from saline solutions to functionalized adsorbents

The information in this chapter chapter is in preparation for publication, co-authored by Jonathan Callura, Kedar Perkins, Newell Washburn, David A. Dzombak and Athanasios K. Karamalidis.

My contributions to this work were the design of adsorption experiments; collection, analysis, and visualization of the data; characterization of materials; statistical and mathematical modeling; and interpretation of results. Development and implementation of the synthesis routine for the adsorbents was performed by Kedar Perkins.

Abstract

The rare earth elements (REE) are commodity elements that drive the development of new technologies. However, the supply chain of the REE is subject to a complex set of technical, environmental, and geopolitical constraints. Some of these challenges may be circumvented if the REE are recovered from naturally abundant alternative sources, such as saline waters and brines. Here we synthesized and tested aminated silica gels functionalized with REE-reactive ligands, diethylenetriaminepentaacetic acid (DTPA), diethylenetriaminepentaacetic dianhydride (DTPA-dianhydride), and phosphonoacetic acid (PAA). A suite of characterization techniques and batch adsorption experiments were used to test the REE-uptake chemistry of the functionalized materials. Results showed that DTPA-dianhydride yielded the most REE reactive adsorbent (maximum observed partitioning coefficient — averaged over Nd, Gd, and Ho — $K_d = 14500$ mL/g at pH 2.2) of the three tested. Additional development is required to implement an REE recovery scheme using these materials, however it is clear that DTPA-based adsorbents offer a highly-reactive adsorbent warranting further study.

6.1 Introduction

Saline waters and brines contain rare earth elements (REE) and are potential sources of REE (Lewis et al. 1998; 1997; Michard 1989; Noack et al. 2014). A promising approach for recovery of REE from saline waters and brines is by adsorption on engineered, highly selective adsorbents followed by elution and then precipitation from the concentrated eluent solution.

Metal extraction from dilute solutions requires selective, high-capacity adsorbents in order to be effective and economical. Numerous ligands exist that have been engineered for their

ability to selectively chelate metals in solution, however the effect of surface attachment on this affinity is not always well understood. Moreover, the prior art in this subject area focus on simple systems (i.e. low concentrations of background electrolytes) and high sorbate concentrations. Thus, there is a need for testing functionalized adsorbents under conditions of elevated salinity and with environmentally-relevant sorbate concentrations.

Silica gel adsorbents are commonly applied because of their low cost and ease of functionalization (Repo et al. 2009; 2013; Shiraishi et al. 2002; Walcarius et al. 2002). Surface hydroxyl groups are used for the attachment of organo-silanes, which can be purchased pre-functionalized with a wide variety of end groups (Walcarius et al. 2002). The most common end-group, because it allows for facile attachment of amino-polycarboxylic acids (e.g. NTA, EDTA, DTPA), is aminopropyl triethoxysilane (APTES; Repo et al. 2013). Additionally, silica gels are resistant to dissolution under acidic conditions, limiting the potential for degradation of the adsorbent with repeated uptake and elution cycles.

The objective of this study was to validate the affinity of surface-attached ligands for the REE using a model solid support and attachment scheme. This was accomplished through (1) qualitative and quantitative characterization of functionalized adsorbents and (2) REE uptake experiments under a range of conditions. The results of this study should be used to better design functionalized adsorbents for REE extraction and recovery from dilute aqueous sources.

6.2 Materials and methods

6.2.1 Chemicals

All adsorbents were functionalized using 3-aminopropyl silica gel (d: 75 – 150 µm; TCI America). The ligands tested were: diethylenetriaminepentaacetic dianhydride (DTPA-dianhydride), diethylenetriaminepentaacetic acid (DTPA), and phosphonoacetic acid (PAA); the structures of the ligands (as received) are illustrated in Figure D.1. All ligands were grafted to the surface through the formation of an amide bond between a free carboxyl group and the surface amines; this process is described subsequently. The related ligands DTPA-dianhydride and DTPA were chosen to compare the effects of forming a targeted amide tether to the surface (i.e. on the lone carboxyl of the DTPA-dianhydride). Upon introduction to an aqueous environment, the anhydride groups should hydrolyze to leave four carboxyl groups free in solution. A third ligand, 1,4,7,10-tetraazacyclododecane-1,4,7,10-tetraacetic acid (DOTA; not pictured), was included in preliminary screening but did not show meaningful uptake and was eliminated from further testing (see Appendix D for results).

Nitric acid (HNO_3; BDH ARISTAR® Plus, VWR) was used to preserve samples for ICP-MS analysis. Hydrochloric acid (HCl; BDH ARISTAR® Plus, VWR) and sodium hydroxide (NaOH; Fischer Scientific) were used for pH adjustments. Background electrolyte solutions were prepared by dissolving NaCl (Sigma Aldrich; $\geq$ 99% purity) in ultrapure water (ASTM Type I, 18.2 MΩ/cm), prepared using a Barnstead NANOpure® water purification system. REE spike solutions were prepared by dissolving $Ln(NO_3)_3 \cdot 6\,H_2O$ salts (Sigma Aldrich or Alfa Aesar) in ultrapure water. Single element standard solutions (1000 µg/L) of the REE were obtained from Inorganic Ventures and used to prepare the calibration curve for ICP-MS analysis.

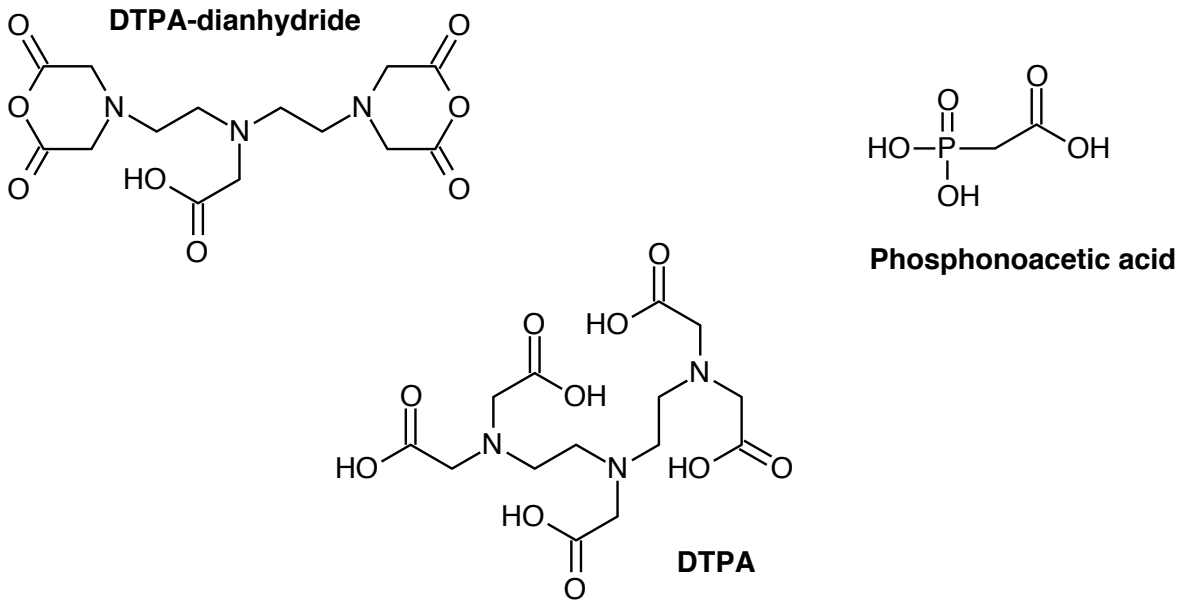

Figure 6.1: Chemical structures of the ligands studied.

6.2.2 Analytical instrumentation

Total dissolved REE concentrations were determined using an Agilent 7700x ICP-MS with HEHe-mode octopole reaction cell. Operating parameters were optimized daily via the auto-tune function of the Agilent MassHunter software using 1000:1 diluted Agilent tuning solutions. Concentrations were determined from a six-point calibration curve (0, 1, 5, 10, 50, and 100 ppb) containing each of the REE. Typical instrument operating parameters and a discussion of instrument operation and data analysis can be found in Appendix C.

An Orion™ 8165BNWP ROSS™ Sure-Flow™ pH electrode (Thermo Scientific), coupled to an accumet™ XL600 meter (Fisher Scientific), was used for pH measurements of high-total dissolved solid (TDS) solutions. The pH meter was calibrated with pH 2.0, 4.0, and 7.0 standards daily.

All samples were prepared gravimetrically using an analytical balance with 0.01 mg precision

(Adam Equipment).

6.2.3 Functionalization

A solution of the desired ligands (128 mM), 4-DMAP (154 mM), 3-aminopropyl functionalized silica (25.7 mM amine), and T3P (77.1 mM) in DMF (35 mL total volume) was stirred at room temperature overnight. The reaction is illustrated schematically in Figure 6.2. The solution was then transferred to a centrifuge tube and centrifuged for 15 mins at 25°C and 4.4 rpm. The supernatant was removed and then the pellet was resuspended in 25 mL of DMF. The solution was centrifuged for 10 mins, the supernatant removed and the pellet resuspended four additional times. The solution was then transferred to a glass vial and the solvent removed under vacuum and heat.

A significantly larger solid support (d: 710 – 1190 µm) was explored to test a material of a more appropriate industrial size. The acid-washed beads were first aminated with 3-aminopropyl triethoxysilane and subsequently functionalized in the same manner as the silica gels. However, preliminary results showed little to no uptake. It was determined that the particles lacked sufficient surface area to support a useful number of reactive sites and were thus abandoned. Details of this analysis are provided in Appendix D.

6.2.4 Characterization

The primary objective of characterization is to confirm the functionalization of the silica surface by the various ligands. The formation of amide bonds between the surface amines and the desired ligand should result in a shift of surface acid/base chemistry from highly basic (amine $pK_a \sim 9-10$) to acidic (ligand $pK_{a1} \sim 2$). This shift was investigated by rapid acid base titrations of particle suspensions and using electrophoretic mobility measurements to

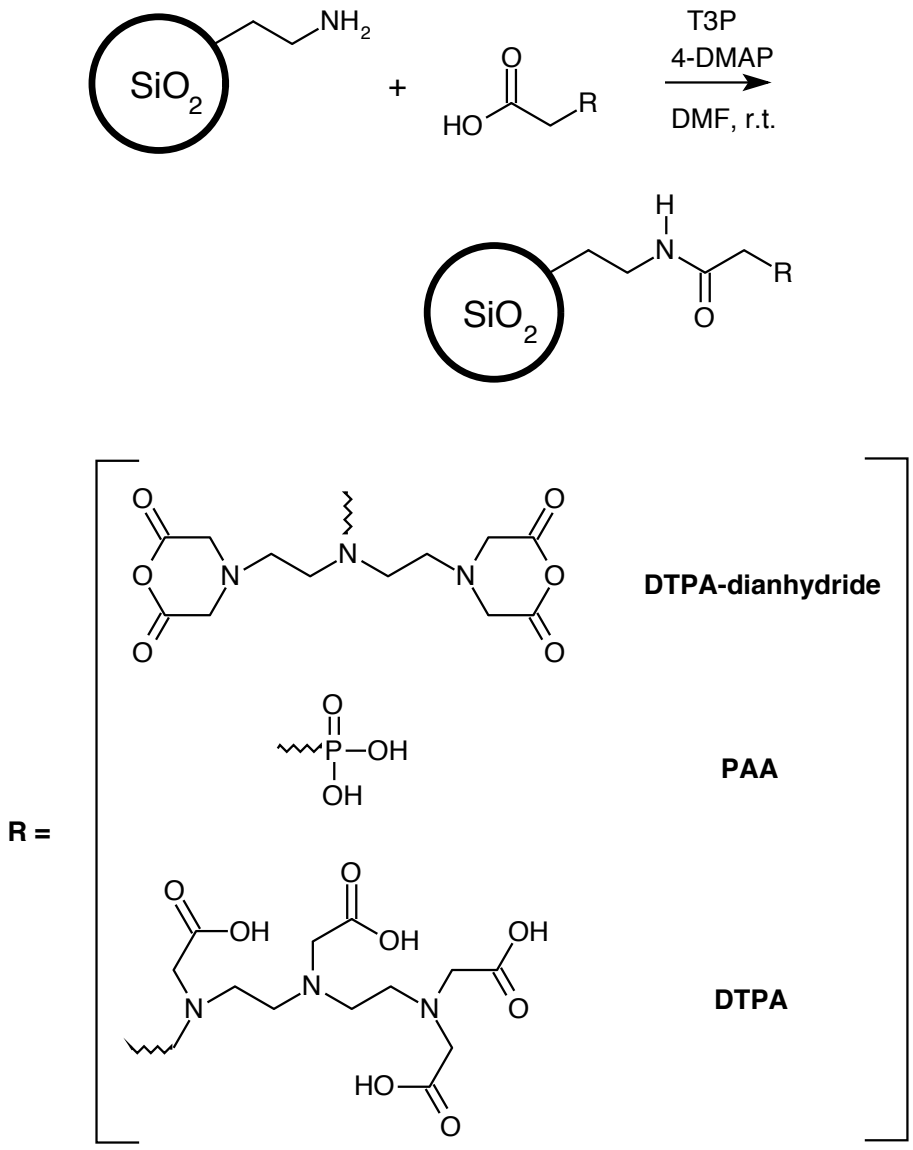

Figure 6.2: Schematic representation of functionalization reaction. Wavy lines denote the attachment point between the ligand and the surface-amide moiety.

infer surface charge. This shift was also tested by inferring surface charge from electrophoretic mobility measurements. The details of these methods are described subsequently.

Rapid titrations of particle suspensions

Acid- and base-neutralizing capacities of the functionalized adsorbents were investigated by rapid titrations of 5 g solid/L suspensions in 0.5 m NaCl. The suspensions were mixed, without any acid or base addition, for 1 minute or until a stable pH reading was achieved (defined here as unchanging at 0.01 pH unit precision over 5 seconds). Small doses (10–20 µL) of either 0.5 N NaOH or 0.5 N HCl were added to the suspensions and a pH was recorded once stable. This process was repeated until the pH exceeded 8.5, for initially acidic suspensions, or was under 5, for initially basic suspensions. The titrant was then switched (i.e. acid for base) and the curve reversed to examine hysteresis effects. Results are presented normalized to the solids concentration of each suspension. Rapid titrations were chosen to avoid effects of surface-site, proton-switching (as described by Dzombak and Morel (1990)) and to avoid complications associated with the high porosity of the silica gel (Walcarius et al. 2002).

Electrophoretic mobility

Measurements of the electrophoretic mobility (EPM) of each adsorbent were made using a Malvern Zetasizer NanoZS with DI water suspensions of particles (100 g solid/L). The pH of the particle suspension was verified just prior to removal of an aliquot for the EPM measurement. The applied voltage was 150 V after a sample equilibration time of 2 min. A minimum of 10 runs and a maximum of 100 runs were performed for each EPM measurement. The runs were averaged to determine the EPM value. Triplicate measurements were performed

at each pH.

6.2.5 REE uptake experiments

Batch experiments were used to study the reactivity of the functionalized adsorbents under a variety of conditions and to probe a variety of adsorbent properties including: uptake kinetics, uptake affinity, and pH dependance.

Adsorption edge and isotherm were performed in 12 mL screw-cap teflon digestion vessels (Savillex). The suspensions were manually agitated and then mixed, end over end, for 3 hours at 30 rpm. After mixing, the suspensions were allowed to settle by gravity, at which point an aliquot of the supernatant was removed and analyzed by ICP-MS and pH was measured.

The chemical and physical stability of the adsorbents was also investigated via adsorption isotherms. Aliquots of the DTPA-dianhydride adsorbent were washed with either 1 N HCl or 1 N NaOH overnight. After centrifugation, the supernatant was decanted and the solids rinsed three times with DI water. After decanting the final DI wash, the slurries were dried overnight at 98°C in polypropylene centrifuge tubes and used in an adsorption isotherm experiment.

6.2.6 Models used to evaluate adsorbent performance

All data analysis and visualization was performed in the `R` language for statistical computing (R Core Team 2014), utilizing additional packages `plyr, dplyr, tidyr, broom`, and `ggplot2` where necessary (Robinson 2015; Wickham 2009; 2011; 2014; Wickham and Francois 2014).

In all experiments, changes in the supernatant concentration (initial, C_i, and final C_e) were used to determine the relevant quantities, either the sorbed fraction (Eq. 6.1) or the mass adsorbed (Eq. 6.2; V is solution volume, m is adsorbent mass). Raw data for the results presented here are found in Appenix D.3.

$$f_{ads} = 1 - \frac{C_e}{C_i} \tag{6.1}$$

$$q_e = \frac{V}{m}(C_i - C_e) \tag{6.2}$$

Isotherms were evaluated using a Freundlich model since the data were log-log linear in all experiments (i.e. adsorbate doses were insufficient to saturate the active sites). This relationship is defined by Equation 6.3, where q_e is defined previously by Eq. 6.2. The relevant parameters are the partition coefficient (or chemical affinity), K_d, and the degree of linearity, n. Parameters were fit to experimental isotherms by first log-transforming the data and using ordinary least squares regression.

$$q_e = K_d \cdot C_e^{\frac{1}{n}} \tag{6.3}$$

Previous researchers have shown that metal sorption on organically modified silica gels, such as those used here, tend to be describable by pseudo-second order kinetics (Repo et al. 2009; Roosen et al. 2014)(Eq. 6.4).

$$\frac{dq}{dt} = k_2 \cdot (q_e - q)^2$$

Which can be integrated and expressed as:

$$q_t = \frac{q_e^2 \cdot k \cdot t}{1 + q_e \cdot k_2 \cdot t} \tag{6.4}$$

6.3 Results and discussion

6.3.1 Characterization

As expected the acid-base titrations of the functionalized particles demonstrate a significant shift from highly basic (dominated by amines) to highly acidic (dominated by carboxyl groups (Figure 6.3). A titration curve for the PAA-adsorbents could not be determined as the solids did not form a well mixed suspension, but rather accumulated at the surface of the solution. In addition to starting as a more acidic suspension, the DTPA acid-form adsorbent showed roughly four times greater base neutralizing capacity (from pH $\sim$4 – 8) than did the DTPA-dianhydride adsorbent. This can possibly be explained by a greater grafting density of the acid-form DTPA, owing to its flexibility of attachment site. The rigid conformation of the DTPA-dianhydride attachment may create steric hindrances to greater grafting densities. Alternatively, the difference in titration curves could reflect and incomplete hydrolysis of the anhydride groups, which would result in fewer solution-facing carboxyl groups and thus less base-neutralizing capacity.

Similar trends are observed for EPM measurements (Figure 6.4). From these zeta-potential measurements, the point of zero charge (PZC) for the various solids can be approximated. In agreement with the acid-base titrations, a large shift is observed from the PZC of the

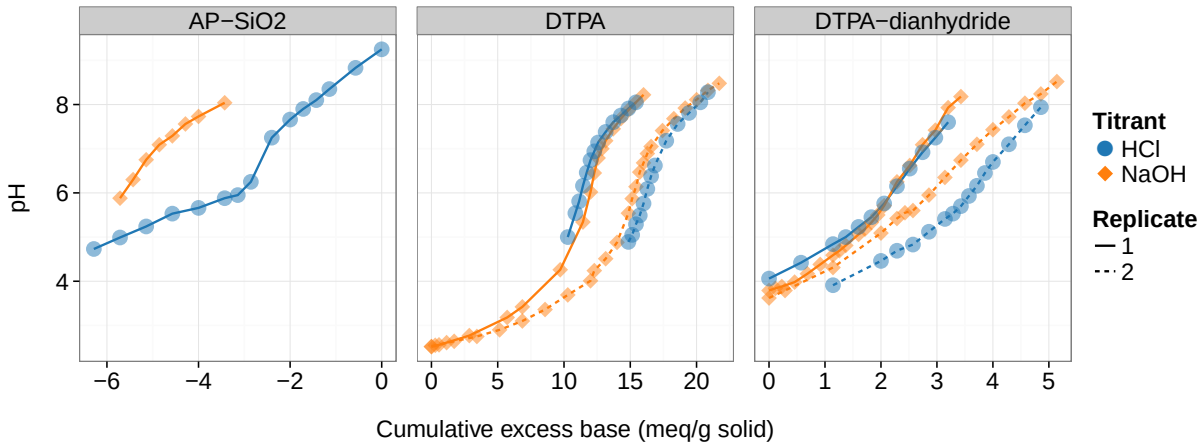

Figure 6.3: Acid-base titration curves for 5 g solid/L suspensions of functionalized adsorbents in 0.5 M NaCl. AP-SiO2 is the as-received starting material. The x-axis value of 0 corresponds to the pH established by the particle suspension prior to any titrant addition.

unfunctionalized SiO_2 (PZC ~ 9.5) to the functionalized adsorbents: ~ 3, $\sim 4-5$, and ~ 7 for DTPA, DTPA-dianhydride, and PAA respectively. In addition to these shifts, complex, non-monotonic relationships were observed for all solids. This reflects the complex surface chemistry of these silica gels, which have been first modified with amine groups and further modified with multiprotic ligands. Thus the measured zeta potential was likely the super position of the amphoteric silanol groups, basic amines, and acidic ligands.

6.3.2 pH dependence of REE uptake

As with metal-oxide surface complexation, adsorption on the functionalized silica will exhibit a strong dependence on pH. For the ligands studied, the relevant surface complexation reactions for a generic REE, Ln^{3+}, are inferred based on solution-phase complexation reactions ("X≡" denotes the aminopropyl-SiO_2):

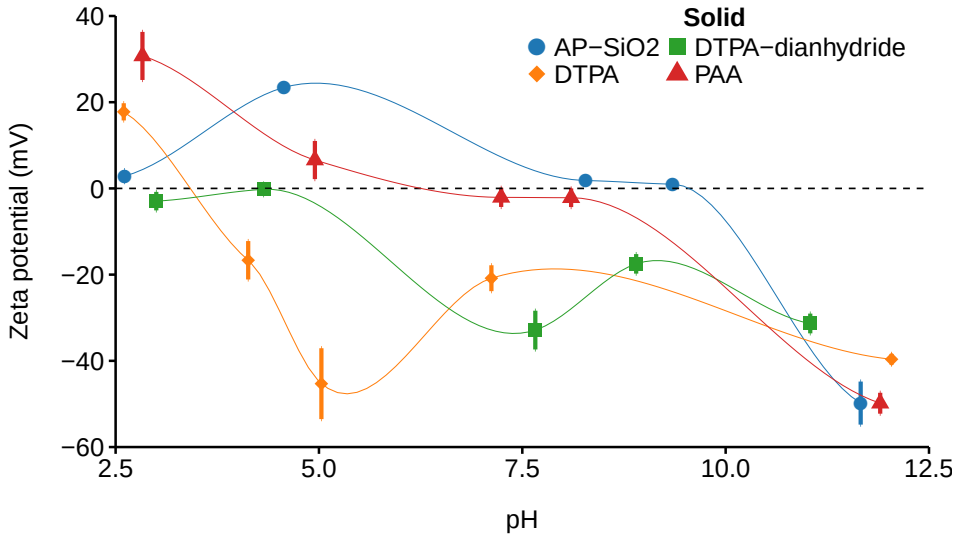

Figure 6.4: Zeta potential of functionalized adsorbents as a function of pH in DI water. Error bars represent $\bar{x} \pm 3 \cdot s_x$ from triplicate measurements. Smoothing lines added for guidance and are not predictive model fits.

$$\mathrm{Ln^{3+}} + \mathrm{X{\equiv}H_2PAA} \rightleftharpoons \mathrm{X{\equiv}(LnPAA^{+})} + 2\,\mathrm{H^{+}}$$
$$\mathrm{Ln^{3+}} + \mathrm{X{\equiv}H_4DTPA} \rightleftharpoons \mathrm{X{\equiv}(LnDTPA^{-})} + 4\,\mathrm{H^{+}}$$
$$\mathrm{Ln^{3+}} + \mathrm{X{\equiv}H_3DTPA^{-}} \rightleftharpoons \mathrm{X{\equiv}(LnHDTPA^{0})} + 3\,\mathrm{H^{+}}$$

By treating the surface bound DTPA (1 mmol DTPA / g adsorbent, 10 g adsorbent / L solution) as *an aqueous* ligand — a significant assumption — and using the stability constants from Grimes and Nash (2014), the fraction of surface-bound REE can be estimated. While the predominant species among the dissolved Ln species is not the free, aquo-ion (i.e. $\mathrm{Ln^{3+}}$) under all conditions (Figures 2.2, 2.3, and 2.4), the equilibrium treatment of the system allows the above reactions to represent the target adsorption reactions. The predicted speciation of the REE in the simple NaCl solutions used in these experiments is shown in Figure 6.5. Figure 6.6 illustrates the high affinity of DTPA for the REE considering competition from

Cl^- and OH^- as aqueous ligands; complete association as DTPA complexes is predicted for all REE by pH 3. At this pH the DTPA exists in a mixture of protonation states as H_5DTPA, H_4DTPA^-, and H_3DTPA^{2-}. While the fully deprotonated $DTPA^{5-}$ constitutes an insignificant portion of the total DTPA at pH 2.5 ($\log_{10} \alpha_{DTPA^{5-}} = -13.3$), the magnitude of the stability constant ($18 < \log_{10} \beta_{ML} < 21.4$) compensates for the mass action disadvantage. Inclusion of moderate amounts of dissolved inorganic carbon in this model (up to 10 mM) — previously shown to be the dominant ligand for REE complexation in natural waters — does not alter the predicted equilibrium speciation (not pictured).

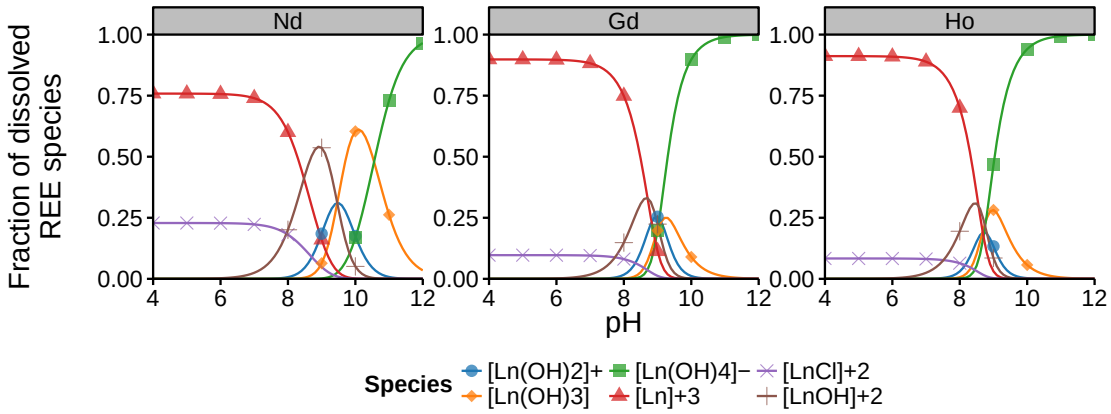

Figure 6.5: Speciation of select REE in 0.5 M NaCl at 25°C. Speciation calculated using `PHREEQC` (Charlton and Parkhurst 2011; Parkhurst and Appelo 2013) in `R` (R Core Team 2014) with the `llnl.dat` thermodynamic database (Table A.2). Total REE concentrations are 100 ppb each. Curves are labeled with plot marker symbols at integer pH values for comparison. Species that make up less than 5% at their maximum concentration are not plotted.

Adsorption pH edges for DTPA-dianhydride under three electrolyte conditions are shown in Figure 6.7. Near complete uptake is observed under acidic conditions (pH < 4 for all background electrolytes). However, contrary to the thermodynamic predictions (Figure 6.6), no metal removal is observed at mid-range and basic pH values. The lack of uptake at mid-ranged pH may be explained by an electrostatic interaction between the negatively charged carboxyl groups of the DTPA molecules and the positive charge of the surface amines (Fig-

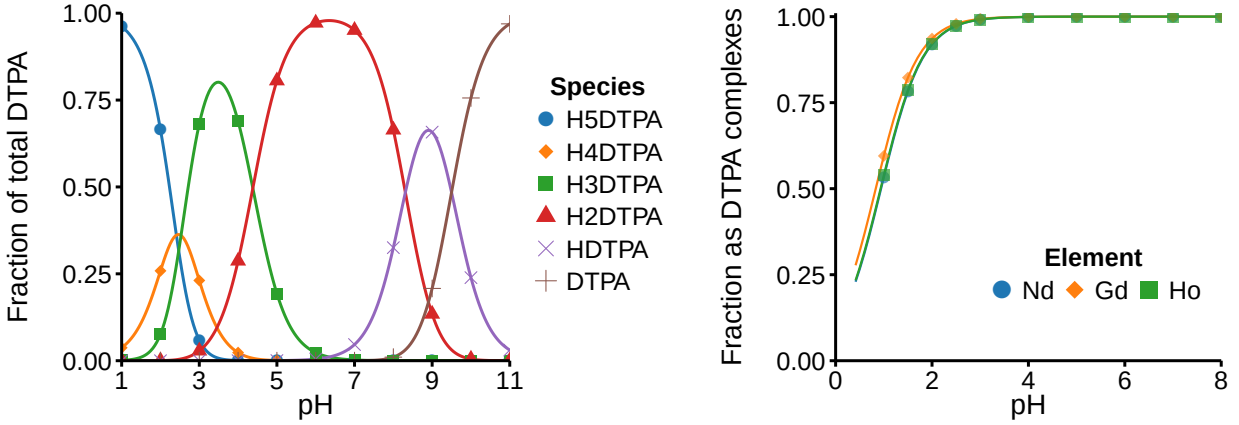

Figure 6.6: Thermodynamic prediction of equilibrium DTPA speciation (left) and DTPA-associated REE (sum of ML and MHL complexes; right) as a function of pH. Conditions of calculation are 0.5 m NaCl, 100 ppb total of each REE, and 10 mM total DTPA at 25°C. Speciation calculated using `PHREEQC` (Charlton and Parkhurst 2011; Parkhurst and Appelo 2013) in `R` (R Core Team 2014) with the `llnl.dat` thermodynamic database (Table A.2) and thermodynamic data for DTPA dissociation and Ln-DTPA complexes from Grimes and Nash (2014). Curves are labeled with plot marker symbols for comparison.

ure 6.8. A similar phenomenon was observed by Shiraishi et al. (2002), where Cu^{2+} adsorption was diminished with increasing pH, though these authors attributed the effect to H^+ from the carboxyl groups interacting with negatively charged silanol groups. Conversely, Repo et al. (2009) reported a traditional adsorption edge onto DTPA-functionalized SiO_2 for Ni^{2+} and Co^{2+}. However, it should be noted that the functionalization scheme for each of these studies was different than the route described here and that their adsorption experiments were performed at higher concentrations of the sorbate (ppm compared to ppb).

Adsorption edges for DTPA- and PAA-functionalized SiO_2 are shown in Figure 6.9. While DTPA acid-form material shows little uptake at any pH, there appears to be a similar trend of decreasing uptake from pH 2–4, though the effect is subtle, decreasing from a maximum of 15–20% removal to a minimum of 3–7%. The PAA-functionalized adsorbent exhibits more typical pH edge behavior, increasing as a function of pH, however there is a noticeable dip in the adsorption edge, reaching a local minima near pH 8.

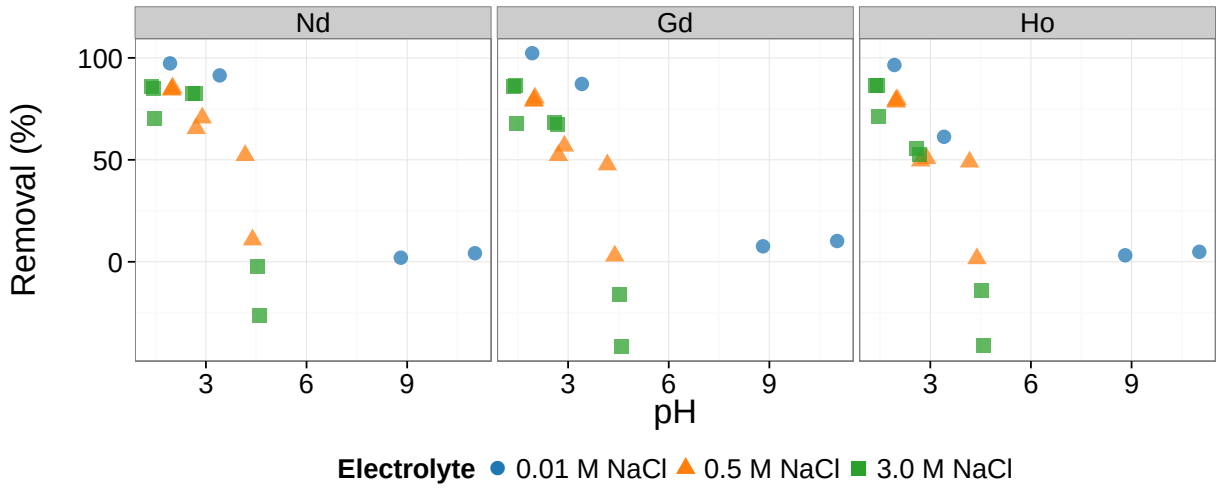

Figure 6.7: Adsorption pH edge for select REE onto DTPA-dianhydride adsorbent under three electrolyte conditions. Adsorbent suspensions (10 g solid/L) were mixed with REE mixtures in NaCl solutions, end over end, for 3 hours and allowed to settle for 15 minutes before removal of supernatant aliquot for ICP-MS analysis and pH measurement.

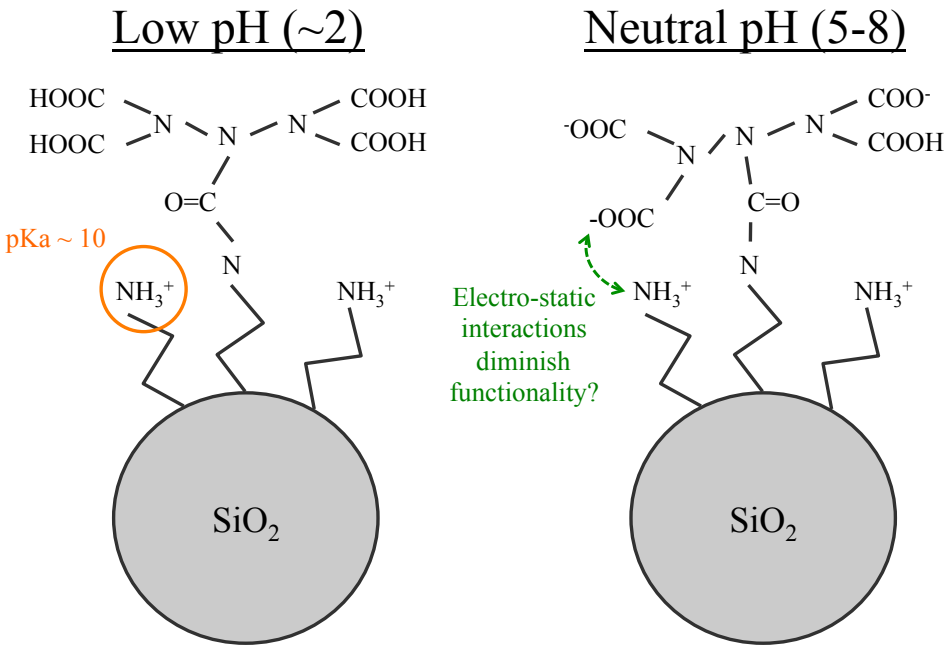

Figure 6.8: Schematic representation of possible electrostatic interactions between unreacted surface amines and ligand carboxyl groups leading to diminished REE uptake by DTPA at mid-ranged pH.

Davis and Leckie (1978) describe a similar behavior for Ag^+ adsorption onto amorphous iron oxide in the presence of thiosulfate ($S_2O_3^{2-}$). As pH increases, the $S_2O_3^{2-}$ desorbs from the oxide surface and competes with the adsorbent for Ag^+, leading to a temporary decrease in Ag^+ adsorption. The experimental systems studied here should be absent a "competing" ligand (by design), meaning this mechanism is unlikely to explain the present observations. Decrease of this effect for Ho vs. Gd vs. Nd suggested some form of differential complexation as the stability constants for most ligands increase or decrease linearly across the REE suite (see: Chapter 2, Tables A.1 and A.2). The uptake by PAA of the REE at mid-ranged pH supports the hypothesis of the DTPA carboxyl groups interacting electrostatically with surface amines, because, while negatively charges, the phosphonate group has little to no freedom of movement, owing to the short single carbon "chain" between the active group and the amide surface-attachment.

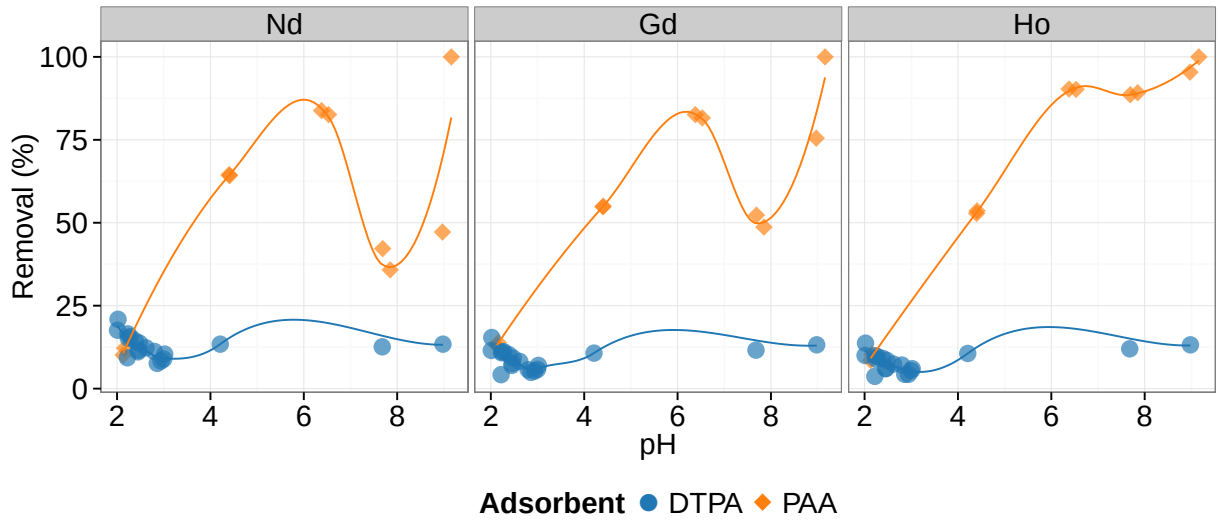

Figure 6.9: Adsorption pH edge for select REE onto PAA and DPTA adsorbents. Adsorbent suspensions (10 g solid/L) were mixed with REE mixtures in 0.5 m NaCl, end over end, for 3 hours and allowed to settle for 15 minutes before removal of supernatant aliquot for ICP-MS analysis and pH measurement. Smoothing lines have been added for visual aid and do not represent a predictive model for these data.

6.3.3 Constant pH isotherms

The ligands chosen for this study are known to have significant affinity for solution-phase complexation of the lanthanides (e.g., Grimes and Nash 2014). Adsorption isotherms were used to quantify the affinity of the surface-attached ligands for the REE under a range of conditions. The three ligands are compared in Figure 6.10 on the uptake of Nd, Gd, and Ho from 0.5 M NaCl, including at two pH values for PAA. In this figure, a more reactive adsorbent (alternatively, an adsorbent with greater affinity) plots further to the left. DTPA-dianhydride (at pH 2) is the clearly superior adsorbent among the three, followed by PAA, and lastly by the acid-form DTPA.

As with the adsorption edge, it is apparent that the ability to attach the DTPA at a single carboxyl group (by performing the synthesis with the dianhydride form) offers significant benefits over a functionalization scheme using the acid-form. This could result from two factors. First, the high affinity for DTPA towards the REE in solution is based on the ability of the ligand to form a highly-coordinated "cage" around the metal. This mechanism utilizes all five of the carboxyl groups in solution to maximally coordinate the ion. The attachment of the ligand to a surface at any of the carboxyl groups will alter the ability to coordinate the ions. We propose that these results suggest this "penalty" is limited by attaching at the lone carboxyl group, emanating from the central tertiary amine of the DTPA molecule. Stated differently, the potential for the attachment of the acid-form DTPA at any of its carboxyl groups results in surface groups that are sterically hindered from forming the desired coordination geometry, and thus relies primarily on electro-static interactions with the ion. Alternatively, because there are no protected carboxyl groups in the acid-form molecule, there is a potential for multiple carboxyl groups from the same molecule to attach to the surface via amide bonds.

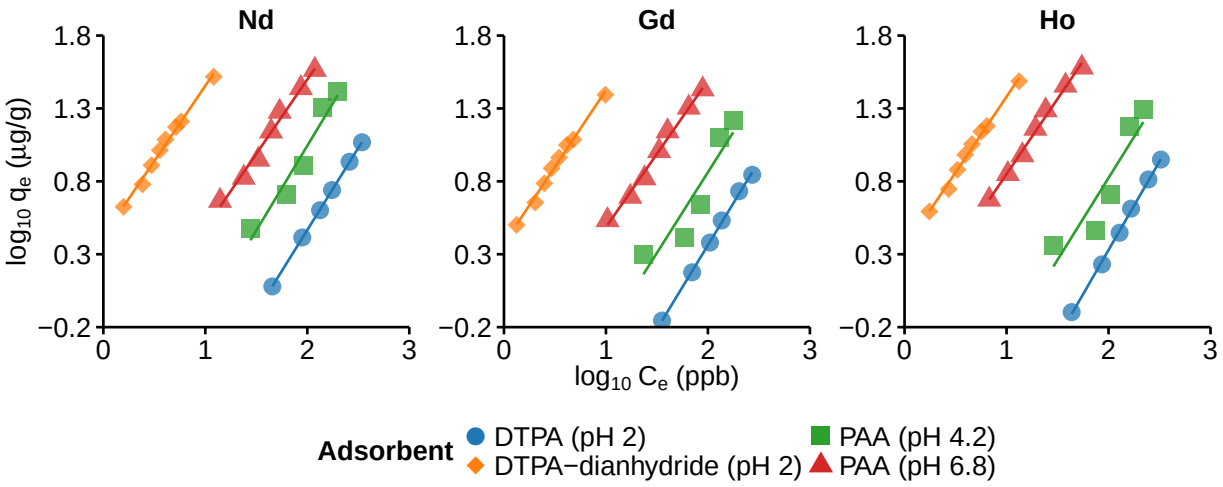

Figure 6.10: Adsorption isotherm for select REE onto functionalized adsorbents. Solution pH for each isotherm is given in the legend. Adsorbent suspensions (10 g solid/L) were mixed with REE mixtures in 0.5 m NaCl end over end for 3 hours and allowed to settle for 15 minutes before removal of supernatant aliquot for ICP-MS analysis and pH measurement.

In order to be economically feasible, the adsorbents must be simple to regenerate (e.g. with an acid elution) and withstand the chemical stresses of the eluent. In addition, the high temperatures of geothermal effluents necessitates the demonstration of a material resistant to thermal decomposition. Elution of the sorbed REE was tested for the pH 2 DTPA-dianhydride resin by mixing the water-washed solids with 10 mL of 5wt% HNO_3 ($\approx$ 0.8 N) for 3 hours. In a single step, 83 – 94 % of the adsorbed mass was eluted (Figure 6.11), with the order of elution being Nd > Gd > Ho. The eluted mass was uncorrelated with the adsorbed mass

Figure 6.12 shows the results of adsorption isotherms for the DTPA-dianhydride adsorbent following either HCl or NaOH wash and drying at 98°C. While the test conditions are slightly different than tests with the untreated materials (i.e. 5 g solid/L vs. 10 g/L), the uptake remains exceptional. These results speak to the chemical and thermal stability of the support as well as the functionalization chemistry.

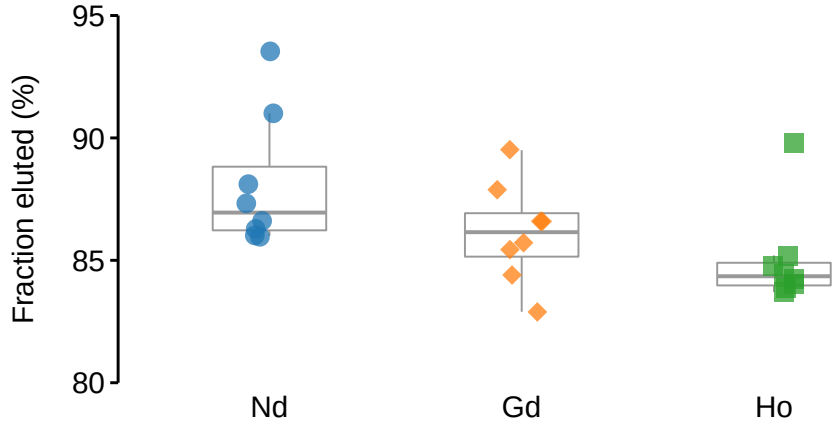

Figure 6.11: Elution of REE from DTPA-dianhydride adsorbent with HNO_3. Plotted values refer to the fraction of the adsorbed mass returned to solution following 3 hour contact with 10 mL of 5wt% HNO_3 (Figure 6.10, DTPA-dianhydride at pH 2).

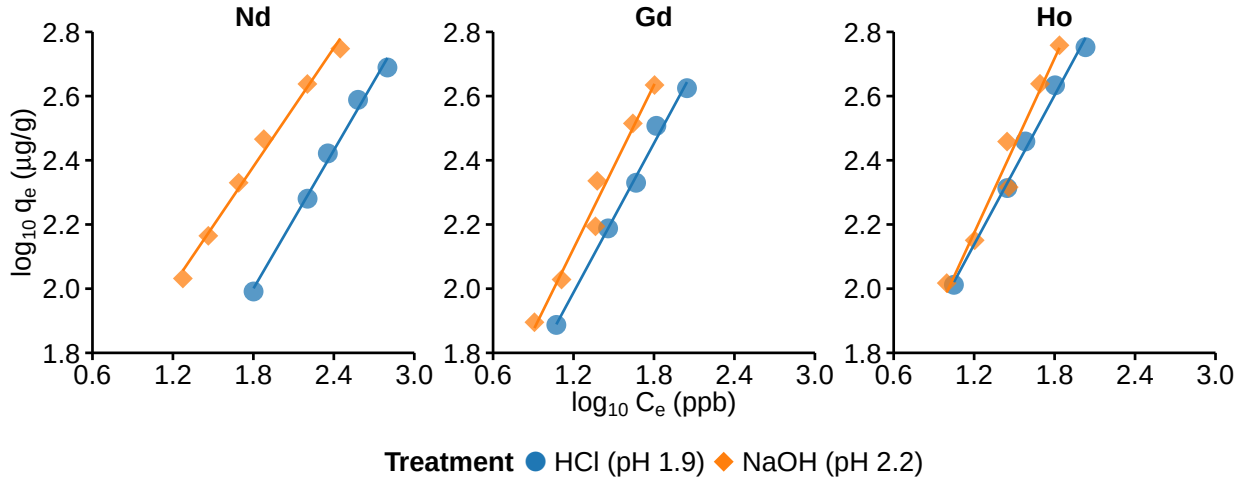

Figure 6.12: Adsorption isotherm for select REE onto DTPA-dianhydride adsorbents following acid or base washing. Washing protocols are described in the main text. Solution pH for each isotherm is given in the legend. Adsorbent suspensions (5 g solid/L) were mixed with REE mixtures in 0.5 m NaCl end over end for 3 hours and allowed to settle for 15 minutes before removal of supernatant aliquot for ICP-MS analysis and pH measurement.

Isotherms were fit using the Freundlich model (Eq. 6.3), with the estimates of K_d reported in Table 6.1. These results further illustrate the large disparity between the DTPA-dianhydride adsorbents and the alternatives. However, it is noteworthy that aside from the HCl washed experiment, the distribution coefficients follow an opposite trend to the stability constants for the aqueous complexes, decreasing with increasing atomic number. The data were insufficient to determine the cause of this difference. The elution data (Figure 6.11) do follow the trend from thermodynamics, where the order of β_{ML} values is Ho > Gd > Nd (Grimes and Nash 2014).

Table 6.1: Summary of Freundlich partitioning coefficients implied by constant pH isotherms. Estimates (and uncertainties) of $\log_{10} K_d$ were made by ordinary least-squares regression on the log-transformed data (q_e v.s. C_e). Freundlich slope parameter, n, was ≈ 1 for all experiments except for DTPA pH 2, where $n = 1.12$, 1.15, and 1.21 for Nd, Gd, and Ho respectively.

Solid	pH_{eq}	$\frac{m}{V}$ (g/L)	$\log_{10} K_d \pm \sigma_{\log_{10} K_d}$ (mL/g)			Notes
			Nd	Gd	Ho	
DTPA	2	10	1.22 ± 0.011	1.06 ± 0.042	0.898 ± 0.051	
PAA	4.2	10	1.72 ± 0.32	1.65 ± 0.5	1.58 ± 0.56	
	6.8	10	2.46 ± 0.094	2.48 ± 0.071	2.82 ± 0.05	
DTPA-dianhydride	2	10	3.42 ± 0.023	3.37 ± 0.022	3.34 ± 0.026	
	2	5	3.71 ± 0.087	4.06 ± 0.063	4.21 ± 0.064	HCl wash
	2.23	5	4.27 ± 0.056	4.11 ± 0.093	4.09 ± 0.13	NaOH wash

6.3.4 Adsorption kinetics

For all equilibrium testing (adsorption edges and isotherms) a 3 hour contact time was chosen to approximate equilibrium conditions. However, process design considerations would likely dictate shorter contact times to be economically viable. Figure 6.13 shows the rapid uptake (within 5 minutes) of the REE by the DTPA-dianhydride adsorbent. A pseudo equilibrium was reached in these tests in under an hour, indicating that the desirable, short contact times could be feasible with these materials.

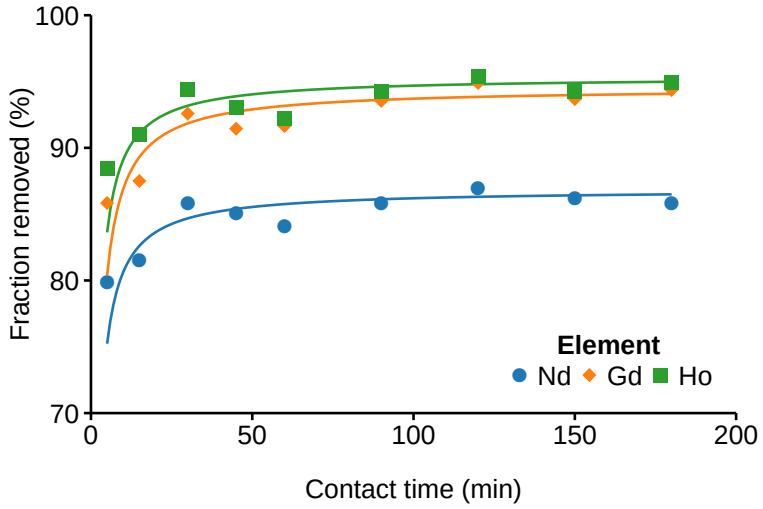

Figure 6.13: Adsorption kinetics for select REE onto DTPA-dianhydride adsorbent at pH 2.06 ± 0.09 ($\bar{x} \pm 3 \cdot s_x$) with pseudo second-order fit (Equation 6.4). Adsorbent suspensions (10 g solid/L) were mixed with REE mixtures (∼100 ppb each) in 0.5 m NaCl end over end for the plotted time (t_{mix} =5, 15, 30, 45, 60, 90, 120, 150, 180 min). Each time point represents and independent batch experiment. Following mixing, samples were immediately centrifuged for 10 minutes and the supernatant immediately sampled for ICP-MS analysis.

6.3.5 Unvalidated properties of functionalized adsorbents

A critical parameter for an adsorbent is the maximum capacity. This value is often estimated from adsorption isotherms, when the isotherm exhibits a Langmuirian shape (i.e. reaches a plateau). However, the isotherm experiments detailed here exhibited log-log linear adsorption up to the maximum adsorbate dose (∼ 3 ppm). Thus, additional testing is required to determine the maximum adsorptive capacity for these materials.

Additionally, some preliminary experiments were conducted (not described here) to test the effect of non-REE sorbate species. Preliminary data indicate that Ca does not significantly alter the adsorptive behavior of the REE under the test conditions, however additional testing is necessary considering other metals for which the β_{ML} values approach those for the REE (e.g. Ni, Co, or Cu).

Similarly, the effect of competing ligands in solution requires study. As described in Chap-

ter 2, complexes with dissolved inorganic carbon typically constitutes the majority of the dissolved REE loads of natural waters. While speciation modeling (assuming no change to the energetics of the REE-DTPA interaction upon surface-attachment) suggests that the adsorption reaction should be preferable, this variable was not studied here.

6.4 References

Charlton, S. R. and Parkhurst, D. L. Modules based on the geochemical model PHREEQC for use in scripting and programming languages. *Computers & Geosciences*, 37(10):1653–1663, 2011.

Davis, J. A. and Leckie, J. O. Effect of adsorbed complexing ligands on trace metal uptake by hydrous oxides. *Environmental Science & Technology*, 12(12):1309–1315, 1978.

Dzombak, D. A. and Morel, F. M. *Surface complexation modeling: hydrous ferric oxide*. John Wiley & Sons, 1990.

Grimes, T. S. and Nash, K. L. Acid dissociation constants and rare earth stability constants for DTPA. *Journal of Solution Chemistry*, 43(2):298–313, 2014.

Lewis, A., Komninou, A., Yardley, B., and Palmer, M. Rare earth element speciation in geothermal fluids from Yellowstone National Park, Wyoming, USA. *Geochimica et Cosmochimica Acta*, 62(4):657–663, 1998.

Lewis, A. J., Palmer, M. R., Sturchio, N. C., and Kemp, A. J. The rare earth element geochemistry of acid-sulphate and acid-sulphate-chloride geothermal systems from Yellowstone National Park, Wyoming, USA. *Geochimica et Cosmochimica Acta*, 61(4):695–706, 1997.

Michard, A. Rare earth element systematics in hydrothermal fluids. *Geochimica et Cosmochimica Acta*, 53(3):745–750, 1989.

Noack, C. W., Dzombak, D. A., and Karamalidis, A. K. Rare earth element distributions and trends in natural waters with a focus on groundwater. *Environmental Science & Technology*, 48(8):4317–4326, 2014.

Parkhurst, D. L. and Appelo, C. Description of input and examples for PHREEQC version 3: a computer program for speciation, batch-reaction, one-dimensional transport, and inverse geochemical calculations. Technical report, US Geological Survey, 2013.

R Core Team. *R: A Language and Environment for Statistical Computing*. R Foundation for Statistical Computing, Vienna, Austria, 2014. URL http://www.R-project.org/.

Repo, E., Kurniawan, T. A., Warchol, J. K., and Sillanpää, M. E. Removal of Co (II) and Ni (II) ions from contaminated water using silica gel functionalized with EDTA and/or DTPA as chelating agents. *Journal of Hazardous Materials*, 171(1):1071–1080, 2009.

Repo, E., Warchoł, J. K., Bhatnagar, A., Mudhoo, A., and Sillanpää, M. Aminopolycarboxylic acid functionalized adsorbents for heavy metals removal from water. *Water research*, 47(14):4812–4832, 2013.

Robinson, D. *broom: Convert Statistical Analysis Objects into Tidy Data Frames*, 2015. URL http://CRAN.R-project.org/package=broom. R package version 0.3.6.

Roosen, J., Spooren, J., and Binnemans, K. Adsorption performance of functionalized chitosan–silica hybrid materials toward rare earths. *Journal of Materials Chemistry A*, 2 (45):19415–19426, 2014.

Shiraishi, Y., Nishimura, G., Hirai, T., and Komasawa, I. Separation of transition metals using inorganic adsorbents modified with chelating ligands. *Industrial & Engineering Chemistry Research*, 41(20):5065–5070, 2002.

Walcarius, A., Etienne, M., and Bessière, J. Rate of access to the binding sites in organically modified silicates. 1. amorphous silica gels grafted with amine or thiol groups. *Chemistry of materials*, 14(6):2757–2766, 2002.

Wickham, H. *ggplot2: elegant graphics for data analysis*. Springer New York, 2009. ISBN 978-0-387-98140-6. URL http://had.co.nz/ggplot2/book.

Wickham, H. The split-apply-combine strategy for data analysis. *Journal of Statistical Software*, 40(1):1–29, 2011.

Wickham, H. *tidyr: Easily tidy data with spread and gather functions.*, 2014. URL http://CRAN.R-project.org/package=tidyr. R package version 0.1.

Wickham, H. and Francois, R. *dplyr: A Grammar of Data Manipulation*, 2014. URL http://CRAN.R-project.org/package=dplyr. R package version 0.3.0.2.

Chapter 7

Summary of novel contributions and suggestions for future work

7.1 Summary of novel contributions

This dissertation has produced several contributions to improve the understanding of the occurrence of REE in waters and the potential for their economic recovery. This knowledge will be useful to compare REE concentrations and values among aqueous sources and to measure and recover these elements.

Novel contributions of this work from this dissertation are summarized here.

7.1.1 Occurence and trends of REE in natural waters

Study of REE in natural and anthropogenically-influenced environments has produced an extensive, but disparate, literature, holding rich insights were it to be compiled, standardized, and analyzed. This objective brought together more than 1000 measurements from 31 studies to constitute the largest aggregation of REE data in the literature. The pub-

lication of this work, in Noack et al. (2014), also includes this database for use by future researchers. This collection, homogenization, and analysis of a disparate literature facilitates inter-study comparison and provides insight into the wide range of variables that influence REE geochemistry.

7.1.2 Efficient and accurate measurement of REE in complex aqueous solutions

The knowledge gaps identified in the first objective of this thesis regarding REE in hyper-saline fluids were partially a lack of a suitable analytical methodology rigorously validated for high-salinity, complex brines. The liquid-liquid extraction used for this object was shown to be robust to a range of solution conditions, and capable of separating part per trillion REE from synthetic solutions (Noack et al. 2015). With proper characterization of the natural samples of interest, this method could be deployed for accurate analysis of REE in small volumes of hyper-saline and chemically complex brines. Additional characterization of these high salinity fluids is necessary for developing extraction and recovery technologies for the REE.

7.1.3 Comparison of solid phase adsorbents

The key to developing dilute aqueous resource streams is the availability of high-capacity and resource-selective adsorbent materials for the passive capture of the resource from large, continuous volumes of feed solution. Numerous ligands have been developed for the express purpose of complexation with the REE, whether for use in medical imaging, or separation of the REE from actinides during nuclear fuel reprocessing. These ligands represent the resource-selective criteria stated above, while their attachment to a high surface area support will create significant capacity. However, few studies have attempted the surface-grafting of

these ligands for this purpose, so little is known about the changes to their reactivity towards the REE.

This study demonstrated the efficacy of surface-grafted DTPA for collection and recovery of REE from saline solutions. This represents a promising surface chemistry for the extraction of the REE from geothermal fluids or other solutions.

7.2 Suggestions for future work

Significant technical and economic hurdles remain before conventional REE mining operations can be displaced or even supplemented by recovery from aqueous sources. However, the work performed as part of this dissertation provides a strong foundation on which to build.

Adequate survey data does not exist to identify high-value aqueous sources of the REE. The analytical technique developed in this dissertation provides other researchers with a tool for making accurate measurements of REE concentrations in brines. However, this technique suffers from being material- and time intensive, limiting sample throughput. An alternative configuration of this process, for example using membrane solvent extraction or micro fluidics, could significantly mitigate these limitations. This work also produced conflicting observations regarding the use of indium as a tracer of the REE in the extraction process. Thus, further study is warranted to determine the most appropriate internal standard to trace REE recovery through the extraction.

The latter portion of this thesis described the batch, pseudo-equilibrium reactivity of DTPA- and PAA-functionalized in idealized systems. On a practical level, these materials need to be validated in a continuous flow design along with further optimization of the solid support.

Divergence of the observed adsorption edges for DTPA (compared to those theoretically predicted) suggest interaction between the ligands and either the support surface (SiO_2) or unreacted amine groups. In addition, this work has yet to identify crucial design parameters including the maximum adsorbate capacity and the selectivity of the adsorbents for the REE over other dissolved solutes.

Results of Chapter 6 demonstrated that the surface attached DTPA-dianhydride was highly reactive towards the REE. Conversely, when using the acid-form DTPA as the precursor, little to no adsorption was demonstrated. This confirmed our hypothesis that surface-attached, REE-selective ligands could remain reactive towards the REE, but that (as with the solution-phase complex) the conformation of the complex would be important. What this work did not explore was the quantitative determination of changes in thermodynamic equilibrium for the surface-attached ligand as compared to the free solution species.

The REE analytical method and selective adsorbent development work described herein necessarily involved use of well-characterized, relatively simple, synthetic saline solutions. Of course, testing of the LLE analytical method and the REE-selective adsorbents developed with natural saline waters and brines is needed. Such testing should start with waters of the type Na-Ca-Cl, Na-Ca-SO_4, and waters with high concentrations of dissolved silica. The effects of temperature must also be quantified for development beyond the laboratory scale.

7.3 References

Noack, C. W., Dzombak, D. A., and Karamalidis, A. K. Rare earth element distributions and trends in natural waters with a focus on groundwater. *Environmental Science & Technology*, 48(8):4317–4326, 2014.

Noack, C. W., Dzombak, D. A., and Karamalidis, A. K. Determination of rare earth elements in hypersaline solutions using low-volume, liquid–liquid extraction. *Environmental Science & Technology*, 49(16):9423–30, 2015.

Appendix A

Supporting information for Chapter 2

A.1 Literature values for stability constants

Table A.1: Compilation of literature equilibrium constants for aqueous complexes of the REE. Stability constant values are for the general reaction: $M^{3+} + aH^{+} + bL^{z-} \overset{\beta}{\rightleftharpoons} MH_aL_b^{(3+a-bz)}$. All values are for 25° C and $I = 0$ M. Values are plotted in Figure 2.1.

Ligand	Complex	Formation constant, $\log_{10}\beta$														Ref.
		La	Ce	Pr	Nd	Sm	Eu	Gd	Tb	Dy	Ho	Er	Tm	Yb	Lu	
CO_3	MHL	—	2.42	—	—	—	2.08	—	—	—	—	—	—	2.33	—	Wood (1990)
CO_3	MHL	2.02	1.95	1.89	1.83	1.75	1.60	1.72	1.71	1.72	1.73	1.76	1.79	1.84	1.90	Millero (1992)
CO_3	ML	6.98	7.31	7.48	7.53	7.71	7.73	7.64	7.71	7.81	7.80	7.86	7.93	8.06	8.00	Liu and Byrne (1998)
CO_3	ML	7.12	7.40	7.56	7.67	7.88	7.95	7.82	7.93	8.00	8.04	8.11	8.19	8.28	8.29	Lee and Byrne (1992)
CO_3	ML	—	7.56	—	—	—	8.00	—	—	—	—	—	—	8.31	—	Wood (1990)
CO_3	ML	6.82	6.95	7.13	7.22	7.30	7.37	7.44	7.50	7.55	7.59	7.63	7.66	7.67	7.70	Millero (1992)
CO_3	ML	7.12	7.40	7.57	7.69	7.93	8.00	7.97	8.08	8.14	8.18	8.24	8.32	8.40	8.43	Lee and Byrne (1992)
CO_3	ML_2	11.86	12.32	12.63	12.73	13.09	13.19	13.04	13.34	13.47	13.56	13.68	13.83	13.86	13.93	Liu and Byrne (1998)
CO_3	ML_2	12.01	12.63	12.91	13.09	13.37	13.40	13.35	13.53	13.66	13.71	13.89	14.03	14.21	14.28	Lee and Byrne (1992)
CO_3	ML_2	—	12.19	—	—	—	12.96	—	—	—	—	—	—	13.81	—	Wood (1990)
CO_3	ML_2	11.31	11.50	11.80	11.96	12.11	12.24	12.39	12.52	12.65	12.77	12.88	13.00	13.08	13.20	Millero (1992)
CO_3	ML_2	11.59	12.18	12.54	12.79	13.37	13.52	13.52	13.73	13.83	13.86	13.98	14.07	14.22	14.29	Lee and Byrne (1992)
Cl	ML	0.65	0.65	0.65	0.65	0.65	0.65	0.65	0.65	0.65	0.65	0.65	0.65	0.65	0.65	Luo and Byrne (2001)
Cl	ML	0.48	0.47	0.44	0.40	0.36	0.34	0.33	0.32	0.31	0.30	0.26	0.25	0.24	0.23	Wood (1990)
Cl	ML	0.29	0.31	0.32	0.32	0.30	0.28	0.28	0.27	0.27	0.27	0.28	0.27	0.16	-0.03	Millero (1992)
F	ML	3.62	3.86	3.84	3.82	4.15	4.27	4.24	4.37	4.39	4.28	4.27	4.29	4.39	4.25	Luo and Byrne (2000)
F	ML	3.72	3.86	4.06	4.14	4.17	4.24	4.36	4.47	4.51	4.57	4.59	4.61	4.63	4.66	Wood (1990)
F	ML	3.12	3.28	3.48	3.56	3.58	3.63	3.75	3.85	3.89	3.95	3.98	3.99	4.02	4.05	Millero (1992)
F	ML_2	6.84	7.30	—	7.27	—	7.96	8.27	7.25	—	—	7.53	—	—	7.78	Wood (1990)
F	ML_3	10.20	—	—	—	—	—	—	—	—	—	—	—	—	—	Wood (1990)
NO_3	ML	—	1.13	—	—	—	1.23	—	0.97	—	—	—	0.67	—	—	Wood (1990)
NO_3	ML	0.58	0.69	0.69	0.79	0.78	0.83	0.47	0.51	0.15	0.25	0.15	0.20	0.25	0.56	Millero (1992)
OH	ML	5.50	—	—	—	6.10	—	—	—	—	—	—	—	—	6.30	Wood (1990)
OH	ML	5.10	5.60	5.60	5.67	5.81	5.83	5.79	5.98	6.04	6.01	6.15	6.19	6.22	6.24	Millero (1992)
OH	ML	5.34	5.59	5.73	5.84	6.04	6.10	6.07	6.14	6.19	6.22	6.27	6.32	6.40	6.41	Lee and Byrne (1992)
OH	ML	5.19	5.66	5.68	5.82	6.16	6.24	6.17	6.36	6.41	6.44	6.48	6.61	6.76	6.73	Klungness and Byrne (2000)
OH	ML_2	9.86	10.40	10.73	10.96	11.49	11.63	11.63	11.82	11.90	11.93	12.04	12.12	12.26	12.33	Lee and Byrne (1992)
OH	ML_3	14.10	14.77	15.37	15.60	16.09	16.59	16.72	16.92	17.17	17.44	17.65	17.82	18.15	18.15	Lee and Byrne (1992)
PO_4	MH_2L	2.50	2.43	2.37	2.31	2.23	2.21	2.20	2.19	2.20	2.21	2.24	2.27	2.32	2.38	Millero (1992)
PO_4	MHL	4.87	4.98	5.18	5.27	5.35	5.42	5.49	5.54	5.60	5.64	5.68	5.71	5.73	5.75	Millero (1992)
PO_4	MHL_2	8.17	8.34	8.66	8.81	8.96	9.10	9.24	9.37	9.49	9.62	9.73	9.84	9.95	10.05	Millero (1992)
PO_4	ML	10.96	11.35	11.60	11.78	12.11	12.22	12.20	12.39	12.52	12.59	12.69	12.82	12.94	12.99	Lee and Byrne (1992)
PO_4	ML_2	17.63	18.48	19.08	19.50	20.42	20.66	20.71	21.02	21.22	21.27	21.41	21.57	21.79	21.90	Lee and Byrne (1992)
SO_4	ML	3.62	—	3.62	3.65	—	3.67	3.66	3.63	3.83	3.60	3.59	3.60	3.59	3.60	Wood (1990)
SO_4	ML	3.21	3.29	3.26	3.34	3.28	3.37	3.25	3.20	3.15	3.16	3.15	3.07	3.06	3.01	Millero (1992)
SO_4	ML_2	5.29	—	4.92	5.15	—	5.42	5.20	5.13	5.03	4.90	5.05	5.15	5.18	5.39	Wood (1990)

A.2 Thermodynamic data used for speciation calculations in PHREEQC

Table A.2: Stability constants, from the LLNL thermodynamic database, used in speciation calculations with `PHREEQC`. Reactions are written as described in the `llnl.dat` database file.

Species	Reaction	$\log_{10} K_{eq}$		
		Nd	Gd	Ho
$LnCl^{2+}$	$Ln^{3+} + Cl^- \rightleftharpoons LnCl^{2+}$	0.3	0.3	0.2
LnF^{2+}	$Ln^{3+} + F^- \rightleftharpoons LnF^{2+}$	4.3	4.5	4.7
$Ln(OH)_2^+$	$Ln^{3+} + H_2O \rightleftharpoons LnO^+ + 2\,H^+$	7.0	6.3	6.0
$LnOH^{2+}$	$Ln^{3+} + H_2O \rightleftharpoons LnOH^{2+} + H^+$	-8.1	-7.9	-7.7
$LnCO_3^+$	$Ln^{3+} + HCO_3^- \rightleftharpoons LnCO_3^+ + H^+$	-2.6	-2.4	-2.2
$LnHCO_3^{2+}$	$Ln^{3+} + HCO_3^- \rightleftharpoons LnHCO_3^{2+}$	1.8	1.6	1.6
$LnHPO_4^+$	$Ln^{3+} + HPO_4^{2-} \rightleftharpoons LnHPO_4^+$	5.4	5.1	5.8
$LnPO_4$	$Ln^{3+} + HPO_4^{2-} \rightleftharpoons LnPO_4 + H^+$	-0.5	-0.1	0.2
$LnH_2PO_4^{2+}$	$Ln^{3+} + HPO_4^{2-} + H^+ \rightleftharpoons LnH_2PO_4^{2+}$	9.5	9.4	9.4
$LnNO_3^{2+}$	$Ln^{3+} + NO_3^- \rightleftharpoons LnNO_3^{2+}$	0.7	0.4	0.2
$LnSO_4^+$	$Ln^{3+} + SO_4^{2-} \rightleftharpoons LnSO_4^+$	3.6	3.6	3.5
$LnCl_2^+$	$Ln^{3+} + 2\,Cl^- \rightleftharpoons LnCl_2^+$	0.0	0.0	0.0
LnF_2^+	$Ln^{3+} + 2\,F^- \rightleftharpoons LnF_2^+$	7.5	7.9	8.2
$Ln(OH)_4^-$	$Ln^{3+} + 2\,H_2O \rightleftharpoons LnO_2^- + 4\,H^+$	7.0	4.4	3.4
$Ln(OH)_3$	$Ln^{3+} + 2\,H_2O \rightleftharpoons LnO_2H + 3\,H^+$	6.3	5.2	4.5
$Ln(CO_3)_2^-$	$Ln^{3+} + 2\,HCO_3^- \rightleftharpoons Ln(CO_3)_2^- + 2\,H^+$	-8.0	-7.5	-7.3
$Ln(HPO_4)_2^-$	$Ln^{3+} + HPO_4^{2-} \rightleftharpoons Ln(HPO_4)_2^-$	9.1	9.6	9.9
$Ln(PO_4)_2^{3-}$	$Ln^{3+} + 2\,HPO_4^{2-} \rightleftharpoons Ln(PO_4)_2^{3-} + 2\,H^+$	-5.1	-3.9	-3.3
$Ln(SO_4)_2^-$	$Ln^{3+} + 2\,SO_4^{2-} \rightleftharpoons Ln(SO_4)_2^-$	5.7	5.1	4.9
$LnCl_3$	$Ln^{3+} + 3\,Cl^- \rightleftharpoons LnCl_3$	-0.3	-0.4	-0.4
LnF_3	$Ln^{3+} + 3\,F^- \rightleftharpoons LnF_3$	9.8	0.4	0.9
$LnCl_4^-$	$Ln^{3+} + 4\,Cl^- \rightleftharpoons LnCl_4^-$	-0.7	-0.8	-0.8
LnF_4^-	$Ln^{3+} + 4\,F^- \rightleftharpoons LnF_4^-$	1.8	2.4	3.0

A.3 References

Klungness, G. D. and Byrne, R. H. Comparative hydrolysis behavior of the rare earths and yttrium: the influence of temperature and ionic strength. *Polyhedron*, 19(1):99–107, 2000.

Lee, J. H. and Byrne, R. H. Examination of comparative rare earth element complexation behavior using linear free-energy relationships. *Geochimica et Cosmochimica Acta*, 56(3): 1127–1137, 1992.

Liu, X. and Byrne, R. Comprehensive investigation of yttrium and rare earth element complexation by carbonate ions using ICP–mass spectrometry. *Journal of Solution Chemistry*, 27(9):803–815, 1998.

Luo, Y.-R. and Byrne, R. H. The ionic strength dependence of rare earth and yttrium fluoride complexation at 25°c. *Journal of Solution Chemistry*, 29(11):1089–1099, 2000.

Luo, Y.-R. and Byrne, R. H. Yttrium and rare earth element complexation by chloride ions at 25°c. *Journal of Solution Chemistry*, 30(9):837–845, 2001.

Millero, F. J. Stability constants for the formation of rare earth-inorganic complexes as a function of ionic strength. *Geochimica et Cosmochimica Acta*, 56(8):3123–3132, 1992.

Wood, S. A. The aqueous geochemistry of the rare-earth elements and yttrium: 1. Review of available low-temperature data for inorganic complexes and the inorganic REE speciation of natural waters. *Chemical Geology*, 82:159–186, 1990.

Appendix B

Supporting information for Chapter 4

B.1 Weighted Kaplan-Meier estimation of survival function for analyzing left-censored data

The weighted Kaplan-Meier (KM) estimator ($\widehat{S}(x_i)$) is expressed as:

$$\widehat{S}(x_i) = \prod_{x \geq x_i} \left(1 - \frac{d_i^w}{Y_i^w}\right) \tag{B.1}$$

where, for application to aqueous chemistry data, $\widehat{S}(x_i)$ is estimate of the probability of any measured concentration, x, from the population being *less* than x_i. It is calculated using the weighted count of uncensored observations at x_i (d_i) and the weighted count of all (censored or uncensored) observed concentrations less than x_i (Y_i^w). The weighting of each data point is calculated here as the inverse of the number of samples from the data source, or $w_i = n_i^{-1}$. This curve can be used to estimate the quantiles of the data distribution as well as make estimates of the mean and variance of the population (Helsel 2012). The computational

methods here are adapted from Xie and Liu (Xie and Liu 2005) and Singh et al. (Singh et al. 2013).

To demonstrate these calculations, random data, drawn from log-normal distributions, will be used, followed by analysis of the groundwater REE dataset. This analysis makes use of functions from the `plyr` (V 1.8.1), `dplyr` (V 0.3.0.2), and `tidyr` (V 0.1) packages which must be installed to run this analysis. Aside from the pipe operator (`%>%`, loaded via the `dplyr` namespace, but part of the `magrittr` package), functions from these namespace are denoted as `package_name::function_name`, e.g. `dplyr::mutate`.

Code, written in R, is shown with a grey-shaded background:

```
# This is an R comment
X <- 10
Y <- rnorm(1000)
```

Conversely, output from R calculations will be shown as:

```
##
## These are results
##
```

B.1.1 Generation of random data

```
## If these packages are not installed,
## un-comment and run these lines
# install.packages('plyr')
# install.packages('dplyr')
# install.packages('tidyr')
library(plyr)
library(dplyr)
```

```
# Data are drawn from three separate log-normal distributions
# Group means
means <- c(1,1.5,2.5)

# Samples in each group
N <- 100

# Generate random data
set.seed(8675309)
R <- data.frame(sapply(means, function(mu) rlnorm(N, mu, 1)))
colnames(R) <- c('Grp1','Grp2','Grp3')
head(R) # Look at first few values of random data, R

# `mutate` adds censoring and site ID
R.g <- tidyr::gather(data = R, key = Dataset,
                     value = Concentration,
                     contains('Grp')) %>%
        # Assume that 60% of samples were analyzed by
        # method with DL = 1 ppb, 40% with DL = 10 ppb
  dplyr::mutate(DL = sample(c(1, 10),
                            size = nlevels(Dataset)*N,
                            replace = T,
                            prob = c(0.6,0.4)),
        # Flag censored values and store at detection limit
        Censored = ifelse(test = Concentration < DL,
                          yes = 1, no = 0),
        Concentration = ifelse(Censored == 1,
                               DL, Concentration),
        # Randomly assign to sites w/ non-uniform probability
        Site = sample(LETTERS[1:10],
                      nlevels(Dataset)*N,
                      replace = T,
                      prob = 1:10/sum(1:10))) %>%
  dplyr::select(Dataset, Concentration, Censored, Site)

# Look at first few rows of fictional, partially censored data.
dplyr::tbl_df(R.g)
```

```
## Source: local data frame [300 x 4]
##
```

```
##    Dataset Concentration Censored Site
## 1     Grp1        10.000        1    D
## 2     Grp1        10.000        1    J
## 3     Grp1        10.000        1    I
## 4     Grp1        20.685        0    H
## 5     Grp1         7.889        0    J
## 6     Grp1        10.000        1    I
## 7     Grp1         2.794        0    H
## 8     Grp1        10.000        1    I
## 9     Grp1         4.817        0    G
## 10    Grp1        10.000        1    F
## ..     ...           ...      ...  ...
```

B.1.2 Functions of the weighted Kaplan-Meier routine

To utilize the weighted KM, the weights of each observation must be calculated.

```
calc_weights <- function(site_vector){
  counts <- data.frame(Site = site_vector) %>%
    dplyr::group_by(Site) %>%
    dplyr::summarise(weight = 1/n())
  return(counts)
}

# Weights of sites are very similar across groups
# Note that no samples were assigned to "Site" A in Grp3,
# thus the weight is NA
plyr::ddply(R.g, .(Dataset), function(df){
    calc_weights(df$Site)
  }) %>%
  tidyr::spread(Dataset, weight)
```

```
##    Site    Grp1    Grp2    Grp3
## 1     A 0.25000 0.20000      NA
## 2     B 1.00000 0.20000 1.00000
## 3     C 0.16667 0.16667 0.20000
## 4     D 0.14286 0.16667 0.14286
```

```
## 5     E 0.25000 0.14286 0.08333
## 6     F 0.08333 0.08333 0.08333
## 7     G 0.12500 0.06667 0.12500
## 8     H 0.05000 0.10000 0.05263
## 9     I 0.06667 0.06667 0.05556
## 10    J 0.04348 0.05263 0.05556
```

Next, the function for calculating the survival estimator is built.

```
Surv_weighted <- function(censored_data){
  # Data should have the following form [R data type]:
  # Column 1 = `Concentration` [double]
  # Column 2 = `Censored` [bool/int]
  # Column 3 = `Site` [factor]

  if(!is.factor(censored_data$Site)){
    censored_data$Site <- factor(censored_data$Site)
  }

  # Get weights
  site_weights <- calc_weights(censored_data$Site)

  # Combine weights with original data
  data_mod <- dplyr::left_join(censored_data,
                               site_weights,
                               by = 'Site')

  # Calculate the `at risk` observations, or
  # weighted # of observations less than each concentration
  data_mod <- dplyr::arrange(data_mod,
                             # Data in descending order
                             desc(Concentration)) %>%
    dplyr::mutate(Yw = sum(weight) - cumsum(weight) + weight)

  # Retain only uncensored (Censored == 0) observations
  observed <- dplyr::filter(data_mod, Censored == 0) %>%
    dplyr::select(-Censored)

  # All observations with identical values are counted
  obs_weight_tab <- dplyr::group_by(observed, Concentration) %>%
    dplyr::summarize(dw = sum(weight))
```

```
  # Combine weighted counts with rest of data and calculate S
  observed <- dplyr::left_join(observed, obs_weight_tab,
                               by = "Concentration") %>%
    # "incremental survival", value inside product
    dplyr::mutate(P = 1 - dw/Yw) %>%
    # Remove duplicated observations
    dplyr::filter(!duplicated(Concentration)) %>%
    dplyr:: mutate(S = cumprod(P),
                   S = ifelse(S<0,0,S))

  return(observed)
}
```

Using the simulated data, these functions can be tested:

```
# Calculate weighted KM for each dataset/group
sim_wKM <- R.g %>% plyr::ddply(.(Dataset), function(df){
  df <- dplyr::select(df,-Dataset)
  wKM <- Surv_weighted(df)
  return(wKM)
})

# Look at results
sim_wKM %>%
  dplyr::select(Dataset, Concentration, weight, S) %>%
  dplyr::tbl_df()
```

```
## Source: local data frame [207 x 4]
##
##    Dataset Concentration  weight      S
## 1     Grp1        20.685 0.05000 0.9950
## 2     Grp1        20.505 0.16667 0.9783
## 3     Grp1        19.803 0.08333 0.9700
## 4     Grp1        19.540 0.04348 0.9657
## 5     Grp1        14.310 0.06667 0.9590
## 6     Grp1        13.423 0.06667 0.9523
## 7     Grp1        13.130 0.04348 0.9480
## 8     Grp1        11.808 0.08333 0.9396
```

```
## 9     Grp1         9.981 0.25000 0.9038
## 10    Grp1         9.503 0.06667 0.8942
## ..     ...           ...     ...    ...
```

To estimate the quantiles of a dataset with censoring, `Surv_quantile` is defined, which calls `Surv_weighted`. This function will choose the observation closest to the desired quantile, without exceeding that quantile. As in the main text, if the calculated survival quantiles, $S(x)$, for adjacent observations were $S(x_1) = 0.94$ and $S(x_2) = 0.96$, then x_1 would be noted as the 95^{th} percentile. If the desired quantile is outside of the range of calculated (e.g. for $Q(0.05)$ when $\min \widehat{S}(x) > 0.05$), the quantile is estimated parametrically through regression on order statistics (ROS). Here the data are assumed to be adequately fit by a log-normal distribution. The parameters of this distribution are estimated from quantile-quantile regression.

```
Surv_quantile <- function(censored_data,
                          # Default to median + IQR
                          percentiles = c(0.25,0.5,0.75),
                          sig.fig = 3){
  # Fraction of data below detection
  cenfrac <- mean(as.logical(censored_data$Censored))

  # Calculate wKM and select relevant columnes
  weighted_km <- Surv_weighted(censored_data) %>%
    dplyr::select(Concentration, S)

  # Warnings about data
  if(any(cenfrac > percentiles)){
    warning(paste('The fraction of censored data is larger ',
                  'than one or more desired percentiles.\n',
                  'This may produce unreliable estimates.',
                  sep = ''))
  }

  out_of_range <- c(F,F)
```

```
if(any(percentiles < min(weighted_km$S))){
  warning(paste('At least one desired percentile below',
                'minimum calculated from data,',
                'will be estimated from ROS.'), sep = ' ')
  out_of_range[1] <- T
}

if(any(percentiles > max(weighted_km$S))){
  warning(paste('At least one desired percentile above',
                'maximum calculated from data,',
                'will be estimated from ROS.'), sep = ' ')
  out_of_range[2] <- T
}

if(any(out_of_range)){
  ROS_data <- dplyr::filter(weighted_km, !is.na(S)) %>%
    transmute(y = log(Concentration), x = qnorm(S))
  ROS <- with(ROS_data,
              lm(y ~ x)
              )

  # Function for returning predictions based on ROS
  pred_ROS <- function(ROS_obj, percentile){
    new_dat <- data.frame(x = qnorm(percentile))
    log_pred <- predict(ROS_obj, newdata = new_dat)
    return(exp(log_pred))
}

fl.h <- function(percentile, S){
  h.temp <- which.min(abs(S - percentile))
  return(h.temp)
}

h.low <- sapply(percentiles, function(p){
    fl.h(p, weighted_km$S)
  })
perc_df <- data.frame(Percentile = percentiles) %>%
  dplyr::group_by(Percentile) %>%
  dplyr::mutate(h.low = fl.h(Percentile, weighted_km$S),
                use_ROS = ifelse(
                  (Percentile < min(weighted_km$S) ||
```

```
                              Percentile > max(weighted_km$S)),
                     T,F)
                   ) %>%
    dplyr::ungroup() %>%
    dplyr::mutate(Xh = ifelse(use_ROS,
                              pred_ROS(ROS, Percentile),
                              weighted_km[h.low,
                                          'Concentration']),
                          Xh = signif(Xh, sig.fig)

  return(perc_df)
}
```

This estimation is demonstrated with the simulated data. Note that in this example the rates of censoring are high in the first two groups, which elicits a warning from the `Surv_quantile` code. However, for clarity here, those warning messages have been suppressed.

```
plyr::ddply(R.g, .(Dataset),
      function(df){
        Surv_quantile(dplyr::select(df,-Dataset),
                      percentiles = c(0.05,0.25,0.5,0.75))
                         }) %>%
  dplyr::select(-h.low)
```

```
##    Dataset Percentile use_ROS     Xh
## 1     Grp1       0.05    TRUE  0.714
## 2     Grp1       0.25   FALSE  2.110
## 3     Grp1       0.50   FALSE  2.900
## 4     Grp1       0.75   FALSE  4.910
## 5     Grp2       0.05    TRUE  1.390
## 6     Grp2       0.25   FALSE  2.790
## 7     Grp2       0.50   FALSE  6.060
## 8     Grp2       0.75   FALSE  8.650
## 9     Grp3       0.05   FALSE  1.900
## 10    Grp3       0.25   FALSE  7.500
## 11    Grp3       0.50   FALSE 10.300
## 12    Grp3       0.75   FALSE 19.400
```

B.2 References

Helsel, D. *Statistics for Censored Environmental Data Using Minitab and R*. Wiley, 2 edition, 2012.

Singh, A., Neuhauser, E. F., Azzolina, N. A., Distler, M., Anders, K. M., Doroski, M. A., and Rabideau, A. J. Statistical techniques for analyzing of soil vapor intrusion data: A case study of manufactured gas plant sites. *Journal of the Air & Waste Management Association*, 63(2):219–229, 2013.

Xie, J. and Liu, C. Adjusted Kaplan–Meier estimator and log-rank test with inverse probability of treatment weighting for survival data. *Statistics in Medicine*, 24(20):3089–3110, 2005.

Appendix C

Supporting information for Chapter 5

C.1 Details of ICP-MS method and subsequent data analysis

C.1.1 Source material

The analytical and data analysis methodologies of Jenner et al. (1990) and McGinnis et al. (1997) — which are used to correct ICP-MS analyses for both spectroscopic (i.e. isobaric overlaps caused by polyatomic or doubly charged species) and non-spectroscopic (i.e. signal alternation due to "matrix effects") interferences as well as instrumental drift — are detailed here.

C.1.2 Preparation of spiked/unspiked sample pairs

Two aliquots of equal mass (or volume) are necessary for each sample; typically 2 g (or 2 mL) is a sufficient size for each aliquot. The first sample is diluted 1:1 with blank, 5%

HNO_3. The second sample is diluted by the same factor using a spike solution of known analyte concentration. The concentration of the spike solution should be designed to exceed the expected unknown concentration, but not in great excess (e.g. 2× not 100×).

At the beginning of each analytical run and after every third sample, an analytical blank (5% HNO_3) should be analyzed. Then, for each sample, the unspiked tube should be analyzed first, followed by the spiked tube, and followed lastly by a system "flush" (5% HNO_3). These flush samples are used to rinse the system and avoid memory effects, their instrumental response can be ignored.

C.1.3 Data analysis

The data necessary for analysis are the averaged counts per second (CPS) instrument response and signal relative standard deviation (RSD) for each unspiked, spiked, and blank sample. The steps of data reduction are as follows:

1. Record initial/final sample masses (if pre-concentrating), mass of sample aliquots, mass of blank diluent, and mass of spiked diluent.
2. Calculate analytical dilution factors (Equation C.1 below).
3. Collect and average all blank samples. There should be at least one blank for every three samples.
4. Subtract the averaged blank signal from all unspiked and spiked samples.
5. Calculate internally calibrated, matrix specific instrument sensitivity (Equation C.2 below).
6. Calculate unknown concentration (Equation C.3 below).

The factors ($D_{i,j}$) used to correct for dilution of signal in i by diluent j and pre-concentration from $m_{initial}$ to m_{final} are calculated as:

$$D_{samp,\,blank} = \frac{m_{samp}}{m_{samp} + m_{blank}} \cdot \frac{m_{initial}}{m_{final}} \tag{C.1a}$$

$$D_{samp,\,spike} = \frac{m_{samp}}{m_{samp} + m_{spike}} \cdot \frac{m_{initial}}{m_{final}} \tag{C.1b}$$

$$D_{spike,\,samp} = \frac{m_{spike}}{m_{samp} + m_{spike}} \tag{C.1c}$$

The internal sensitivity of the analyte ($S_{internal}$) can be determined using instrument responses for blank-subtracted spiked (I_s) and unspiked (I_u) samples, dilution factors, and spike concentration:

$$S_{internal} = \frac{I_s - I_u \cdot \frac{D_{samp,\,spike}}{D_{samp,\,blank}}}{D_{spike,\,samp} \cdot C_{spike}} \tag{C.2}$$

Finally, the unknown concentration is calculated by:

$$C_{unk} = \frac{I_u}{S_{internal} \cdot D_{samp,\,blank}} \tag{C.3}$$

C.2 Multiple linear-regression of organic-aqueous distribution coefficients

The raw data for the MLR optimization of the LLE method are plotted in Figure C.1.

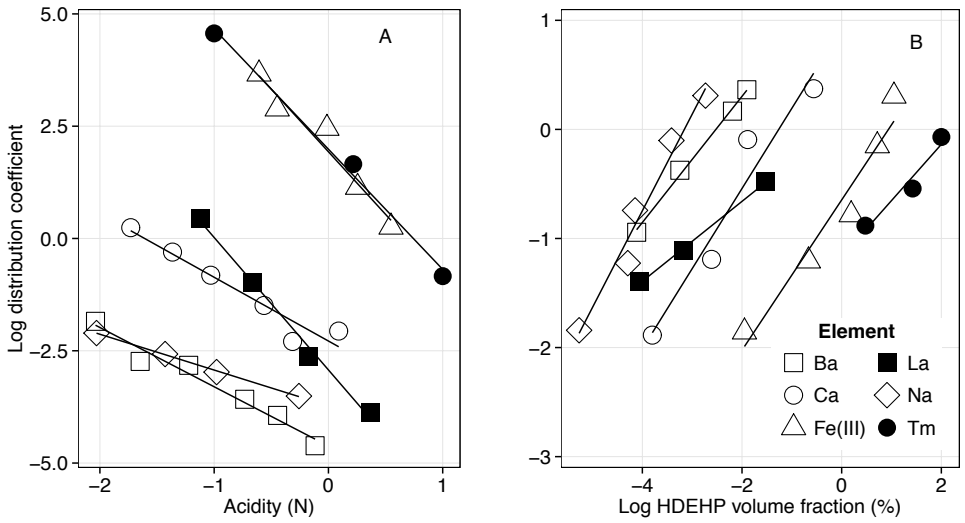

Figure C.1: Distribution coefficients for elements between HCl solutions and HDEHP-toluene solutions. Data were extracted from Figure 1 of Kimura (1960) for K_d vs. $[ACY]$ at constant $[L]$ and from Figure 1 of Kimura (1961) for K_d vs. $[L]$ at constant $[ACY]$. Note that the constant parameter (e.g. $[L]$ in A or $[ACY]$ in B) does not necessarily take the same value for all elements in the panel.

The parameter estimates for Equation 5.1 along with 95% confidence interval were estimated by least squares regression. The results are reported in Table C.1. As described in Chapter 5, this was a qualitative exercise; thus it is acceptable that many of the parameters have significant uncertainty (i.e. are not statistically significantly different than 0). Moreover, the experimental results (e.g. Figure 5.2) demonstrate that the condition changes suggested by the model were effective.

Table C.1: Model (Eq. 5.1) parameter estimates and associated 95% confidence interval (CI). Model fit to data in Figure C.1 by least squares.

Element	$\beta \pm 95\%$ CI		
	β_{ACY}	β_L	β_0
Ba	-1.39 ± 0.77	-0.52 ± 0.18	-3.69 ± 0.96
La	-2.93 ± 0.19	0.41 ± 0.05	-3.61 ± 0.17
Na	-0.85 ± 1.2	-0.29 ± 0.18	-3.12 ± 1.57
Tm	-1.57 ± 2.26	1.78 ± 3.03	-2.38 ± 4.88

C.3 Barium removal and background REE concentrations

A primary objective in analyzing REE in natural water samples is the separation of Ba, which may lead to isobaric interferences with Eu. Figure C.2A illustrates the effective rejection of Ba by the LLE method presented here, however Figure C.2C shows that even with $\sim 0.2\%$ $^{135}Ba^{16}O^{+}$:$^{135}Ba^{+}$, the $^{151}Eu^{+}$ is indistinguishable from $^{135}Ba^{16}O^{+}$ in the vast majority of samples prior to barite precipitation. Following precipitation (Figures C.2B,D), these issues are resolved.

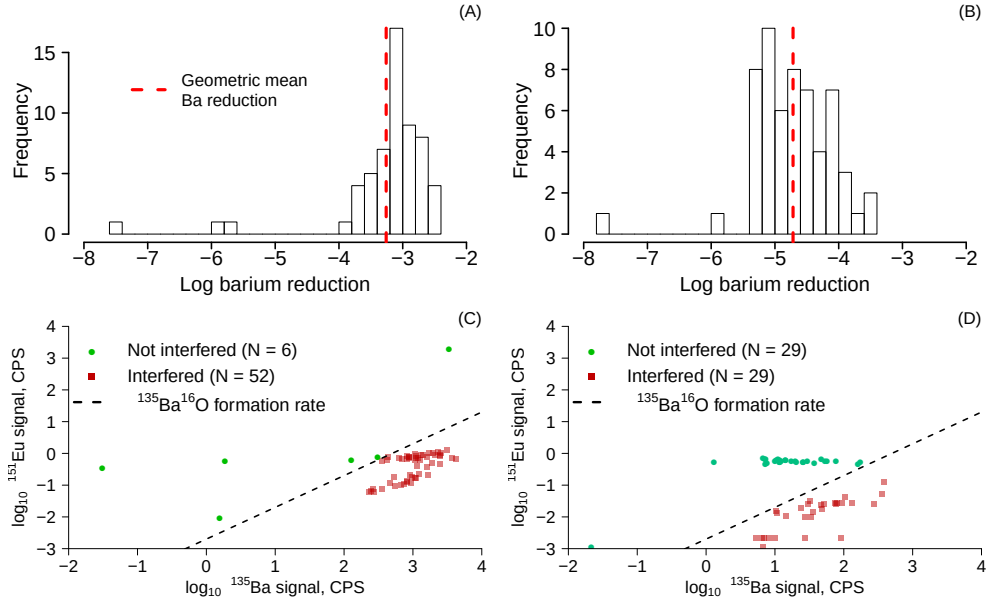

Figure C.2: Efficiency of Ba removal by LLE method (A, C) and ICP-MS octopole collision cell (B, D). Results are for samples without (A, C) and with (B, D) H_2SO_4 addition to precipitate barite. In (B) and (D), $^{135}Ba^{16}O^{+}$ rate is inferred from 23 replicate analyses of a 200 ppb Ba standard after blank subtraction. Interfered samples are those where accurate Eu determination could not be made due to excessive $^{135}Ba^{16}O^{+}$ interference. In (D) the interfered samples were all unspiked experiments.

Other experimental work in our shared lab space involves high concentrations ($\sim$mM) of Gd. We ascribe the uniformly high Gd background in all experiments to cross contamination in this shared space. In the "Blank" experiment (i.e. pH adjusted ASTM Type I water), all

analytes were below detection (IDL $\sim 5 - 20$ ppt for 1% false negative rate) except for Ba, La, and Gd. This indicates that the high La background could either be a result of laboratory cross-contamination (as with Gd) or an impurity in the organic phases used. The latter supposition was investigated by direct contact of the mixed organic phases used (i.e. 3 mL 0.25 M HDEHP in heptane + 1 mL octanol) with 4 mL of 6 N HCl, followed by analysis of the acid phase. These results were below detection (not pictured), indicating no significant REE contamination of the organic phases. While all chemicals were purchased at high purity, we can assume that the observed background concentrations in other experiments are due to trace contamination of these reagents. Paradoxically, the level of these contaminations cannot be determined by ICP-MS without applying a separation/preconcentration technique such as the LLE method; this makes source apportionment of the observed background concentration challenging.

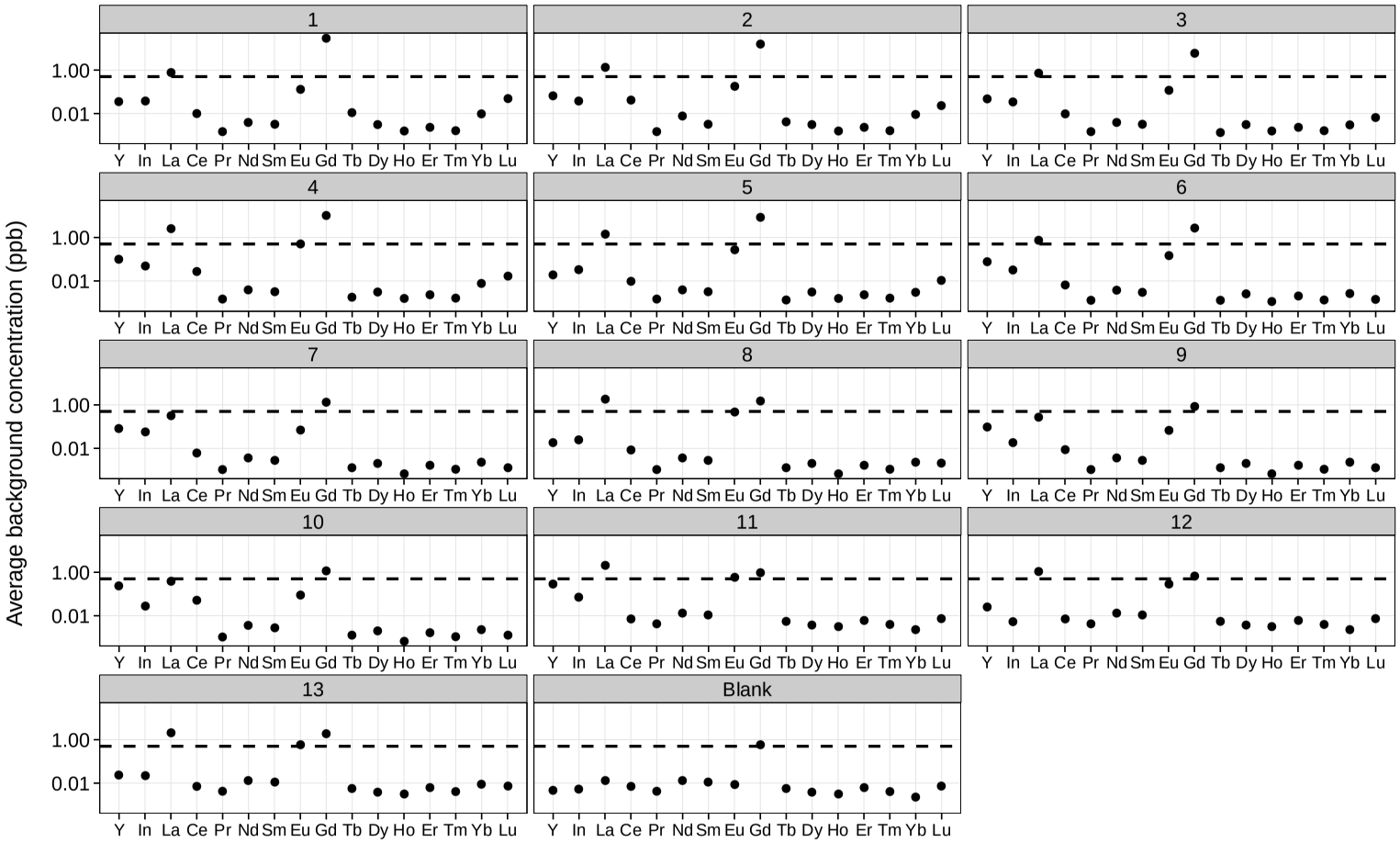

Figure C.3: Average (from $n \geq 2$ replicates, except for Blank and experiments 6, 13) background concentrations of target analytes in samples without $BaSO_4$ precipitation. Dashed line at 500 ppt indicates the input concentration for all spiked samples. Note that the y-axis is a logarithmic scale. Blank experiment represents pH adjusted ASTM Type I water.

C.4 Doehlert experimental results

Experiment- and replicate ordered results of Doehlert matrix tests are shown in Figure C.4. Each experiment number represents a unique set of solution conditions ([NaCl], [Fe], and [DOC]); values for each of these parameters in each experiment is given in Table C.2.

Table C.2: Actual variable values for Doehlert matrix experiments. Proposed values are shown in Table 5.2.

Experiment	[NaCl] (m)	[Fe] (ppm)	[DOC] (ppm)
1	1.797	41.5	165.3
2	3.713	59.0	218.3
3	2.733	63.6	185.6
4	2.715	22.7	304.3
5	0.503	10.3	149.0
6	1.263	21.4	43.5
7	1.232	40.9	24.7
8	2.729	14.0	148.4
9	2.763	69.8	41.0
10	1.367	125.1	187.9
11	2.052	121.7	36.7
12	1.266	51.4	304.3
13	2.065	19.5	318.9

Table C.3: Fractional elemental recovery in Doehlert matrix samples by LLE methodology. Recovery values for Eu were determined after dosing the LLE eluent with H_2SO_4 to precipitate barite; all other recoveries were determined without barite precipitation. Elements where the background concentration was determined to 250 ppt or greater (see Figure C.3) were excluded (i.e. La and Gd in all experiments and Y in experiment 11). Experiment numbers correspond to conditions described in Table C.2.

Exp.	Rep.	Y	In	Ce	Pr	Nd	Sm	Eu	Tb	Dy	Ho	Er	Tm	Yb	Lu
1	1	1.030	1.400	1.040	1.000	1.020	0.953	1.150	1.110	1.020	1.000	0.997	0.999	0.891	1.410
1	2	1.090	1.130	1.130	1.100	1.100	1.060	1.130	1.230	1.090	1.120	1.130	1.150	0.978	1.580
1	3	1.050	1.070	1.100	1.060	1.040	1.030	1.100	1.170	1.080	1.100	1.090	1.110	0.993	1.550
1	4	0.919	0.948	0.966	0.941	0.963	0.926	1.000	1.060	0.971	0.963	0.974	0.966	0.943	1.370
2	1	1.040	1.110	1.100	1.140	1.140	1.130	1.130	1.130	1.170	1.150	1.110	1.140	1.100	1.110
2	2	0.907	0.931	0.892	0.952	0.955	0.900	0.922	0.949	0.946	0.982	0.955	0.967	0.936	0.937
3	1	1.200	1.220	1.190	1.200	1.170	1.150	1.150	1.190	1.190	1.210	1.220	1.180	1.220	1.150
3	2	0.917	0.927	0.944	0.950	0.913	0.965	0.872	0.958	0.988	0.978	0.975	0.955	0.948	0.957
4	1	1.010	1.030	1.070	1.050	1.070	1.020	1.030	1.070	1.060	1.070	1.060	1.060	1.050	1.030
4	2	1.020	1.090	1.090	1.090	1.060	1.070	1.050	1.090	1.110	1.090	1.100	1.110	1.090	1.070
4	3	1.020	1.030	1.080	1.060	1.110	1.070	1.070	1.090	1.080	1.100	1.090	1.080	1.050	1.060
5	1	1.100	1.070	1.100	1.110	1.090	1.050	0.963	1.090	1.110	1.100	1.100	1.120	1.110	1.020
5	2	1.120	1.130	1.110	1.100	1.100	1.010	1.100	1.100	1.130	1.130	1.140	1.110	1.130	1.090
6	1	1.040	1.000	1.040	1.030	0.982	0.974	0.936	1.010	1.090	1.050	1.040	1.030	1.030	0.967
7	1	1.110	1.120	1.080	1.070	1.110	1.040	1.030	1.050	1.050	1.100	1.070	1.090	1.090	1.010
7	2	1.160	1.160	1.150	1.120	1.100	1.100	1.130	1.130	1.130	1.160	1.150	1.140	1.130	1.060
8	1	1.060	1.070	1.070	1.040	1.070	1.020	1.020	1.070	1.040	1.090	1.090	1.070	1.080	1.010
8	2	1.060	1.020	1.080	1.040	1.010	1.020	0.981	1.020	1.080	1.060	1.060	1.060	1.050	1.010
9	1	1.120	1.070	1.080	1.070	1.030	1.000	0.883	1.030	1.020	1.090	1.090	1.070	1.070	0.997
9	2	1.040	1.060	1.040	1.060	1.020	1.000	0.831	1.010	1.040	1.040	1.030	1.040	1.040	0.979
10	1	0.932	1.040	1.030	1.030	1.010	1.020	1.010	1.020	1.000	1.040	1.040	1.030	1.040	0.989
10	2	0.981	1.090	1.070	1.060	1.080	1.070	1.050	1.070	1.060	1.080	1.110	1.120	1.120	1.020
11	1	—	1.000	1.100	0.997	1.020	0.997	1.030	0.971	1.020	1.020	0.990	0.996	1.000	0.932
11	2	—	1.240	1.200	1.190	1.230	1.180	1.150	1.170	1.200	1.220	1.220	1.210	1.180	1.130
12	1	1.010	1.010	1.030	1.000	0.928	0.983	0.956	0.990	1.000	1.020	1.000	1.010	0.999	0.945
12	2	1.060	1.050	1.070	1.050	0.959	0.948	0.978	1.020	1.030	1.050	1.040	1.060	1.070	0.966
13	1	1.040	1.030	1.090	1.050	1.030	1.010	1.040	1.050	1.060	1.080	1.050	1.070	1.140	1.060

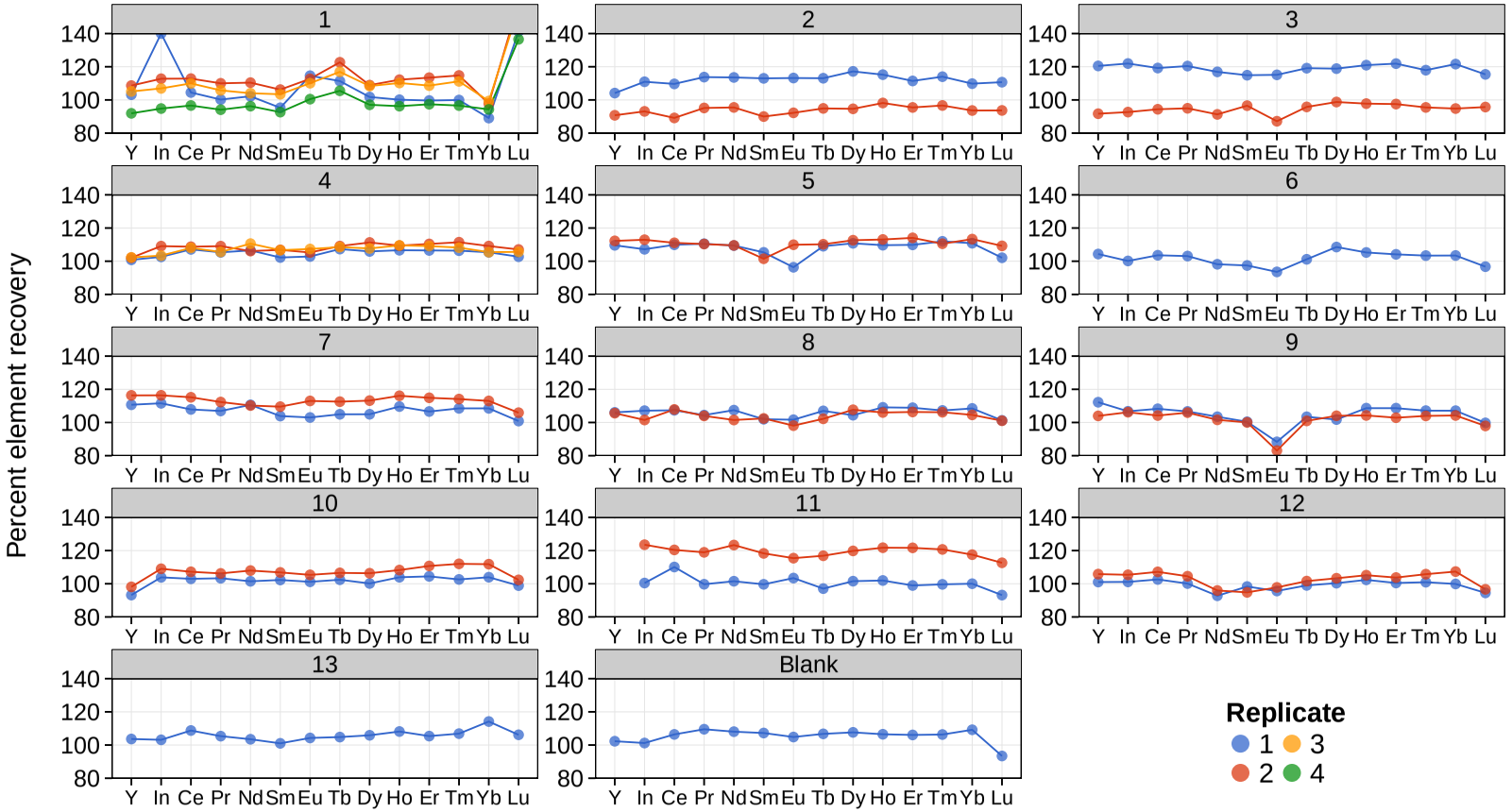

Figure C.4: Elemental recovery in Doehlert matrix samples by LLE methodology (see Table 5.2 for experimental conditions). Recovery values for Eu were determined after dosing the LLE eluent with H_2SO_4 to precipitate barite; all other recoveries were determined without barite precipitation. Elements where the background concentration was determined to 250 ppt or greater (see Figure C.3) were excluded (i.e. La and Gd in all experiments and Y in experiment 11).

Table C.4: Hodge-Lehman (HL) estimators of differences in median recovery between elements by LLE method. The HL estimator describes the median difference between all permutations of experimental observations in two groups. Estimates are reported with respect to the elements in the row, e.g. the median recovery of In is 1.4% lower than the recovery for Y. Statistical significance is noted with the asterisks for the following levels: $* = p < 0.05$, $** = p < 0.01$, and $*** = p < 0.005$.

	In	Ce	Pr	Nd	Sm	Eu	Tb	Dy	Ho	Er	Tm	Yb	Lu
Y	-0.014*	-0.025***	-0.014	-0.002	0.018	0.013	-0.026	-0.022*	-0.032***	-0.026**	-0.026**	-0.014	0.007
In	—	-0.008	0.003	0.013	0.034***	0.036***	0.003	-0.002	-0.017*	-0.012	-0.011	-0.001	0.033*
Ce	—	—	0.013*	0.021*	0.044***	0.041***	0.006	0.008	-0.006	-0.002	0.001	0.007	0.042
Pr	—	—	—	0.009	0.03***	0.028*	0.003	-0.006	-0.02***	-0.013**	-0.012***	-0.002	0.035*
Nd	—	—	—	—	0.024***	0.018	-0.013	-0.013	-0.026***	-0.021***	-0.021***	-0.009	0.019
Sm	—	—	—	—	—	0.001	-0.03***	-0.034***	-0.048***	-0.042***	-0.044***	-0.028**	0.005
Eu	—	—	—	—	—	—	-0.036***	-0.032***	-0.048***	-0.042***	-0.041***	-0.038*	-0.015
Tb	—	—	—	—	—	—	—	-0.005	-0.021*	-0.014	-0.012	-0.009	0.029*
Dy	—	—	—	—	—	—	—	—	-0.012*	-0.004	-0.005	0.007	0.038*
Ho	—	—	—	—	—	—	—	—	—	0.005	0.008	0.016*	0.054*
Er	—	—	—	—	—	—	—	—	—	—	-0.002	0.01	0.048*
Tm	—	—	—	—	—	—	—	—	—	—	—	0.008	0.045*
Yb	—	—	—	—	—	—	—	—	—	—	—	—	0.043*

C.5 Summary of Doehlert matrix regression

Effects of solution conditions on element recovery, R, were evaluated by linear regression according to the model:

$$\begin{aligned} R =& \beta_0 + \beta_{NaCl}[NaCl] + \beta_{Fe}[Fe] + \beta_{DOC}[DOC] + \\ & \beta_{NaCl\cdot Fe}[NaCl]\cdot[Fe] + \beta_{NaCl\cdot DOC}[NaCl]\cdot[DOC] + \beta_{Fe\cdot DOC}[Fe]\cdot[DOC] + \\ & \beta_{NaCl\cdot Fe\cdot DOC}[NaCl]\cdot[Fe]\cdot[DOC] \end{aligned} \tag{C.4}$$

Table C.5: Summary of parameter estimates from regression of element recovery versus (actual) Doehlert experimental values, including interaction terms. Parameters, β_i, correspond to those defined in Equation C.4. Statistical significance, determined from regression, is noted with the asterisks for the following levels: $* = p < 0.05$, $** = p < 0.01$, and $*** = p < 0.005$.

Element	Parameter estimate							
	β_0	β_{NaCl}	β_{Fe}	β_{DOC}	$\beta_{NaCl\cdot Fe}$	$\beta_{NaCl\cdot DOC}$	$\beta_{Fe\cdot DOC}$	$\beta_{NaCl\cdot Fe\cdot DOC}$
Y	1.02**	0.019	0.00243	0.000785	-0.000699	-0.000323	-2.2e-05	6.05e-06
In	0.91*	0.0828	0.0062	0.00127	-0.00271	-0.000601	-3.54e-05	1.5e-05
Ce	0.989***	0.0185	0.00381	0.000683	-0.00121	-0.000166	-2.06e-05	5.11e-06
Pr	1.18***	-0.0782	-0.00113	-0.000524	0.000899	0.000316	2.76e-06	-3e-06
Nd	1.06***	-0.0331	0.00365	-6.03e-05	-0.00111	0.000157	-2.06e-05	6.13e-06
Sm	1.04***	-0.0322	0.00238	-0.000244	-0.000603	0.000216	-1.02e-05	2.48e-06
Eu	0.542	0.195	0.017*	0.00306	-0.00755*	-0.00122	-9.22e-05*	4.04e-05*
Tb	0.934***	0.0632	0.00542	0.00103	-0.00251	-0.000433	-3.22e-05	1.39e-05
Dy	1.16***	-0.0618	0.000645	-0.000241	2.24e-05	0.000206	-8.7e-06	2.14e-06
Ho	1.11***	-0.0301	0.00149	-4.35e-05	-0.00038	8.6e-05	-1.08e-05	3.16e-06
Er	1.15***	-0.0496	0.000377	-0.000382	9.3e-05	0.000233	-2.15e-06	-6.68e-07
Tm	1.11***	-0.0346	0.00128	-0.000121	-0.000312	0.000132	-7.58e-06	1.74e-06
Yb	1.24***	-0.117	-0.00232	-0.000913	0.00157	0.000562	1.24e-05	-8.31e-06
Lu	0.186	0.486	0.0222	0.00595	-0.0112	-0.00286	-0.000129	6.05e-05

C.6 References

Jenner, G., Longerich, H., Jackson, S., and Fryer, B. ICP-MS - a powerful tool for high-precision trace-element analysis in earth sciences: evidence from analysis of selected USGS reference samples. *Chemical Geology*, 83(1):133–148, 1990.

Kimura, K. Inorganic extraction studies on the system between bis (2-ethyl hexyl)-orthophosphoric acid and hydrochloric acid (i). *Bulletin of the Chemical Society of Japan*, 33(8):1038–1046, 1960.

Kimura, K. Inorganic extraction studies on the system between bis (2-ethyl hexyl)-orthophosphoric acid and hydrochloric acid (ii). *Bull. Chem. Soc. Japan*, 34, 1961.

McGinnis, C. E., Jain, J. C., and Neal, C. R. Characterisation of memory effects and development of an effective wash protocol for the measurement of petrogenetically critical trace elements in geological samples by ICP-MS. *Geostandards Newsletter*, 21(2):289–305, 1997.

Appendix D

Supporting information for Chapter 6

D.1 Preliminary adsorption experiments

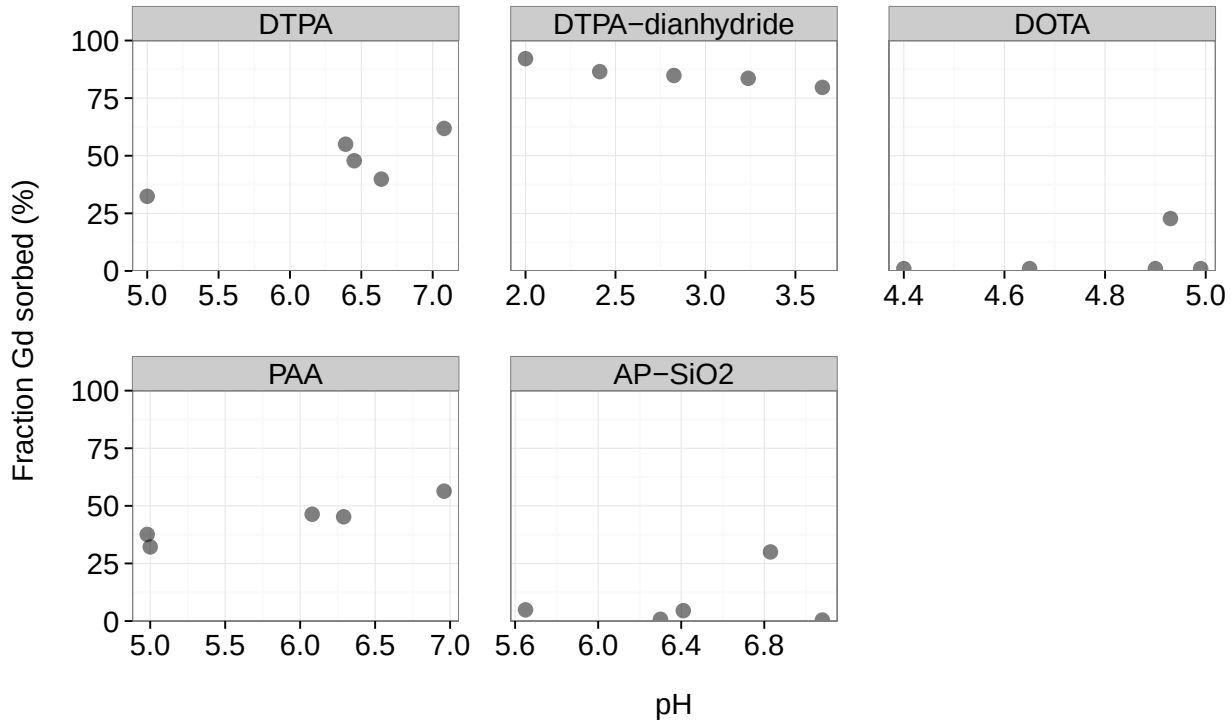

Figure D.1: Preliminary experimental results screening candidate functionalized adsorbents. Gd removal measured from 1 mM solution of Gd in 0.5 M NaCl after 3 hours of contact time.

D.2 Calculation of maximal binding sites for 1 mm glass beads

To determine the per gram concentration of ligands in a batch of beads ($[x]$) we first calculate the number of sites per bead and then the mass of an individual bead. For a bead with a 0.5 mm radius (r_{bead}) and an amine site density (Γ_{amine}) of 3 sites nm^{-2} (taken as the maximum value from Walcarius et al. (2002), and likely represents a best-case scenario), this results in:

$$
\begin{aligned}
r_{bead} &= 0.5 \text{ mm} \\
\Gamma_{amine} &= 3 \text{ sites nm}^{-2} \\
SA = 4\pi r_{bead}^2 &= 3.14 \times 10^{-6} \text{ m}^2 \\
&= 3.14 \times 10^{12} \text{ nm}^2 \\
[x] &= 9.42 \times 10^{12} \text{ sites bead}^{-1} \\
&= 1.56 \times 10^{-11} \text{ mol bead}^{-1}
\end{aligned}
$$

Next, assuming that each bead is a non-porous, soda-lime glass sphere ($\rho_{SiO_2} = 2.5$ g cm^{-3}), we calculate the mass of an individual bead.

$$
\begin{aligned}
V_{bead} &= \frac{4}{3}\pi r^3 = 5.24 \times 10^{-4} \text{ cm}^3 \\
m_{bead} &= V_{bead} \cdot \rho_{SiO_2} = 1.31 \times 10^{-3} \text{ g}
\end{aligned}
$$

Dividing the moles of site per bead by the mass per bead yields $[x]$ in the desired units of mol-sites g-1, 1.2×10^{-8}, or 12 nmol-sites g^{-1}. For 10 g/L solids concentration, this is effectively 120 nmol-sites L^{-1}. At 100 ppb, the molar concentration of Gd in solution is 640 nmol L^{-1}. These result in a sorbent-sorbate (mole-mole) ratio of 0.19.

However, these calculations are highly sensitive to: the size of the bead (spec'd at diameter = 710 – 1190 µm), the density of the material (ranging from 2.1 – 2.65 g cm^{-3} depending on crystalline phase (Lide 2012)), and density of surface sites (ranging between 1.9 and 2.9 in silica gels according to Walcarius et al. (2002))

By assigning statistical distributions to these values, we can better assess the likely range of conditions that might be occurring through simulation. Material density (ρ_{SiO_2}) and amine site density (Γ_{amine}) are both given uniform distributions with the noted endpoints. Particle diameter is generated from a truncated log-normal distribution with the noted endpoints, log mean 6.8 (geometric mean of endpoints), and log standard deviation 0.36 (geometric standard deviation of endpoints). From this simulation, the 95% confidence interval on the sorbent to sorbate ratio is 0.12–0.25, indicating that it is highly likely that there are insufficient sites for Gd binding (under these assumptions).

The maximum potential amine site density can be estimated from the crystal geometry of various quartz polymorphs. While likely incorrect, we can assume that the surface geometry is equivalent to the bulk geometry. Holleman and Wiberg (1995) provide the following Si-O-Si bond angles (θ) and Si-O bond distances (d_{Si-O}) for a variety of quartz phases. From these data, the Si-Si distance can be approximated from a triagular geometry ($d_{Si-Si} = 2x\sin(\theta/2)$). Assuming that the amino-propyl, triethoxy-silane binds to three of these Si atoms (spaced in an equilateral triangle, $A = \sqrt{3}/4 \cdot d_{Si-Si}$), the area of an individual silane group can be determined. The reciprocal of this value gives the maximal amine density per nm^2, ignoring further geometric/coordination constraints.

Table D.1: Silica mineral geometries and maximal amine site density calculation results. Silica geometry data from Holleman and Wiberg (1995).

Mineral	$\theta_{Si-O-Si}$ (°)	d_{Si-O} (nm)	d_{Si-Si} (nm)	$\max \Gamma_{\text{amine}}$ (sites nm^{-2})
α-Quartz	144	0.161	0.306	7.7
β-Quartz	153	0.162	0.315	7.1
α-Cristobalite	147	0.160	0.307	7.7
β-Cristobalite	151	0.158	0.306	7.7

Thus, even by more than doubling the surface sites, compared to the estimates of Walcarius et al. (2002), and under the most favorable calculation conditions (low diameter, low density to maximize specific surface area), the maximum possible sorbent to sorbate ratio achieved is 0.81.

D.3 Raw data from adsorption experiments

Table D.2: Raw data for REE adsorption edges onto DTPA-dianhydride (DTPA-a) functionalized adsorbents under three electrolyte conditions. Contact time was 3 hours. For experiments in 0.5 and 3.0 M NaCl, the adsorbent mass is approximately 0.1 g.

Electrolyte	Adsorbent mass (g)	pH	Concentration (μg/L)		
			Nd	Gd	Ho
0.01 M NaCl	0.10433	1.93	2.3	<0.1	2.8
	0.10444	3.41	7.4	8.3	31
	0.9818	8.81	84	60	78
	0.9950	11.02	82	58	77
	Initial conc. (µg/L)		86	65	81
0.5 M NaCl	—	2.01	17	16	22
	—	1.99	18	17	23
	—	1.97	18	18	23
	—	2.71	40	40	54
	—	2.89	34	36	53
	—	4.39	103	81	105
	—	4.17	55	44	54
	Initial conc. (µg/L)		115	84	107
3.0 M NaCl	—	1.37	16	12	15
	—	1.43	17	11	14
	—	1.47	34	27	31
	—	2.6	20	27	47
	—	2.68	20	27	51
	—	4.54	118	97	122
	—	4.6	146	119	150
	Initial conc. (µg/L)		115	84	107

Table D.3: Raw data for REE adsorption edges onto PAA functionalized adsorbents. Contact time was 3 hours in 0.5 M NaCl.

Solid	Adsorbent mass (g)	pH	Concentration (μg/L)		
			Nd	Gd	Ho
PAA	0.0996	2.16	71	52	65
	0.1005	2.13	73	52	66
	0.1019	4.4	29	27	34
	0.0991	4.41	29	27	34
	0.099	6.53	14	11	7.1
	0.102	6.38	13	10	7.0
	0.1009	7.69	47	29	8.2
	0.0989	7.85	52	31	7.8
	0.1	8.97	43	15	3.3
	0.101	9.16	<0.1	<0.1	<0.1
Initial conc. (µg/L)			81	60	72

Table D.4: Raw data for REE adsorption edges onto DTPA (acid-form) functionalized adsorbents. Contact time was 3 hours in 0.5 M NaCl. Experiments that were performed on different days are divided by their respective initial concentrations.

Solid	Adsorbent mass (g)	pH	Concentration (μg/L)		
			Nd	Gd	Ho
DTPA	0.09903	2.01	70	56	68
	0.10312	2.02	67	53	66
	0.09942	2.28	71	56	69
	0.09835	2.23	71	56	68
	0.10005	2.24	72	56	69
	0.09975	2.22	77	60	73
	0.09928	2.48	73	57	69
	0.10376	2.39	73	56	69
	0.10039	2.45	75	58	71
	0.10072	2.46	75	58	71
	0.10218	2.80	75	59	71
	0.10230	2.62	74	58	70
	0.10464	2.94	78	59	73
	0.10093	2.86	78	60	73
	0.09932	3.00	77	59	72
	0.10031	3.02	76	58	71
	Initial conc. (µg/L)		85	63	76
	0.09812	4.21	74	58	72
	0.09877	7.68	75	57	71
	0.09926	8.98	74	56	70
	Initial conc. (µg/L)		86	65	81

Table D.5: Raw data for REE adsorption isotherms onto DTPA-dianhydride (DTPA-a) functionalized adsorbents. Contact time was 3 hours in a 0.5 m NaCl background electrolyte.

Solid	Adsorbent mass (g)	pH		Concentration (μg/L)		
				Nd	Gd	Ho
DTPA-a	0.09822	2.1	C_e	1.6	1.3	1.7
			C_i	43	32	40
	0.10314	2.08	C_e	2.4	2.0	2.7
			C_i	64	49	60
	0.10194	2.04	C_e	3.0	2.5	3.3
			C_i	86	65	81
	0.10067	2.1	C_e	3.6	2.9	3.9
			C_i	107	81	101
	0.10224	2.03	C_e	4.1	3.5	4.6
			C_i	129	97	121
	0.09773	2.05	C_e	5.2	4.1	5.6
			C_i	150	114	141
	0.10228	2.03	C_e	5.8	4.8	6.4
			C_i	172	130	161
	0.10073	2.08	C_e	12	10	13
			C_i	344	259	322

Table D.6: Raw data for REE adsorption isotherms onto PAA functionalized adsorbents. Contact time was 3 hours in a 0.5 m NaCl background electrolyte.

Solid	Adsorbent mass (g)	pH		Concentration (μg/L)		
				Nd	Gd	Ho
PAA	0.1007	6.55	C_e	14	10	7
			C_i	61	45	54
	0.1005	6.74	C_e	24	17	10
			C_i	91	67	82
	0.0991	6.91	C_e	33	24	14
			C_i	121	90	109
	0.0993	6.8	C_e	44	33	19
			C_i	182	134	163
	0.0997	6.81	C_e	54	40	24
			C_i	242	179	217
	0.1007	6.83	C_e	86	65	38
			C_i	364	269	326
	0.0998	6.83	C_e	118	89	55
			C_i	485	358	435
	0.09968	4.14	C_e	28	23	29
			C_i	58	43	52
	0.10102	4.1	C_e	63	59	74
			C_i	115	85	104
	0.10000	4.21	C_e	91	85	105
			C_i	173	128	156
	0.10136	4.27	C_e	141	129	160
			C_i	346	256	311
	0.10017	4.24	C_e	199	177	220
			C_i	461	342	415

Table D.7: Raw data for REE adsorption isotherms onto DTPA (acid-form) functionalized adsorbents. Contact time was 3 hours in a 0.5 m NaCl background electrolyte.

Solid	Adsorbent mass (g)	pH		Concentration (μg/L)		
				Nd	Gd	Ho
DTPA	0.09934	2.07	C_e	45	36	43
			C_i	58	43	52
	0.10041	2.18	C_e	89	70	86
			C_i	115	85	104
	0.09916	2.23	C_e	133	105	128
			C_i	173	128	156
	0.10081	2.25	C_e	175	137	166
			C_i	230	171	208
	0.10022	2.26	C_e	260	202	246
			C_i	346	256	311
	0.10017	2.25	C_e	344	272	326
			C_i	461	342	415

Table D.8: Raw data for REE adsorption isotherms onto DTPA-dianhydride functionalized adsorbents following overnight washing with either acid (1 N HCl) or base (1 N NaOH) and drying at 98°C. Contact time was 3 hours in a 0.5 m NaCl background electrolyte.

Treatment	Adsorbent mass (g)	pH		Conc. (μg/L)		
				Nd	Gd	Ho
HCl	0.05189	2.01	C_e	63	12	11
			C_i	572	412	545
	0.0516	1.95	C_e	160	29	28
			C_i	1144	824	1090
	0.0492	1.96	C_e	227	46	38
			C_i	1525	1099	1453
	0.0492	1.9	C_e	381	66	64
			C_i	2288	1648	2179
	0.0495	1.92	C_e	631	111	107
			C_i	3050	2197	2906
NaOH	0.0514	2.23	C_e	19	8	10
			C_i	572	412	545
	0.0502	2.23	C_e	29	13	16
			C_i	763	549	726
	0.0512	2.27	C_e	49	23	29
			C_i	1144	824	1090
	0.0496	2.27	C_e	75	24	28
			C_i	1525	1099	1453
	0.049	2.22	C_e	159	44	49
			C_i	2288	1648	2179
	0.0495	2.16	C_e	281	64	69
			C_i	3050	2197	2906

Table D.9: Raw data for time-dependent adsorption of REE onto DTPA-dianhydride functionalized adsorbents. Background electrolyte was 0.5 m NaCl. Each time point represents a separate batch experiment that was centrifuged and sampled at the noted time point.

Time (min.)	Mass solid (g)	Final conc. (µg/L)		
		Nd	Gd	Ho
5	0.10501	16.3	8.7	8.7
15	0.10444	15.0	7.7	6.7
30	0.09674	11.5	4.6	4.2
45	0.09716	12.1	5.3	5.2
60	0.09895	12.9	5.1	5.8
90	0.09921	11.5	4.0	4.3
120	0.09975	10.6	3.1	3.4
150	0.1023	11.2	3.9	4.3
180	0.09999	11.5	3.5	3.8
Initial conc. (µg/L)		81.2	61.6	74.9

D.4 References

Holleman, A. F. and Wiberg, E. *Lehrbuch der anorganischen Chemie*. Walter de Gruyter, 1995.

Lide, D. R. *CRC handbook of chemistry and physics*. CRC press, 2012. ISBN 1439880492.

Walcarius, A., Etienne, M., and Bessière, J. Rate of access to the binding sites in organically modified silicates. 1. amorphous silica gels grafted with amine or thiol groups. *Chemistry of materials*, 14(6):2757–2766, 2002.